G-27-17

Characterization Study of Temper Embrittlement of Chromium-Molybdenum Steels

API PUBLICATION 959
MAY 1982

American Petroleum Institute
2101 L Street, Northwest
Washington, D.C. 20037

Characterization Study of Temper Embrittlement of Chromium-Molybdenum Steels

Refining Department

API PUBLICATION 959
MAY 1982

American
Petroleum
Institute

Nothing contained in any API publication is to be construed as granting any right, by implication or otherwise, for the manufacture, sale, or use in connection with any method, apparatus, or product covered by letters patent.

This publication may be used by anyone desiring to do so. The Institute hereby expressly disclaims any liability or responsibility for loss or damage resulting from its use; for the violation of any federal, state, or municipal regulation with which an API publication many conflict; or for the infringement of any patent resulting from the use of an API publication. Every effort has been made by the Institute to assure the accuracy and reliability of the data presented.

PREFACE

At the October 1973 API Refining meeting, it was brought to the attention of the Committee on Refinery Equipment that 2-1/4Cr-1 Mo steel, an alloy frequently used to build hydrotreater reactors, was susceptible to temper embrittlement. Reactors constructed of this alloy could potentially experience a considerable loss of toughness. The embrittlement occurs partly during shop fabrication heat treatments, but more significantly, as a result of operating in the embrittling temperature range. Responding to this problem, CRE established a Task Group on Temper Embrittlement with members from the Subcommittees on Corrosion and on Pressure Vessels and Tanks. The task group was given two objectives:

1. To review the existing metallurgical data and research programs, and to recommend what approach should be taken to avoid embrittlement problems with existing vessels.
2. To recommend what further work was required to develop steels for future pressure vessels which would be immune or less susceptible to temper embrittlement.

On July 30, 1974, the API issued a cautionary letter prepared by the task group to managers of all refineries in the United States and Canada. It alerted plant operators to the concern for in-service embrittlement of low alloy chrome-moly steels, and especially of 2-1/4Cr-1 Mo in thick sections. It also suggested precautions that should be taken to minimize the probability of brittle fracture in embrittled material.

Earlier, at the May 1974 Refining meeting, CRE accepted a task group proposal that API support a multiyear program to characterize the temper embrittlement susceptibility of commercial plate, forging, and welds used in reactors. The program would investigate the extent of embrittlement that might exist in operating vessels and how best to predict the embrittlement that could occur. In the spring of 1975, Westinghouse Research Corporation was selected as contractor for a 5-year characterization research program as outlined by the task group, with Dr. Bevil J. Shaw as principal investigator. A total of 64 samples, mostly 2-1/4Cr-1 Mo, but a few of 1-1/4Cr-1 Mo and 3Cr-1 Mo compositions, were provided by member companies, by steel suppliers, and by vessel fabricators. The 64 samples represented a large range of commercially produced steels, and included qualification welds, croppings from forgings, and nozzle and manway cutouts from plate ranging in thickness up to 6 inches.

The characterization program was divided into Phases I and II. Phase I included a 64-sample study of the microstructure, grain size tensile properties, hardness, chemistry, including tramp elements, heat treatments, and toughness. Toughness data included determination of transition temperatures before and after short time step-cool embrittlement heat treatment and of the shift in transition temperature resulting from the induced embrittlement.

For Phase II, 25 heats were selected for additional embrittlement study. These heats were chosen to represent both the typical and the extremes in chemistry and in susceptibility to temper embrittlement as measured by the step-cool test. The main thrust of Phase II was the characterization of these alloys for embrittlement during isothermal exposure at five temperatures from 650 F to 950 F for times up to 20,000 hours. These temperatures were chosen to span the range typical of service conditions.

The report which follows is a summary covering the Westinghouse characterization work and several ancillary studies, which developed during the nearly 6 years of work by the task group and Dr. Shaw.

At the outset, the API program recognized that the characterization study could provide much needed information about the temper embrittlement behavior of commercial low alloy Cr-Mo steels used in reactors. It was not designed, however, to probe the temper embrittlement mechanism. Coincidentally, in late 1974, the Metals Properties Council Task Group on Tramp Elements in Pressure Vessel Steels was considering a proposal by Dr. C. J. McMahon, Jr., Department of Materials Science and Engineering, University of Pennsylvania, to study the mechanism of temper embrittlement, particularly with respect to the effect of tramp elements. The API task group also reviewed the proposed program and concluded that it was a highly desirable supplement to the characterization study. As a result, API entered into an agreement with the Metals Properties Council for joint API/MPC support of McMahon's three-phase, 5-year mechanism study. The primary objective was to study, using laboratory heats of controlled chemistry, the individual and synergistic embrittling potency of the elements manganese, phosphorus, silicon, antimony, and tin. A number of significant conclusions on the effects of these elements were derived from this study. Some of these data have been published in an article appearing in Vol. 102, 1980, of the Transactions ASME, Journal of Engineering Materials and Technology. Other supplementary papers are in process of publication, and a final report is now being prepared by Dr. McMahon.

The API Temper Embrittlement Characterization Study benefited strongly from the support of steel manufacturers and vessel fabricators. Their representatives were active ex-officio members of the task group; their industrial backgrounds made their input to the program especially valuable. This is an outstanding example of the benefits to be derived from close cooperation between supplier and user.

As a result of the API characterization study and the jointly supported API/MPC mechanism study, along with large individual research programs by some steel suppliers and vessel fabricators, which were at least partly stimulated by the API program, there is now a much better understanding of the causes and implications of temper embrittlement for reactors built up to about 1975. As a result of the cooperative effort, it is now possible to obtain hydrotreator reactors, both in the United

States and abroad, with far greater initial toughness and with relatively little susceptibility to temper embrittlement. It is with a strong sense of achievement that the task group submits this summary report. Readers are cautioned that the conclusions it draws are applicable to materials in reactors produced up to about 1975. They are not applicable to the plate, forgings, and weld metal available today from those manufacturers utilizing the necessary controls to produce material having low temper embrittlement susceptibility. Finally, it should be recognized that the user has the responsibility to specify that material with low embrittlement susceptibility is required, and that it cannot be assumed that all low alloy Cr-Mo material available today meets this criterion.

API TASK GROUP ON TEMPER EMBRITTLEMENT
APRIL 1982

CONTENTS

CHARACTERIZATION STUDY OF TEMPER EMBRITTLEMENT OF CHROMIUM-MOLYBDENUM STEELS

B. J. Shaw
Westinghouse R&D Center
Pittsburgh, Pennsylvania 15235

ABSTRACT

A comprehensive evaluation of the step-cooled and isothermal embrittlement of Cr-Mo pressure vessel steels (A387) has been carried out. The prime purpose of this project was to characterize typical commercial reactors steels and weldments in terms of toughness and other physical properties prior to being placed in service and the changes anticipated in toughness due to long term service at elevated temperatures. In Phase I of the program, 64 supplied steels were characterized in terms of tensile properties, metallographic features and analytical chemistry. In this phase the change in the transition temperature due to step-cooled embrittlement was evaluated from Charpy impact curves. In Phase II, 25 selected samples were isothermally embrittled for 1,000, 10,000 and 20,000 hours at 650, 725, 800, 875 and 950°F. Specific relationships between sample chemistry, strength level or structures were studied. Based upon comparison of Phase I and II data, an approximate relationship between the step-cooled embrittlement and the isothermal embrittlement is derived. This paper includes the study of repeated de-embrittlement on two isothermally embrittled steels and the effect of strength level and structure on the isothermal embrittlement of one sample of steel. Subsidiary experiments performed in Phase II of the program include the effect of high pressure hydrogen (3500 psig) on temper embrittlement, fracture toughness measurements (J_{Ic}) on one sample, fractographic evaluation of isothermally embrittled steels and an Auger Electron Spectroscopic evaluation of grain boundary segregation of isothermally embrittled samples. As a result of the API Temper Embrittlement Committee efforts, the National Bureau of Standards has produced a solid standard of 2-1/4Cr - 1Mo steel (Standard Reference Material 1270). Since the interpretation of the data depends upon the experimental scatter an appendix has been devoted to the characterization of the Charpy impact test procedure.

KEY FOR ABBREVIATIONS AND SYMBOLS

40 ft-lb TT	40 ft-lb Transition Temperature also T(40)
FATT	Fracture Appearance Transition Temperature (50% Shear)
ΔT(40)	Shift in 40 ft-lb TT Due to Temper Embrittlement
ΔFATT	Shift in FATT Due to Temper Embrittlement
ΔTT	Shift in Transition Temperature

Subscripts to FATT and 40 ft-lb TT

U	Unembrittled or as received condition (i.e. the degree of embrittlement derived from cooling through the temper embrittlement range of temperatures after the final heat treatment)
D	De-embrittled condition - (1100°F, 2 hrs, water quench to remove all temper embrittlement)
E	Step-cooled embrittled condition (see page 11)
1,000, 10,000, 20,000	stand for the number of hours of isothermal embrittlement

SEM	Scanning Electron Microscope
AES	Auger Electron Spectrograph
IG	Intergranular
CL	Cleavage
DM	Dimpled Rupture
CBI	Chicago Bridge and Iron
JSW	Japan Steel Works
WRDC	Westinghouse R&D Center
FOR	Forging
PLA	Plate
SAW	Submerged Arc Weld
ESW	Electroslag Weld
SMA	Shielded Metal Arc Weld

Material Key

1	1-1/4Cr - 1/2Mo
2	2-1/4Cr - 1Mo
3	3Cr - 1Mo
M	Martensitic Structure
QBM	Quenched Martensite-Bainite Structure
B	Bainite Structure
F-P	Ferrite-Pearlite Structure
J_{Ic}	A Fracture Toughness Parameter Used in Assessing Low Strength High Ductility Metals
J	An Embrittlement Factor, $(Mn + Si)(P + Sn) \times 10^4$ (wt%)
X	An Embrittlement Factor, $(P + 4Sn + 5\,As + Sb) \times 10^{-2}$ (ppm)

Characterization Study of Temper Embrittlement of Chromium-Molybdenum Steels

I. INTRODUCTION

In 1975 the API awarded a contract to Westinghouse R&D Center (WRDC) to evaluate the temper embrittlement characteristics of Cr-Mo pressure vessel steels. The steels are designated A387 in Part 4 of the ASTM Book of Standards. Most of the samples supplied were of Grade 22(2-1/4Cr - 1Mo) and a few samples of Grades 11 and 21 were also included (1-1/4Cr - 1/2Mo, 3Cr - 1Mo). The 64 samples received represented a large range of commercially produced steel including qualification welds in 1-in. and 6-in. plate, large nozzle cut-outs and randomly shaped pieces of forging and plate material. These materials had received heat treatment typical of hydro-treater reactor fabrication. The samples were typified by a simple code as follows:

FOR	Forging
PLA	Plate
SAW	Submerged Arc Weld
ESW	Electroslag Weld
SMA	Shielded Metal Arc Weld
1	1-1/4Cr - 1/2Mo
2	2-1/4Cr - 1Mo
3	3Cr - 1Mo

Thus, throughout the text, 1 PLA means 1-1/4Cr - 1/2Mo Plate material, 2 SAW means 2-1/4Cr - 1Mo Submerged Arc Weld material and so on.

The objective of this program was to characterize typical commercial reactors steels and weldments in terms of toughness and other physical properties prior to being placed in service and the changes anticipated in toughness due to long time service at elevated temperature. It is important to note that these materials were typical of commercial production and fabrication up to about 1975, and are not representative of the plate, forgings and weld metal, having low temper embrittlement susceptibility available today [1]. Phase I of the project included the metallography and grain size, the tensile properties and the Rockwell Hardnesses, the analytical chemistries including the tramp elements, the heat treatments and Charpy impact test data. The latter yielded the Fracture Appearance Transition Temperatures (FATT) and the 40 ft-lb Transition Temperatures (40 ft-lb TT) for the steels in the unembrittled and step-cooled embrittled condition. The terms ΔFATT and ΔT(40) refer to the change in FATT and the 40 ft-lb TT due to temper embrittlement.

The main part of Phase II was the characterization of the isothermal embrittlement of 25 steels assessed in Phase I. Five isothermal embrittlement temperatures were chosen at 75°F intervals from 650° to 950°F. Tests to measure the amount of temper embrittlement were carried out after 1,000, 10,000 and 20,000 hours. A number of studies were also performed in this time. These were:

- o The effect of repeated de-embrittlement of the steel.
- o The effect of strength level and structure.
- o Auger analysis of grain boundaries of embrittled steels.
- o J_{Ic} measurements.
- o Effect of high pressure hydrogen on temper embrittlement.
- o Isothermal embrittlement of 1-1/4Cr and 3Cr steels.

By the end of 1976 the first phase of the program had been completed. At this juncture in the program a number of discrepancies, between the data generated at WRDC and other laboratories, were brought to light. These included the visual readings of the percentage of brittle fracture on the Charpy specimens, the conclusion that ΔFATT was not always equal to ΔT(40), absolute differences in the Charpy impact energy curves and the results of the analytical chemistries. In addition, it was found that in Phase I of the program WRDC had used a Charpy specimen orientation which was different than the one conventionally used by API.

As a consequence, a number of subsidiary experiments were initiated to clarify the various issues. These included a comparative Charpy impact test study between Japan Steel Works (JSW) and WRDC and a comparative fracture surface evaluation study between Chicago Bridge and Iron (CB&I) and WRDC (see Appendix). At the same time, since the specimens for Phase II of the program were machined in the conventional API orientation, experiments designed to establish the relationship between the Phase I and Phase II orientations were carried out.

In addition, the API Task Group initiated a round robin comparative analysis of samples and also requested the National Bureau of Standards to establish a solid 2-1/4Cr - 1Mo Standard for spectrographic analysis. As a direct result of the API Task Group efforts, this standard designated SRM 1270, is now available for public purchase from NBS. The subsidiary experiments were carried out during Phase II of the project which was concluded in 1980. This paper reviews the primary results of the program.

II. GENERAL CONCLUSIONS

This paper has been organized so that the value of the experimental results can be assessed and then the information generated has been reviewed in terms of these considerations.

It can be observed that a small portion of the samples in the unembrittled (as received) condition exhibited transition temperatures above normal ambient temperature (+50°F). Similarly, the number of samples exhibiting TT above normal ambient temperature significantly increased after step cooling or long-time isothermal exposure. Since the samples were selected to be typical of commercial reactor materials, these results can be compared to reactors prior to service (unembrittled sample condition) and after prolonged service (step cooled or isothermally exposed sample condition). See Figure 44.

In the Appendix, "Discussion of the Charpy Test," it was concluded that the Fracture Appearance Transition Temperature (FATT) was a subjective measurement and was open to considerable error. For this reason most of the discussion has been based upon the 40 ft-lb Transition Temperature (40 ft-lb TT) which is relatively nonsubjective measurement of the effect of temperature. Even so, it was found that considerable scatter could exist in the 40 ft-lb TT.

A universal industrial problem is the prediction of long-term (usually years) service degradation of a material component. The usual approach is to make predictions based upon carefully constructed short-term screening tests. The constant inevitable question is "how well do the screening methodologies represent the long-term characteristics?" The API program addresses this problem for temper embrittlement very directly. In Phase I the short-term screening test for temper embrittlement (the step-cooled embrittlement test) is evaluated and then compared with isothermal embrittlement data up to 20,000 hr. in Phase II.

Even though significant experimental scatter existed in the data, enough experiments were carried out to formulate approximate expressions relating the isothermal embrittlement to the step-cooled embrittlement. The results generated from the data base of this program appear to show that the step-cooled embrittlement can be related to the Isothermal embrittlement but is not equal to the very long-term embrittlement of a steel. In fact the step-cooled embrittlement appears to correlate with 250-hr. isothermal embrittlement at 875°F. However the step-cooled embrittlement screening test should not be replaced with 250-hr. isothermal embrittlement without further experiments to confirm

the prediction from Equation (4), page 21. This equation is primarily for 2 1/4 Cr 1 Mo steels. The equation, developed from the complete data set, suggests that the 30-year in-service embrittlement, or ΔT (40) ft-lb TT is equal to 3 times the step-cooled 40 ft-lb Transition Temperature shift.

Attempts to correlate the composition of a steel to the observed embrittlement indicated too many variables were present to formulate a reasonable regression analysis with the (statistically) disorganized data available. The correlation with the often employed "J-factor" [2] viz. (Mn + Si) (P + Sn) x 10^4 was relatively poor for data from weld metal, plate and forgings - Figures 4 (a) and (b). However, this correlation is not intended for weld metal and the correlation for plate and forging (black points) is comparable with that of similar studies [3]. Some of the scatter in the data for the plate and forging may indicate that the steel processing procedure is an important variable in the A387 Class 22 steel.

The results of the Phase II isothermal embrittlement tests may be summarized as follows:

(1) The maximum isothermal embrittlement occurred in the 800-950°F range.

(2) Embrittling susceptibility varied widely in the 25 samples. Some reached peak embrittlement at 800°F or 875°F after 20,000 hr. exposure, while some had apparently not reached maximum embrittlement after 20,000 hr. at 950°F.

(3) A possibility of embrittlement was found in half of the samples isothermally embrittled at 650°F.

(4) After 20,000 hr. exposure, the extremes and average values of the 40 ft-lb Transition Temperature for the 2 1/4 Cr - 1 Mo samples were as follows:

Exposure Temperature (°F)	Average 40 foot-pound Transition Temperature (°F)	Range of 40 foot-pound Transition Temperature (°F) Min*	Max*
650	- 11	- 115	+ 55
725	- 8	- 100	+ 60
800	+ 22	- 75	+ 100
875	+ 34	- 75	+ 140
950	+ 24	- 55	+ 100

*Minimum and Maximum values are not for the same sample but illustrate the range of transition temperatures observed.

(5) Of the twenty three 2 1/4 Cr, one 1Cr and one 3Cr samples isothermally aged, a total of twelve samples exhibited a 40 ft-lb transition temperature higher than 50°F - which is frequently used to typify the ambient temperature - at one or more of the 5 aging temperatures, and for one or more of the 3 aging times. The breakdown by materials type and alloy type is given in Table 29(a) and (b).

(6) Even though the data base is small, it suggests strongly that 2 1/4 Cr weld metal has a higher susceptibility to temper embrittlement than plate or forgings - Table 29(b).

(7) Because of the small data base, no firm conclusion can be drawn about the isothermal embrittlement of 1Cr and 3Cr alloys, but it would appear weld metal of both alloys have some susceptibility to embrittlement.

In general, the upper shelf impact energy, which reflects the toughness of the steel, was not significantly changed from the unembrittled condition to either the step cooled embrittlement or the isothermally embrittled condition.

The effect of repeated de-embrittlement at 1100°F for 2 hrs. on 875°F isothermal embrittlement (in fully post weld heat treated specimens) showed that the de-embrittled condition was approximately a constant. It was concluded that temper embrittlement is reversible and that the embrittlement is due to diffusion of the tramp elements.

The effect of strength level and structure was reasonably clear. The quenched (bainite-martensite) and tempered steel had lower transition temperatures than the slow-cooled (ferrite-pearlite) steel on the single composition tested. However, after 20,000-hr. isothermal embrittlement at 875°F the quenched and tempered steel had embrittled to the same level as the slow-cooled steel which had de-embrittled slightly. The untempered (high strength) steel, which does not represent the typical strength levels of PWHT steels except possibly in the heat affected zone, had very high initial transition temperatures but de-embrittled substantially after 20,000-hr. at 875°F.

The effect of high pressure hydrogen (3,500 psig) at 875°F after 1,000 hr. was most pronounced in the ferrite-pearlite sample which was degraded due to the hydrogen exposure. Bainite samples in the same autoclave did not show a radical change in their properties.

The Auger Electron Spectroscopic (AES), analyses of the embrittled grain boundaries showed high concentrations of the embrittling element P and to a much lesser extent Sn. Interestingly, steels with high contents of As did not reveal segregation of this element. This information supports the form of the embrittlement factor $\overline{X}$ = (10P + 5Sb + 4Sn + As) proposed by Bruscato. [4] The most surprising conclusion

from the AES study was that Cu segregates to the grain boundaries. This effect is not normally found and the role of Cu at the grain boundaries is far from clear.

Overall, this program has served to identify the primary temper embrittlement characteristics of the commercial Cr-Mo pressure vessel steels used for vessel construction up to about 1975. General guidelines of the material degradation for industrial applications have been deduced.

III. PHASE I: STEP-COOLED EMBRITTLEMENT EXPERIMENTS AND MATERIAL CHARACTERIZATION

Primary Objectives for Phase I

Phase I represented the primary characterization of the supplied steel samples. The characterization consisted of

(i) Metallographic structure

(ii) ASTM grain size

(iii) Rockwell B Hardness

(iv) Tensile properties

- (a) 0.2% yield strength
- (b) Ultimate tensile strength
- (c) Reduction in area
- (d) Elongation

(v) Analytical chemistry which consists of analyses for C, Cr, Mo, Mn, Si, Ni, Cu, P, S, Sn, Sb, O, N, As.

(vi) The generation of Charpy impact curves of unembrittled and step-cooled temper embrittled samples yielding

- (a) $FATT_U$; 40 ft-lb TT_U
- (b) $FATT_E$; 40 ft-lb TT_E
- (c) $\Delta FATT$ (or amount of embrittlement, $FATT_U - FATT_E$)
- (d) $\Delta T(40)$ (or embrittlement judged by shift in 40 ft-lb transition temperature).

Material Key

The samples listed according to the material key are as follows: (see page 1)

Material Key	Sample Number
1 PLA	2, 50, 52, 60
2 PLA	1, 7, 12, 13, 14, 33, 36, 45, 46, 47, 48, 54, 55, 70, 71, 72, 74, 75
3 PLA	64
1 FOR	77
2 FOR	9, 10, 15, 56, 57, 58, 59, 78
3 FOR	61
1 SAW	4
2 SAW	18, 19, 20, 21, 22, 23, 24, 25, 34, 35, 37, 38, 39, 40, 41
3 SAW	65
2 ESW	8, 16, 26, 27, 76
2 SMA	63, 67, 68, 69
3 SMA	66

Metallography

Metallographic sections were prepared from each sample and etched so as to show the prior austenitic grain size and structure. Photographs were taken at X200 and X500, two typical examples are shown in Figures 1 and 2. The structure of each sample is listed in Table 1.

ASTM Grain Size (Table 1)

The ASTM grain size was judged by comparison with standard charts either directly on the microscope or by comparison with the photographs. The error in these determinations is about ±1 in ASTM grain size (ASTM E112-74 Plate 1).

Tensile Properties (Table 1)

The tensile properties were judged from one tensile test on each sample. In the forged and plate material the tensile specimens were standard 0.505 inches diameter gauge as shown in Figure 3, type 1. The longitudinal axes of these specimens were parallel to the rolling direction in the plate. Transverse tensile samples were taken from the weldments. A standard tensile could not be taken from most of the weld samples without including the heat affected zone (HAZ) within the gauge length. Since the base plate or HAZ could possibly yield prior to the weld material, it was decided to use reduced size samples which included only weld metal within the gauge length. Thus, the tensile data produced for weld samples relates solely to the weld. Since the grain size is sufficiently small in each sample, grain size effects on the tensile properties should be negligible. (The effect of grain size on tensile properties is only apparent if there are less than about 5 grains in a cross section). A diagram of the tensile samples used is given in Figure 3. The size of the weld tensile samples is as follows:

Sample No.	Tensile Specimen Type from Fig. 36
4	3
8	3
16	3
34	4
35	3
37	3
38	4
39	3
40	3
41	3
42	3
43	3
44	3
67	2
68	2
69	2
76	2

Rockwell B hardness measurements were also taken on each sample (Table 1).

Analytical Chemistry (Table 2)

The analytical chemistry was done by the following techniques:

C	LECO - Combustion - IR Detection
S	(IR Infra-Red)
O	LECO - High Temperature Fusion - Thermal Conductometric
N	(LECO is a trade name)
Cr	
Mo	
Si	Emission Spectrometer
Cu	
Ni	
Mn	
P	
As	Phosphor-Molybdate Technique
Sn	
Sb	

The latter four tramp elements were evaluated at Westinghouse Research Center and the rest were evaluated at Lukens Steel Research.

It should be noted that the tables give three significant figures, whereas in fact, the error in most is such that only two significant figures are warranted.

Specifically the claimed precision is as follows (ppm means parts per million):

Element	Precision	Element	Precision
C	± .002%	Cu	± .01%
S	± 3 ppm	Ni	± .01%
O	± 5 ppm	Mn	± .01%
N	± 3 ppm	As	± 10%
Cr	± .05%	Sb	± 5%
Mo	± .08%	Sn	± 5%
Si	± .01%	P	± 5 ppm or better

Also it should be noted that the analyses for samples 12, 13 and 14 showed a significant variation in Mn as follows:

Sample	Mn (site A)	Mn (site B)
12	.67	.42
13	.59	.39
14	.53	.37

The quoted values of Mn in the tables are the average of the above estimates:

Charpy Impact Data (Table 3)

The data generated for this report stemmed from two sources: (1) Westinghouse Research on Samples not hitherto evaluated and (2) samples evaluated at the various suppliers' laboratories. In order to reduce the total scope and expense of the program, the data supplied by various sources was accepted and the remaining data generated at Westinghouse Research Center. Since the standard step-cooled embrittlement treatment, termed the SOCAL step-cooled embrittlement, has been used in the API industry, viz:

1100°F — 1 hr	Cool at 10°F/hr
1000°F — 15 hr	Cool at 10°F/hr
975°F — 24 hr	Cool at 10°F/hr
925°F — 60 hr	Cool at 5°F/hr
865°F — 100 hr	Cool at 50°F/hr to
600°F — air cool	

This embrittlement treatment was used throughout the series.

Discussion of Phase I Data

An attempt to fit an equation to the data generated in Phase I was carried out using regression analysis techniques. Unfortunately, the distribution of elements, grain sizes and strength levels among the set was such that no specific major trend or coefficients associated

with each variable could be found. At first sight this is surprising, since there appears to be a sufficient range of each variable within the number of samples taken. However, a statistically designed experiment for 14 elements plus grain size and strength, i.e. 16 variables would require considerably more than the 65 samples available. Moreover, the variables would be arranged according to the design rather than taken at random. Consequently, it was not possible to find a fitted equation to the Phase I data for two reasons, viz. insufficient data and unfortunate organization of the variables. The correlation between the often employed "J-factor" and ΔT (40), shown in Fig. 4 (a), is relatively poor for both plate and weld metal.

The data can, however, be expressed in the form of the histograms and a few useful observations made. The histograms are shown in Figures 5 through 18. The upper histogram in each of these figures represents all the weld and plate and forged samples, whereas the weld metal contribution alone is represented by the hatched areas within the total histogram. The dashed curves are an approximation to the shape of the histogram for the plate and forged samples and similarly the solid curve represents the welds. Thus, a comparison of weld and plate plus forged sample characteristics can be made within each histogram.

There is a question of how well the histograms represent the Cr-Mo A387 steels. The samples were drawn from many sources, some of which were from actual pressure vessels and others from heats or weldments produced to simulate the normal vessel steels. A few of the samples were included in the program because they were "interesting" in that they had anomalously high temper embrittlement fracture appearance transition temperature ($FATT_E$) or represented some extreme in composition. These samples might put a bias on the accumulated data and hence in this respect the histograms may not truly represent the class of steel. However, there are sufficient samples that the histograms should give a reasonable approximation to the normal characteristics.

Figures 5, 6 and 7 show the FATT data. The $FATT_U$ (unembrittled) and $FATT_E$ (embrittled) show that as a class the weld have a higher FATT than the plate and forgings. Both $FATT_E$ and $\Delta FATT$, due to temper embrittlement, reveal that certain 2 1/4 Cr - 1Mo submerged arc weldments (2 SAW) have poorer embrittlement characteristics than the rest. Overall, one can conclude that weld may be more prone to embrittlement and may have a higher unembrittled $FATT_U$ than the plate and forged material.

Figures 8 through 17 show the distribution of most of the elements in the steels. Figures 8, 9 and 10 show significant differences between the weld metal and plate and forgings for C, Mn and Si. In general, higher levels of Mn and Si lead to higher FATT values in the presence of P. [4,5,6]

With regard to the tramp elements, P, Sn, As and Sb, Figures 11 through 14, little difference is found between weld metal and plate for P and As, whereas plate and forgings exhibit a higher content of Sn and Sb. A secondary high peak in P is associated with 2 SAW samples. This again confirms the secondary high ΔFATT peak in Figure 7 for 2 SAW materials. (See page 8 for sample numbers)

The histogram for S does not indicate a specific trend, whereas the histograms for N and O, Figures 16 and 17, show very much higher concentrations of these elements for the welds. It is interesting to note that the electroslag weld (ESW) samples exhibit the lowest oxygen content of the weld class. The role of these two elements on temper embrittlement is not known.

The J embrittlement factor $(Mn + Si) \times (P + Sn) \times 10^4$ does not show a strong difference between plate and weld metal, even though it is not intended to be used for welds. Interestingly, the ESW samples all fall in the 50-100 range. If they were taken out of the weld set, then the weld metal would show a greater population at 200 to 250 compared with 100 to 150 for the plate and forgings (Figure 18).

Even though the histograms show reasonable correlations between the FATT data and compositions, especially Mn, Si and P and C, any interpretation of the trends must be treated with caution. Simple plots of $FATT_U$, $FATT_E$ or FATT versus any <u>one</u> of the compositional elements or the J embrittlement factor show no specific trend whatsoever. This observation only confirms the fact that the expression for FATT in terms of composition is a complex function which represents the multiple interactions of the primary alloying elements and the tramp elements.

IV. PHASE II: ISOTHERMAL EMBRITTLEMENT EXPERIMENTS

The primary objective in Phase II was to characterize the isothermal embrittlement of 25 selected steels and to ultimately compare this data with the step-cooled embrittlement data of Phase I. The isothermal embrittlement matrix was as follows:

Temperature (°F)		Time (hr)
650		1,000
725		
800	X	10,000
875		
950		20,000

The samples were selected on the basis of

i) Material availability
ii) Extremes in step-cooled embrittlement
iii) Extremes in compositional elements
iv) Structure and strength level

The primary data gathered was the 40 ft-lb TT and FATT. Wherever possible an indication of the upper shelf value was also obtained. The basic data gathered is given in Tables 4 through 12.

Figures 19 through 43 show the 40 ft-lb TT and FATT plotted as a function of the isothermal embrittlement temperature for 1,000, 10,000 and 20,000 hr. For reference, the unembrittled (U) and step-cooled embrittled (E) transition temperatures are indicated by bench marks in the same figures. Samples tested with Phase II orientation are indicated with an asterisk in Table 3. Further data is given in Table 16 where the effect of specimen orientation is shown. The supplied data for sample 26 (Table 3) was probably incorrect and the bench mark U represents an independent test. Where U and E data for the Phase II specimen orientation were not available, Phase I data adjusted according to the relationship given in Section VI below were used.

For the samples which exhibit distinct embrittlement (or increase in the transition temperature), the maximum effect is in the range 800°F to 950°F. (See Figures 19 to 43)

Histograms of the 40 ft-lb TT in the unembrittled and step-cooled embrittled conditions are compared with the maximum embrittlement

after 1,000 and 20,000 hr isothermal embrittlement in Fig. 44. These histograms give a clear indication of the general trend of embrittlement after long term isothermal exposure.

V. THE EFFECT OF DE-EMBRITTLEMENT

Samples received from various sources had received a number of different heat treatments including a range of post-weld heat treatments (PWHT). In Phase I these samples were tested in the "as-received" condition which was termed the "unembrittled" condition. The Fracture Appearance Transition Temperature for this condition was abbreviated to $FATT_U$, where the subscript U designates "unembrittled." In fact, due to the slow cooling through the temper embrittlement range, various degrees of temper embrittlement might well have been experienced by each sample in this condition. The same samples were subjected to the SOCAL Step-Cooled Temper Embrittlement treatment and given the designation E. (See page 11)

It was thought that the possible correlations between sample characteristics (structure, yield strength and composition) and the degree of temper embrittlement would be better revealed by comparison of the E condition with samples in a de-embrittled condition. Samples were de-embrittled by heat treating at 1100°F for 2 hr and water quenching. This condition is given the designation D. Thus, a number of samples have been tested in three conditions.

U - Unknown degree of embrittlement or as-received
E - Step-cooled embrittlement from condition U
D - De-embrittled condition from condition U

In Phase I, ΔFATT was defined as $FATT_E - FATT_U$ and similarly the change in the 40 ft-lb TT was $\Delta T(40) = T(40)_E - T(40)_U$.

The data from Phase I and the current tests are given in Tables 13, 14 and 15.

Since the U condition might be slightly temper embrittled, one should expect the $FATT_U$ and $T(40)_U$ to be greater than $FATT_D$ and $T(40)_D$ and less than $FATT_E$ and $T(40)_E$, respectively. Inspection of Tables 13 and 14 shows that in general this is not the case.

In order to explore the reason for the many discrepancies in the data, the curves of the D, U and E condition were compared. In nearly every instance, the upper shelf of D > U > E as is also obvious from Table 15. Thus on embrittlement the curves are definitely changed in the upper shelf or 100% ductile region. Also the gradient of the Charpy curves becomes less steep with embrittlement.

Data similar to the above was found for 3.5Ni-Cr-Mo-V rotor steel by Dr. J. Watanabe. [6] He pointed out that intergranular fracture extends to lower temperatures as the degree of temper embrittlement increased. It is reasonable to suggest that the introduction of an extra mode of fracture, i.e., intergranular fracture by temper embrittlement, serves also to change the gradients of the Charpy curves. A. S. Tetelman and A. J. McEvily, Jr. [7] point out that the Charpy curve gradient is difficult to define and depends strongly on microstructural variables. They state that in general a process which lowers the upper shelf value will tend to broaden out the 100% ductile-to-brittle range (or change the Charpy curve slope to a lower gradient).

It follows from this study that the relationship between the (D) and (U) condition is far from simple. Consequently a clarification of the ambiguity in the data caused by variable degrees of embrittlement stemming from a range of cooling rates is not possible.

VI. THE EFFECT OF SPECIMEN NOTCH ORIENTATION

The two specimen notch orientations used in this program are shown in Figure 45. In Phase I of the program, the orientation of the notch was parallel to the plate or weld surface, designated L-S and T-S, respectively, whereas in Phase II the notch was perpendicular to the surface, L-T and T-L, respectively.

In order to compare Phase I and Phase II data, a comparative study was carried out on a few samples from which sufficient material was available. The data for the Phase II unembrittled (U) and step-cooled embrittled (E) condition was derived from only five specimens per Charpy curve. Some of the data was scattered to a point that estimates of transition temperature could only be made to ±50°F (Table 16). A plot of this data, in which the poorer estimates have been omitted, is shown in Figure 46. The error bands, represented by bars and circles, have been included in order to give a clear representation of the comparative experiment.

A least squares analysis of the data yielded the expression (in °F)

$$\text{(Phase I data)} = 0.96\ \text{(Phase II data)} - 10.5 \qquad \text{Eq. (1)}$$

with a standard deviation of 25.8 and a correlation coefficient, r = 0.92. (See page 20 for discussion of r)

By eye it would appear that

$$\text{(Phase I data)} = \text{(Phase II data)} - 10^{\circ}\text{F},\ \pm 25^{\circ}\text{F}. \qquad \text{Eq. (1a)}$$

Based upon this study, it is possible to adjust Phase I orientation data to that of Phase II by adding 10°F to the FATT or 40 ft-lb TT. In this way, where the direct measurements were not made, the step-cooled embrittlement data of Phase I can be compared with the isothermal embrittlement data of Phase II. Overall there is little change in the data due to the change in orientation shown in Figure 45.

VII. PREDICTION OF LONG-TERM ISOTHERMAL EMBRITTLEMENT

The prediction of long-term service embrittlement of pressure vessel steels is of considerable importance. Consequently various methods of assessing potential embrittlement have been employed; the main ones being the step-cooled embrittlement screening test and correlations with composition. The API program allows for the comparison of these correlations with isothermal embrittlement up to 20,000 hr.

There are two models (often referred to as embrittlement factors) in the literature which relate temper embrittlement to composition in 2 1/4 Cr - 1 Mo steels. The first by Bruscato,[4] primarily for weld metal, delineated high and low embrittlement areas on a two dimensional plot of (Mn + Si) and $\bar{X}$ = (10 P + 5 Sb + 4 Sn + As)/100. Recognizing that the iso-embrittlement curves in this plot are approximately hyperbolic, the embrittlement can be represented by a function of the form

$$\Delta TT = f_1 [\bar{X} (Mn + Si)]$$

where ΔTT stands for the shift in the transition temperature.

The second model, by Murakami, et al,[2] is primarily for plate material and is given by

$$\Delta TT = f_2 [(P + Sn) (Mn + Si) \times 10^4]$$

which is similar in form to that of Bruscato. The function f_2 is usually called the J-factor.

Two of the most commonly used predictive methods have been examined in this section: the SOCAL step-cooled embrittlement screening test and the J-factor.

There is greater scatter (or subjectivity) in the FATT data, therefore, the 40 ft-lb TT data has been used for the analysis. The basic data, extracted from previous tables, is given in Table 17. All of this data is for the Phase II orientation.

The values used for the unembrittled condition U are shown in Figures 19 to 43 (Section IV). The maximum amount of isothermal embrittlement, which usually occurred in the range 800-950°F, was used in the analysis. The equations derived therefore yield predictions for

an approximation to the maximum embrittlement found in the temper embrittlement range and not to a specific isothermal embrittlement temperature.

Since there is scatter in the 40 ft lb data, the best approach to the comparison of the isothermal embrittlement with the step-cooled or J-factor measurements is via a least-squares fitted equation. In the analysis of the differences between the two orientations above, it was noted that the standard deviation was about 25°F. In a study of differences between these measurements, the standard deviation should be 25 x $\sqrt{2}$ or approximately 36°F.

The regression analysis leads to a model or an expression relating the dependent variable (e.g., ΔFATT) to terms which are independent variables or combinations of the independent variables. For example, a quadratic model includes terms such as Mo, Cr^2, CCr, MnP, etc. One measure of the quality of the model is the correlation coefficient between the observation and the model prediction, signified by r, which lies between 0 and 1. If $r < .5$, the model is usually considered to be quite poor, i.e., the predictions of the model are not closely representative of the observations. As r approaches 1, the predictions are close to the observations. However, the number of terms included in the model should be significantly less than the number of observations to ensure that the model is meaningful.

The regression analyses yielded the following equations:

Fitted Equation (°F)	Correlation Coefficient	Standard Deviation (°F)
$\Delta T(40)_{E-U} = -1.7 + .72\Delta T(40)_{1,000-U}$	.57	34
$\Delta T(40)_{E-U} = .34 + .50\Delta T(40)_{10,000-U}$	.57	34
$\Delta T(40)_{E-U} = -1.5 + .44\Delta T(40)_{20,000-U}$	.57	34
$J = 142 + .80\Delta T(40)_{1,000-U}$	.39	57
$J = 131 + .70\Delta T(40)_{10,000-U}$	.52	54
$J = 145 + .45\Delta T(40)_{20,000-U}$	.35	58
$J = 148 + .9\Delta T(40)_{E-U}$	.62	48

where the notation $\Delta T(40)_{E-U}$ stands for the change in the transition temperature in the unembrittled condition, U to the step-cooled embrittled condition, E, etc. See Key for Abbreviations and Symbols, page iii.

As bad as these fitted equations are, it can be seen that overall $\Delta T(40)_{E-U}$ has a greater correlation with the isothermal embrittlement than the J-factor, and that the standard deviation is in the range that would be expected for this quality of data.

Looking at these expressions in a simplified form, we have approximately

(1,000 hr isothermal embrittlement) = 1.4 (Step-Cooled Embrittlement)

(10,000 hr isothermal embrittlement) = 2 (Step-Cooled Embrittlement)

(20,000 hr isothermal embrittlement) = 2.3 (Step-Cooled Embrittlement)

Eq. (2)

It can be seen that the coefficient increases with time, as would be expected. Also the step-cooled embrittlement is (on the average, as represented by this method) less than the isothermal embrittlement.

A least-squares fitted equation to the coefficients versus log (isothermal embrittlement time) yielded

log (isothermal embrittlement time) = .91 + 1.5 (Coefficient) Eq. (3)

with a standard deviation of .066
and a correlation coefficient = .995

It follows then that very approximately the isothermal embrittlement after time t hr can be expressed by

$$I(t) = .67\ (\log_{10}(t) - .91) \times (S.C.E.) \qquad \text{Eq. (4)}$$

where I(t) stands for isothermal embrittlement and S.C.E. stands for the step-cooled embrittlement.

Interestingly, the time required for the isothermal embrittlement to equal the step-cooled embrittlement, from Eq. (4), is approximately 250 hr. This is roughly comparable with the total embrittlement time (200 hr) used in the step-cooled embrittlement procedure. Equation 4 also leads to the conclusion that 30 years of in-service embrittlement is about equal to three times the step-cooled embrittlement.

VIII. THE EFFECT OF REPEATED DE-EMBRITTLEMENT ON ISOTHERMAL EMBRITTLEMENT AT 875°F

The selected samples, nos. 18 and 38, were exposed to a series of thermal cycles and a blank of each steel taken for testing at each stage. The thermal cycles, the Fracture Appearance Transition Temperature (FATT) and 40 ft-lb Transition Temperatures (40 ft-lb TT) associated with each stage are given in Table 18.

The FATT and the 40 ft-lb TT were the same for each steel after the de-embrittlement stage (1 and 4 in Table 18). Similarly the transition temperatures after 1000-hr isothermal embrittlement at 875°F were the same (stages 2 and 7 in Table 18). After 5000-hr isothermal embrittlement sample 38 had not changed significantly from the 1000-hr stage. However, sample 28, after 5000 hr, showed an increase from the 1000-hr transition temperatures after the second de-embrittlement stage and a reduction after the third de-embrittlement stage. It is implied therefore that temper embrittlement is reversible and that the embrittlement is due to the diffusion of the tramp elements (P, Sn, Sb, As). The possibility of irreversible temper embrittlement by (irreversible) carbide precipitation may have been precluded by the PWHT of these samples which was

1100°F for 8 hr +
1200°F for 15 hr +
1275°F for 7 hr +
Cool at 50°F per hour.

IX. THE EFFECT OF STRENGTH LEVEL AND STRUCTURE ON TEMPER EMBRITTLEMENT

Heat Treatment and Structures

This section of the API contract required that three structures, viz. martensite (M), bainite (B), and ferrite-pearlite (F-P) be tempered from one sample to the same strength level, and that one structure, bainite, be tempered to three strength levels. Figure 47 shows the continuous cooling transformation diagram for an A387D steel with a composition very similar to that of sample 75, which was assigned to this study.[8]

It was relatively difficult to produce the three structures at the same strength level. Whereas the M or B structure could be tempered down to a minimum strength level corresponding to Rockwell B (R_B) of 87, the F-P structure was always in the R_B range of 78-87. The higher strength level corresponds to a short time, two hours, at 1200°F. Figure 47 shows that this is sufficient time to cross the F+C transformation curve and the metallographic section shown in Figure 48 confirms that the F-P structure was formed. The samples were water quenched from 1200°F to give the equivalent to a de-embrittled F-P condition. Slow cooling through the range 1100°F to 600°F could, of course, lead to a small degree of temper embrittlement.

The transformation diagram indicates that bainite is formed at all quenching rates. In order to form martensite, the blanks (0.5 x 2 x 4.5 in.) were quenched from the austenitizing temperature of 1700°F into stirred water. The percentage of bainite formed in this process should be quite small but has not been determined. There is little difference between the metallographic sections of what will be referred to as the "quenched bainite-martensite" (QBM) and the bainite (Figure 49).

The bainite structure was formed by forced air cooling the sample from 1700°F to 950°F and holding at 950°F for one hour (3.6×10^3s) at which point the transformation is complete. The cooling rate was arranged in such a way that the sample surface remained above 950°F (i.e., above the M_s temperature of 869°F) while the center of the sample cooled to 950°F fast enough not to form ferrite. After 67 hr at 1275°, the bainite structure had the same strength level, $R_B = 87$, as it had after 24 hr. This appears to be the lower strength level for this particular sample with a bainitic structure and, coincidently, it is exactly the same as the starting condition. It was, therefore, decided to use the "as-received" material for the lower strength bainitic sample. A $R_B = 98$ was obtained by tempering at 1275°F for 4 hr. The

upper strength level was obtained by using the material in an untempered condition (R_B = 108).

The high and low strength bainite samples were de-embrittled prior to testing. Thus all the samples were in a de-embrittled starting condition. Table 19 gives the complete heat treatments.

Three specimen blanks in each of the five conditions were placed in a furnace at 875°F, the temperature designated as T_{MAX} earlier program. The three blanks were isothermally temper embrittled for 1,000, 10,000 and 20,000 hr.

Isothermal Embrittlement Results and Discussion

The basic Charpy impact test data for the isothermal embrittlement of the five samples for the de-embrittled, 1,000, 10,000 and 20,000 hr isothermal embrittlement conditions are given in Table 20. The 40 ft-lb TT for the five samples is shown as a function of isothermal embrittlement time in Figure 50. The trends of the FATT for these samples are similar to those shown in Fig. 50.

The effect of strength level in the bainitic structure is reasonably clear after 20,000 hr isothermal embrittlement. The lower the strength level, the lower the FATT. However, the embrittlement characteristics as a function of time are a little more complex. The highest strength level B(108), which is a re-austenitized and untempered steel, continuously de-embrittles. The intermediate strength level steel B(98) appears at first to be superior to the lowest strength level steel B(87). Both steels embrittle with time but the lower strength steel relatively less than the intermediate. If one takes into consideration the maximum scatter band, it can be seen that there is not necessarily a great difference between B(87) and B(98).

The effect of structure at the one strength level (Rockwell B Hardness of 87) can also be clearly seen in Fig. 50. The ferrite-pearlite structure, FP(87), has a transition temperature over 150°F greater than the other two in the de-embrittled condition. It de-embrittles slightly but in reality changes very little after 1000-hr isothermal embrittlement. In contrast the quenched structure representing martensite, QBM(87), starts at a relatively very low de-embrittled condition but continuously embrittles with time to almost the same level as the FP(87) sample. The embrittlement characteristics of QBM(87) are almost identical to those of B(98).

The conclusions from the structure study are that for sample 75 the ferrite-pearlite structure has a greater transition temperature than either the martensitic or bainitic structures. After 20,000-hr isothermal embrittlement, the martensitic structure has a transition temperature comparable with that of ferrite-pearlite and slightly higher than that of bainite. It is possible that samples with a different chemistry may exhibit different degrees of embrittlement for each structure.

X. THE SEGREGATION OF ELEMENTS TO GRAIN BOUNDARIES IN Cr-Mo STEELS AFTER 20,000 HR ISOTHERMAL EMBRITTLEMENT ASSESSED BY AUGER ANALYSIS

Selection of Samples for AES Study

In order to select the samples for the Auger Electron Spectroscopic (AES) study of grain boundary segregation, it was necessary to determine which samples had an intergranular fracture mode (IG) as opposed to cleavage or dimpled rupture modes (CL and DM). Based on the fractographic study, see Appendix Section (b), candidate samples were chosen and Auger specimens were machined from broken Charpy specimens. The list of the samples and the analytical chemistries is given in Table 21.

Experimental Results

The experimental procedure used was identical to that described by Joshi and Stein.[9] Specimens were broken in a vacuum of 10^{-9} to 10^{-10} torr and a surface analysis was carried out* using a 5 μm diameter beam. The beam position on the fracture surface was adjusted to give a maximum reading in P, thus indicating a grain boundary position. The profile of the concentration of elements adjacent to the surface was obtained by removing the surface material by ion sputtering. The analyses were carried out at depths of 25, 50, 100, 200, 400, 800 and 1600Å from the original fracture surfaces.

The first set of seven samples were broken at room temperature since their FATT was at or above this temperature. Post-mortem scanning electron microscope (SEM)† evaluations revealed that all the samples fractured at RT had DM mode except No. 56, which had IG. The FATT for No. 56 was 225°F. The DM fracture surfaces all had a very small P segregation. Detailed SEM evaluation of these fracture surfaces revealed very small areas of intergranular fracture, thus accounting for the observation. The second series of six specimens was broken at about 0°F by using a cooling stage on the AES. Two of the samples, No. 27 and No. 37, still had DM fracture mode and the remainder failed by IG. Consequently, five complete sets of data were obtained. Since No. 56 had a very high level of As (243 ppm), a second run was carried out

*Physical Electronics AES No. 545 modified.
†Cambridge Stereoscan 150, MK2 (1978).

on this sample specifically to evaluate the possibility of As on the grain boundary. It was concluded that As was not present, at least within the resolution of the AES used, which for As is approximately 1.0 wt %.

The grain boundary concentrations for Mo, Cr, Fe, C, Cu and P for each of the five samples are shown in Figs. 51 to 55. The maximum levels of the elements at or adjacent to the grain boundary are given in Table 22. Profiles of the grain boundary concentrations of Ni and Sn were not drawn because most of the data were on the limit of resolution in the experiment. The elements S, O and N could be detected but they revealed no particular trend. Sulfur and oxygen are normally found on a fracture surface after ion sputtering, not necessarily as an element in the steel but rather as a surface environmental contaminant. Similarly, the level of carbon often increases due to readsorption. Manganese and silicon were below the limit of resolution of the AES.

The fracture surfaces of the broken Auger specimens were inspected on a SEM and all found to contain intergranular facets.

Interpretation of the Data

Figures 51 through 55 show the primary concentration profiles of elements found on the grain boundaries. In each of the five samples for which data was obtained, there was a very distinct peak of P in the range of 3 to 4 wt %. In each instance, the phosphorus level fell very rapidly from the grain boundary to 25 angstrom from the surface. This indicates that the phosphorus segregates to form a very thin film on the grain boundaries. Phosphorus is well known to be the primary embrittling element in temper embrittlement of Cr-Mo steels.

The limit of resolution of Cu is approximately 1 wt % and any reading below this level should be regarded as quasi-qualitative. Specimen No. 56 shows a very clear Cu peak (2 wt %) which drops to low (qualitative) values within 200Å from the surface. Since the presence of Cu on the grain boundary in this specimen is unambiguous, the profile was drawn in Fig. 54. The response from Cu can be seen in Fig. 56. For this reason the profile obtained for the remaining specimens were drawn, since the qualitative data appeared to conform with the data from No. 56. Sample No. 63 shows no segregation of the Cu. This is quite consistent with the level of Cu in this sample (0.02 wt %) being somewhat lower than the rest (0.1 to 0.21 wt %). There is no clear correlation between the amount of Cu segregation and the wt % of Cu in the steel (Tables 21 and 22).

The levels of C, Cr and Mo at the grain boundaries or adjacent to the boundaries are all high compared with the bulk composition. Undoubtedly, carbides on the grain boundary may account for the high C level up to 1600Å from the surface.

Segregation of Ni is clear in Sample No. 56 which has the highest Ni content of the set (.23 wt %). The grain boundary concentration of Ni in Samples 20, 26 and 43 is quasi-qualitative and the lack of Ni on the GB in Sample 63 is consistent with the low Ni level (.06 wt %). Similarly, the segregation of Sn in Sample 56 is clear, whereas the data for Samples 26 and 43 is quasi-qualitative.

Discussion of Results

The segreation of P to the grain boundaries is normally associated with temper embrittlement. However, segregation of Cu is not commonly found. A concentration of 1 wt % Cu on the grain boundaries is greater than the solid solubility of Cu in iron or steels. The maximum solubility at room temperature is ~0.35 wt %.[10] Consequently, the Cu is probably present on the grain boundaries in the form of small Cu-rich precipitates. The role of Cu in embrittlement of steels[11] has been of considerable concern in nuclear vessels where embrittlement of the steel after irradiation damage has been associated with higher levels of Cu (~0.4 wt % Cu) as well as P. It is reported that 4.2 wt % Cu in 2.25Cr - 1Mo - 0.2Si - 0.1C weld steel caused a shift of 535°F in the transition temperature (after irradiation at 550°F). Interestingly, the Auger analysis of steels embrittled this way showed no Cu on the fracture surfaces. The embrittlement was thought to be due to the combination of radiation and Cu solute-defect aggregate hardening.

More recent research by Takaku et al.[12] demonstrated that the addition of Cu to Fe-induced intergranular fracture after irradiation but they could not detect Cu on the grain boundaries using an electron microprobe. Pope et al.[13] in an investigation of an SA533-B steel, found Cu on the intergranular fracture surface after a stress relief treatment at 1135°F for 6 hr. They comment that Cu is not normally associated with embrittlement in steels.

The same report[13] noted that in the AES work, As was not found on the grain boundaries even though the As level was ~650 ppm. They suggested that the other segregating elements (P, Sn, Sb, S, N, etc.) may have occupied the available segregation sites and therefore precluded As. The maximum level of As in the set testing in the API study was ~250 ppm.

The presence of Sn on the grain boundaries coincides with the observed segregation of Ni, which is also consistent with the level of Ni in each sample. Tin has been regarded as an embrittling element in Ni-Cr-Mo-V rotor steels,[14] whereas Yu and McMahon[15] found that Sn did not (alone) embrittle the Cr-Mo steels used in their study. Significantly, the steels used in the latter study had no Ni. In a study of Ni-Cr-Mo-V steel,[16] based upon a statistical design, it was found that the expression for the shift in the transition temperature after temper embrittlement included significant terms in Ni x Sn and P x Sn.

Consequently, it may be implied that either high P or high Ni are necessary to bring about embrittlement by Sn. The data generated in the API study are consistent with the significance of the Ni x Sn interaction, but there are too many variables available to clearly demonstrate this point.

The high carbon level adjacent to the grain boundaries is associated with GB carbides. The high level of Mo may be associated with the formation of Mo-rich carbides[17] at the temper embrittlement temperature or due to Mo segregation. Similarly, the Cr at the grain boundaries can be associated with carbides or with the result of segregation. Without a careful analysis of the carbides, the effects cannot be readily separated.

XI. FRACTURE TOUGHNESS EVALUATION (J_{IC}) OF UNEMBRITTLED AND ISOTHERMALLY EMBRITTLED SAMPLE NO. 75

Introduction

As part of the API program on temper embrittlement, a comparison between the upper shelf toughness behavior of unembrittled and temper embrittled 2 1/4 Cr - 1Mo steel is being made. Whereas the original intention was to use a steel highly susceptible to temper embrittlement, in fact no sample with this characteristic was large enough to make twelve compact tension specimens. Amongst the large plate and forged steel samples available, No. 75 was selected. It had a shift in transition ΔFATT of (55°F) and ΔT (40) of (80°F) after step-cooled embrittlement. (Table 3).

From this plate sample twelve blanks for 2T compact tension specimens were cut. Six of the blanks were tested in the "as-received" condition and the remaining six placed in a furnace at 875°F (468°C) for 20,000-hr. isothermal embrittlement.

Experimental Background

The tensile properties, hardness, chemistry and step-cooled temper embrittlement properties, etc. for Sample No. 75, are listed in Tables 1, 2 and Table 3. Since this sample had a low yield strength (~60 ksi), the largest possible compact tension specimens (2T) were made from the available material in order to give the greatest probability of obtaining valid data. Also due to the extreme ductility of this material it was necessary to use a J_{Ic} testing procedure in order to determine the toughness. The recommended methods for J_{Ic} testing were released recently, consequently this was an opportune time to test the material according to the procedures which are outlined in the proposed standard.[18]

A single specimen J_{Ic} procedure using the unloading compliance technique was used to determine the J_{Ic} value at a 50°F to 300°F in 50°F intervals. The specimens were heated with heater tapes and the temperature controlled to within ±4°F. The load and displacement data was fed into a Westinghouse 2500 computer via a 12-bit data acquisition system. The values of both J and crack extension, a, were calculated by a data reduction program described in a paper by Clarke and Brown.[19] The initial test at 100°F was taken to an arbitrary displacement value of 5.10 mm in the hope that sufficient crack extension would occur.

However, only crack extension values defined as crack tip blunting occurred at this displacement. The remainder of the tests were loaded in order to develop displacements up to 12.7 mm. The test results are shown in Table 23. The values of J and Δa for the various temperatures tested can be seen in Figure 57.

Discussion

From Figure 57 it can be seen that at 50°F and 150°F the value of J_{Ic} is at some value greater than 1500 kJ/m^2. This high value of J_{Ic} results in apparent crack extensions due to crack tip blunting of at least 15 mm prior to the intersection of the R-line and the blunting line. The recommended J_{Ic} procedure was designed to test materials with less blunting than developed at these two temperatures. The values of J_{Ic} for the tests at 350°F, 250°F and 200°F are 700, 927 and 1050 kJ/m^2, respectively. While the test data at 100°F is not sufficient to determine the value of J_{Ic}, it is reasonable to assume the value is also greater than 1500 kJ/m^2.

Since the J_{Ic} values are in doubt below 200°F, a plot of the load displacement curves normalized to the remaining ligament was generated (Figure 58).

The curves generated for the same steel after an isothermal embrittlement treatment of 20,000 hr. at 985°F were identical to those of the unembrittled condition. This probably reflects the fact that the transition temperature is comparable with or below 50°F, the lowest temperature used in J_{Ic} evaluations.

An approximate estimate of a value of K_{Ic} may be obtained from the expression

$$K_{Ic} = \left[\frac{E\ J_{Ic}}{(1-\nu^2)}\right]^{1/2}$$

where F is Young's modulus and ν is Poisson's ratio.

Conclusions

The high ductility and toughness of this material resulted in extreme crack tip blunting prior to stable crack growth. The toughness of the material at temperatures below 200°F could not be determined using the procedure as outlined by the ASTM recommended practice for J_{Ic} determination. After 20,000-hr. isothermal embrittlement at 875°F, the toughness was the same as measured prior to embrittlement.

XII. A STUDY OF THE EFFECT OF HIGH PRESSURE HYDROGEN ON THE TEMPER EMBRITTLEMENT CHARACTERISTICS OF Cr-Mo STEELS

Background

In 1979 a small "add-on" program was incorporated into the API Temper Embrittlement study. The program was designed to establish the effect of high pressure hydrogen at temper embrittlement temperatures (650 and 875°F) on the known temper embrittlement characteristics of steels embrittled in air. Some of the data were so unusual that the API Committee on Temper Embrittlement requested further research to confirm the observed effects. The additional tasks, analytical chemistry, metallography, carbide morphology evaluations and fractography served to clarify to some extent the reason for the extreme embrittlement of one of the samples.

Experimental Background

From the inventory of remaining samples, three were selected for this study. These were sample nos. 46, 56 and 59. At the 10,000 hr. isothermal embrittlement stage in air, no. 46 showed no temper embrittlement, 56 the greatest amount of embrittlement (a shift in the transition temperature of 200°F) and 59 an intermediate degree of embrittlement of about 50°F.

Sixteen Charpy specimens were machined from each of the 3 selected steel samples. Eight specimens from each sample were placed in an autoclave at 650°F and the remainder in an autoclave at 875°F. The hydrogen pressure in the autoclaves was maintained at 3,500 psig. After 1,000 hr. exposure the specimens were taken out and tested in a Charpy impact machine. The data generated was then compared with similar data from Phase II of the program for specimens embrittled in air for 1,000 hr. (Section IV).

Experimental Results and Discussion

(a) Initial Experiments

The Charpy impact curve data from the hydrogen-environment tests is given in Table 24, along with data previously obtained for specimens isothermally embrittled in air. The data recorded in Table 24 gives an

estimate of the upper shelf value or, alternatively, if the upper shelf is not obtained, the greatest impact energy observed (indicated by >).

Based upon these considerations the data is analyzed as follows.

No. 46 (Ferrite-Pearlite Structure). This sample exhibits little or no temper embrittlement in air over the range 650 to 950°F. The 650°F hydrogen-environment data indicates a slight degree of embrittlement, relative to the air data, but the shift in the 40 ft-lb TT is barely significant. The 875°F hydrogen-environment exposure resulted in a radical change in properties. The FATT increased by 50°F and the upper shelf was reduced from 240 ft-lb to 25 ft-lb. Comparison of the 40 ft-lb TT was therefore not possible (see Figure 59).

No. 56 (Bainitic Structure). This sample has the greatest shift in FATT (ΔFATT) of the series selected for Phase II of the program. After 1,000 hr isothermal exposure in air the shift in the transition temperatures was approximately 100°F. After 1,000 hr. in the hydrogen-environment at 650°F a significant increase in the transition temperature was found whereas, paradoxically, at 875°F the shift in FATT was relatively less than that resulting from exposure in air (see Figure 60).

No. 59 (Bainitic Structure). The 1,000 hr. exposure to the hydrogen-environment and air at both 650 and 875°F resulted in essentially the same degree of embrittlement (see Figure 61).

(b) Further Research

Since the results of the hydrogen-environment embrittlement tests were so inconsistent, especially for sample 46, a few additional tasks were undertaken in an attempt to confirm the data. These tasks were:

(i) Compare analytical chemistry of samples taken from no. 46;

(ii) Compare hardness of specimens;

(iii) Compare metallographic sections of specimens from sample no. 46;

(iv) Compare carbide extraction replicas from specimens of sample no. 46;

(v) Examine fracture surface of sample no. 46 after environmental exposure.

(i) Analytical Chemistry of Specimens from Sample No. 46

The analytical chemistry of three specimens from no. 46 was very kindly provided by Mr. R. L. Brooks of Phoenix Steel. The chemical analysis was performed by standard spectographic analysis without any special procedures. The three specimens were from Charpy specimens which had been exposed to

875°F for 1,000 hr. in air (46/A47)
650°F for 1,000 hr. in H_2 (46/EN8)
875°F for 1,000 hr. in H_2 (46/EN16)

These chemistries are compared with data from an "as-received" or unexposed specimen obtained earlier in the program in Table 25. The agreement is very good and therefore the possibility of specimen identification error is unlikely.

(ii) Hardness Readings

Rockwell B hardness measurements were taken from specimens which had been exposed to the hydrogen-environment at 650 and 875°F for 1,000 hr. and compared with measurements from specimens in the "as-received" or unexposed condition and specimens exposed in air at 875°F for 1,000 hr. The data is presented in Table 26. Normally there is a degree of scatter (±1 to 2 points) in hardness measurements even though the hardness measurement machine is calibrated with standards whenever it is used. As a trend, based upon the hardness measurements, it appears that there is a slight hardening after the 875°F air exposure and the 650°F H_2 exposure and a softening of the steels after the 875°F H_2 exposure. The softening is particularly significant in the sample no. 46.

(iii) Metallography of Sample No. 46

Metallographic sections of specimens in the "as-received" condition, exposed to air for 1,000 hr. at 875°F and exposed to H_2 at 650 and 875°F, were prepared. Apart from the H_2-875°F specimen, the metallographs are essentially similar in appearance. The structure is ferrite-pearlite and the grain sizes are comparable. The H_2-875°F specimen has the same grain size as the other specimens, but the ferrite-pearlite structure has apparently been replaced by ferrite grains with large carbides on the grain boundaries. Since ferrite is normally softer than ferrite-pearlite, the change in hardness with the structure change is consistent. Comparison of the metallographs may be made from Figures 62 and 63.

(iv) Carbide Extraction Replicas from Sample No. 46

In order to obtain a better documentation of the changes in the structure of sample no. 46 after exposure to the high pressure environment at 875°F, carbide extraction replicas were prepared from the three

specimens A, B and C for which the analytical chemistry was carried out, viz.

A. 875°F for 1,000 hr. in air (46/A47)
B. 650°F for 1,000 hr. in H_2 (46/EN8)
C. 875°F for 1,000 hr. in H_2 (46/EN16)

Transmission Electron Microscope (TEM) examination of the replicas was carried out and a number of high magnification micrographs taken. A few of these are reproduced in this report for comparison. Figure 64 shows a relatively low magnification micrograph of each of the three specimens. The distribution of carbides in A and B are distinctly different to those in C. Enlargements of the structures, including the grain boundaries, are shown in Figure 65. Figure 65 shows the presence of acicular carbides, which were found to a lesser extent in the other two specimens. A comparison of acicular carbides at a higher magnification is shown in Figure 66. It is clear that these carbides have grown significantly in the 875°F hydrogen environment.

(v) Fractographic Examination of Samples After Environmental Exposure

Typical areas from the Scanning Electron Microscope (SEM) examination of the fracture surface of a Charpy specimen from sample no. 46 after 1,000 hr. at 875°F in 3,500 psig H_2 are shown in Figure 67. The lower magnification overview (X1500) shows a mixture of cleavage and intergranular fracture. The intergranular faces, seen in detail in the higher magnification (X5000), exhibit polyhedral voids. These voids are not typical of dimpled rupture since they do not have the symmetrical cup-cone configuration normally associated with this mode of failure.

After the same exposure sample no. 56 had a typical intergranular and cleavage fracture surface (Figure 68). The higher magnification picture of the intergranular face does not show any sign of void formation (or dimpled rupture). It is possible that micro-voids beyond the resolution of the SEM employed may exist. However, void formation of the size and type found in sample 46 was not present.

(c) Discussion and Conclusions

At first sight the results of the study appear to be contradictory since the steel that showed the least embrittlement in isothermal embrittlement in air (no. 46) had the most radical change in properties after exposure to high pressure hydrogen in an autoclave at 875°F. The metallography and the carbide extraction replica study of specimens from no. 46 revealed, however, that the carbides had changed radically after the 875°F/1,000 hr. hydrogen exposure. This is consistent with the change in R_B hardness (Table 26). The pearlite structure had dissolved and large clusters of carbides were formed on the grain boundaries. This observation coupled with the void formation on the grain boundaries

leads to the possible conclusion that the extreme changes in Charpy impact properties may be due primarily to grain boundary weakening (carbides and/or voids) caused by the effect of hydrogen. This cannot be explained within the limited work performed for this project.

XIII. ISOTHERMAL EMBRITTLEMENT OF 1-1/2Cr-1/2Mo AND 3Cr-1Mo SAMPLES AT 875°F

Three additional samples were assessed for isothermal embrittlement at 875°F. These were

Sample No.	Type	Key
52	1Cr-1/2Mo Plate	(1 PLA)
61	3Cr-1Mo Forging	(3 FOR)
66	3Cr-1Mo Shielded Metal Arc Weld	(3 SMA)

The only other specimens tested in Phase II in the 1Cr or 3Cr category were

4, 1Cr - 1/2Mo Submerged Arc Weld (1 SAW)
and 65, 3Cr - 1Mo Submerged Arc Weld (3 SAW)

for which the embrittlement data is reproduced above in Section IV.

The isothermal embrittlement data is given in Table 27. A comparison of the step-cooled embrittlement data $\Delta T(40)_{U-E}$ and the embrittlement due to isothermal embrittlement $\Delta T(40)_{(1000-U)}$, $\Delta T(40)_{(10,000-U)}$ and $\Delta T(40)_{(20,000-U)}$ is given in Table 28 along with the predicted data for isothermal embrittlement based upon Eqs. (5) given in Section VII.

The predicted isothermal embrittlements are reasonably good for the 3Cr-1Mo samples, 61 and 66, but poor for the 1,000 and 10,000 hr condition of the 1-1/4Cr-1/2Mo, sample 52. Here the term "reasonably good" means within the standard deviation of 35°F for the predictive equations developed in Section VII.

XIV. ACKNOWLEDGMENTS

It is my sincere desire to acknowledge the patient and kindly help in this large program of all members of the API Task Group on Temper Embrittlement:

R. L. Brooks
A. R. Ciuffreda
E. H. Edwards (Chairman)
J. J. Heller
G. B. Kohut
C. A. Robertson
J. W. Thomas

I have also been aided considerably in the following areas:

Specimen layout and organization: G. E. Parker, R. Burland

Metallography: G. E. Parker, R. Burland, G. A. Blann

Analytical Chemistry: L. E. Creasy (Lukens Steel)
J. Penkrot (Westinghouse R&D Center)

Charpy Testing: R. B. Hewlett, R. R. Hovan, G. A. Mullen, Jr.

Tensile Properties: J. J. Dufalla

Computer Tabulation: B. J. Taszarek

The 64 samples were provided by the following sources:

Amoco
Ashland
Chicago Bridge and Iron
Exxon
Gulf
Japan Steel Works
Lukens Steel
Socal
Sohio
Sun Oil
Texaco

XV. REFERENCES

1. E. H. Edwards, Private Communication (1981).

2. Y. Murakami, T. Nomura and J. Watanabe, May (1980), MPC/ASTM Symposium, Denver Colorado. Also published as Japan Steel Works Report No. Ac80-5-21.

3. J. Watanabe and Y. Murakami, "Prevention of Temper Embrittlement of CrMo Steel Vessels by Use of Low Si Forged Steels," to be published, API Spring Meeting, Chicago, May (1981).

4. R. Bruscato, Welding Journal, 49, 148-S (1970).

5. G. C. Gould, ASTM Publication STP 407, p. 59 (1967).

6. J. Watanabe, Private Communication to E. H. Edwards, July 17 (1975).

7. A. S. Tetelman and A. J. McEvily, Jr., "Fracture of Structural Materials," Wiley and Sons, New York, p. 325 (1966).

8. R. E. Lorentz, Jr., Welding Jnl., 41, p. 4405 (1962).

9. A. Joshi and D. F. Stein, "Temper Embrittlement of Low Alloy Steels," ASTM STP 499, 59 (1971).

10. "Copper in Cast Steel and Iron," Copper Development Association Publication No. 29, p. 37 (1937).

11. L. E. Steele, "Neutron Irradiation Embrittlement of Reactor Pressure Vessel Steels," Int. Atomic Energy Agency, Vienna, Report No. 163, p. 187 (1975).

12. H. Takaku, et al., Jnl. Nuc. Matls. 80, 57 (1979).

13. D. P. Pope, et al., "Elimination of Impurity-Induced Embrittlement in Steel," EPRI, NP-1501, September (1980).

14. D. L. Newhouse, et al., ASTM STP 499, 3 (1971).

15. J. Yu and C. J. McMahon, Jr., Met. Trans. 11A, 277 and 291 (1980).

16. B. J. Shaw, "A Temper Embrittlement Free Low Alloy Steel," U.S. Patent 3,954,454 (1976).

17. C. J. McMahon, Jr., Third International Conference on the Effect of Hydrogen Behavior of Materials, Jackson Lake (1980).

18. G. A. Clarke, W. R. Andrews, J. A. Begley, J. K. Donald, G. T. Embley, J. D. Landes, D. E. McCabe and J. H. Underwood, "A Procedure for the Determination of Ductile Fracture Toughness Values Using J Integral Techniques," Jnl. Testing and Eval., JTEVA, Vol. 7, No. 1, January (1979), pp. 49-56.

19. G. A. Clarke and G. M. Brown, "Computerized Methods for J_{Ic} Determination Using Unloading Compliance Techniques," presented at ASTM Symposium on Computer Automation of Material Testing, Philadelphia, PA, November (1978), to be published.

Table 1

Grain Size, Tensile Test Data and Rockwell B Hardness Measurements of Samples Evaluated in Phase I

Sample Number	Key	Grain Size		0.2% Yield	Ultimate Tensile Strength	Elongation	Reduction/ Area	Rockwell B
		ASTM Number	Structure[a]	ksi		Percent		
1	2 PLA	5.0	B	81.8	99.3	20.9	66.4	95.0
2	1 PLA	8.0	F	45.5	76.4	32.1	68.8	79.0
4	1 SAW	8.0	B	69.9	86.5	14.9	56.5	91.0
7	2 PLA	8.0	F	46.4	80.9	29.8	74.0	78.0
8	2 ESW	6.5	F	43.3	76.8	27.9	72.9	78.0
9	2 PLA	5.5	F	65.2	83.4	28.8	59.8	83.0
10	2 FOR	3.5	B	71.8	87.2	23.2	69.2	84.0
12	2 PLA	7.0	B	65.8	83.7	27.7	77.6	88.0
13	2 PLA	6.0	B	69.3	86.9	25.9	73.5	89.0
14	2 PLA	6.5	B	60.5	80.9	30.6	77.8	87.0
15	2 FOR	6.5	B	71.5	87.7	27.5	76.3	89.0
16	2 ESW	8.0	B	66.2	85.7	25.0	72.1	87.5
18	2 SAW	7.0	B					91.0
19	2 SAW	4.0	B					83.0
20	2 SAW	4.5	B					87.0
21	2 SAW	4.0	B					81.0
22	2 SAW	6.5	B					80.0
23	2 SAW	4.5	B					88.5
24	2 SAW	4.0	B					86.0
25	2 SAW	4.0	B					89.5
26	2 ESW	2.5	B					83.0
27	2 ESW	6.0	B					88.0
33	2 PLA	5.0	B	95.0	111.7	22.0	68.0	90.0
34	2 SAW	6.0	B	90.5	105.3	18.6	63.5	95.0
35	2 SAW	5.0	B	92.7	107.5	19.1	66.9	96.0
36	2 PLA	5.0	B	85.5	100.6	23.1	73.0	94.0
37	2 SAW	3.5	B	62.3	82.4	26.7	67.5	89.0
38	2 SAW	4.0	B	59.6	79.4	24.1	71.0	86.5
39	2 SAW	9.0	B	55.1	83.5	25.4	71.9	86.0
40	2 SAW	7.5	B	68.2	77.6	24.5	72.1	88.0
41	2 SAW	5.0	B	64.1	81.5	26.3	74.6	87.0
42	2 SAW	6.5	B	63.5	81.4	23.6	72.6	85.0
43	2 SAW	6.0	B	62.9	81.0	26.0	74.2	84.0
44	2 SAW	3.0	B	60.7	78.5	23.6	71.4	89.0
45	2 PLA	6.5	F	44.9	76.2	32.7	79.0	79.0
46	2 PLA	7.0	F	49.1	79.3	30.4	79.0	81.0
47	2 PLA	8.0	B	68.2	85.5	28.0	81.0	89.0
48	2 PLA	8.0	B	69.2	86.4	27.2	81.0	90.0
50	1 PLA	7.5	F	50.4	74.5	34.5	69.4	81.0
52	1 PLA	.0	F	50.9	77.1	33.8	69.9	82.0
54	2 PLA	8.0	B	71.8	91.4	28.9	75.4	89.0
55	2 PLA	7.0	B	73.5	82.1	30.3	78.1	84.0
56	2 FOR	5.5	B	65.0	87.7	27.1	75.0	85.5
57	2 FOR	4.5	B	67.4	86.8	27.5	79.1	85.0
58	2 FOR	5.0	B	63.3	82.9	29.0	79.2	83.5
59	2 FOR	6.0	B	61.5	82.1	28.1	80.8	86.0
60	1 PLA	7.5	B	66.7	85.9	28.5	75.5	83.5
61	3 FOR	5.5	B	64.3	85.4	27.3	78.1	87.5
62	2 SAW	5.5	B	77.6	92.6	33.7	70.8	90.0
63	2 SMA	5.0	B	77.1	91.9	24.4	73.7	88.0
64	3 PLA	8.0	B	58.1	80.6	31.8	78.7	82.0
65	3 SAW	6.0	B	64.0	82.1	27.3	71.6	87.0
66	3 SMA	7.0	B	63.6	87.2	28.4	69.1	83.5
67	2 SMA	6.5	B	63.0	80.4	57.4	70.2	87.0
68	2 SMA	5.0	B	68.0	83.6	54.4	72.1	88.5
69	2 SMA	4.5	B	63.1	80.3	54.6	73.3	88.5
70	2 PLA	5.0	B	62.4	79.7	26.3	72.5	84.0
71	2 PLA	5.0	B	63.4	82.4	27.2	71.0	87.5
72	2 PLA	5.5	B	63.9	82.4	29.1	76.7	86.5
74	2 PLA	4.0	B	60.4	78.8	30.2	79.1	83.5
75	2 PLA	5.0	B	60.4	83.8	31.2	74.5	87.0
76	2 PLA	7.0	B-F	53.0	77.2	56.5	74.6	81.0
77	1 FOR	6.5	F	41.7	75.6	32.3	70.5	78.5
78	2 FOR	8.0	F	45.6	77.8	30.3	72.6	80.0

[a] B — Bainite
F — Ferrite-Pearlite

Table 2 - Analytical Chemistries of Samples Evaluated in Phase I

	in Weight Percent							in Parts per Million							
Sample	C	Cr	Mo	Mn	Si	Ni	Cu	P	S	Sn	Sb	O	N	As	Key
1	.150	2.15	1.02	.42	.25	.18	.19	84.	211.	146.	29.	70.	99.	118.	2 PLA
2	.134	1.29	.47	.52	.59	.14	.13	100.	208.	230.	30.	32.	90.	80.	1 PLA
4	.046	1.17	.44	.91	.53	.12	.28	79.	139.	87.	16.	1187.	108.	63.	1 SAW
7	.139	2.20	1.00	.45	.26	.15	.16	100.	192.	140.	34.	16.	102.	108.	2 PLA
8	.121	2.27	.91	.47	.17	.24	.12	73.	126.	86.	17.	158.	121.	88.	2 ESW
9	.120	1.98	1.00	.44	.40	.12	.11	72.	104.	86.	13.	33.	129.	63.	2 PLA
10	.116	1.95	1.05	.39	.20	.08	.06	52.	129.	56.	13.	42.	109.	52.	2 FOR
12	.129	2.29	1.09	.53	.24	.16	.13	54.	160.	87.	17.	190.	139.	84.	2 PLA
13	.125	2.13	.98	.48	.22	.21	.11	74.	148.	118.	17.	185.	125.	62.	2 PLA
14	.133	2.25	.98	.45	.21	.17	.09	69.	154.	93.	12.	133.	108.	52.	2 PLA
15	.123	1.99	.92	.44	.35	.10	.08	120.	93.	57.	16.	28.	118.	54.	2 FOR
16	.140	2.11	.91	.61	.21	.15	.09	97.	130.	68.	38.	188.	129.	67.	2 ESW
18	.075	1.94	.87	.81	.51	.20	.13	48.	173.	135.	20.	758.	153.	118.	2 SAW
19	.070	2.35	1.10	.39	.24	.16	.05	124.	145.	58.	8.	266.	109.	66.	2 SAW
20	.121	1.97	.86	.52	.28	.13	.21	100.	121.	147.	20.	337.	123.	100.	2 SAW
21	.055	2.20	1.05	.62	.42	.14	.02	75.	188.	47.	6.	739.	167.	58.	2 SAW
22	.078	2.22	.90	.64	.39	.12	.02	79.	162.	62.	8.	760.	110.	50.	2 SAW
23	.081	1.89	.94	.82	.48	.14	.21	103.	145.	149.	19.	575.	126.	29.	2 SAW
24	.047	2.14	.85	.70	.47	.13	.05	175.	184.	63.	6.	769.	147.	139.	2 SAW
25	.095	1.92	.86	.81	.47	.14	.21	98.	160.	162.	19.	482.	119.	78.	2 SAW
26	.146	2.25	.93	.61	.25	.15	.10	91.	127.	188.	25.	144.	127.	47.	2 ESW
27	.168	2.22	.92	.59	.21	.13	.08	64.	135.	75.	15.	93.	121.	92.	2 ESW
33	.119	1.96	.98	.38	.31	.21	.21	78.	195.	172.	29.	178.	119.	88.	2 PLA
34	.078	2.01	.85	.84	.45	.23	.29	85.	165.	102.	21.	602.	149.	97.	2 SAW
35	.079	2.01	.91	.89	.45	.23	.34	103.	95.	86.	21.	564.	182.	71.	2 SAW
36	.107	2.09	.93	.34	.21	.29	.17	57.	187.	109.	24.	53.	72.	78.	2 PLA
37	.067	2.15	.77	.96	.54	.12	.02	118.	110.	43.	11.	653.	125.	34.	2 SAW
38	.072	2.21	1.20	.77	.44	.12	.02	110.	140.	39.	9.	932.	115.	31.	2 SAW
39	.053	2.40	.95	.73	.32	.12	.15	174.	107.	76.	19.	376.	122.	142.	2 SAW
40	.066	2.35	.90	.73	.28	.10	.12	139.	115.	78.	19.	452.	100.	150.	2 SAW
41	.056	2.26	.87	.72	.37	.10	.13	163.	93.	78.	19.	368.	125.	146.	2 SAW
42	.055	2.40	.91	.74	.31	.12	.14	162.	100.	68.	19.	474.	125.	113.	2 SAW
43	.058	2.41	.97	.67	.32	.10	.16	190.	77.	69.	21.	412.	137.	200.	2 SAW
44	.056	2.28	.81	.69	.38	.07	.13	167.	95.	83.	20.	394.	120.	213.	2 SAW
45	.108	2.25	.80	.44	.19	.17	.24	113.	32.	161.	30.	29.	90.	123.	2 PLA
46	.108	2.34	1.08	.43	.17	.25	.19	103.	31.	149.	30.	28.	92.	119.	2 PLA
47	.111	2.21	.84	.43	.23	.16	.24	88.	30.	157.	30.	24.	86.	127.	2 PLA
48	.110	2.30	.97	.43	.19	.19	.25	111.	30.	157.	30.	21.	86.	128.	2 PLA
50	.141	1.20	.42	.48	.60	.13	.08	212.	131.	81.	21.	40.	131.	328.	1 PLA
52	.143	1.29	.44	.54	.63	.22	.11	168.	107.	140.	35.	29.	136.	380.	1 PLA
54	.125	2.19	.93	.47	.47	.13	.09	143.	42.	106.	21.	51.	142.	249.	2 PLA
55	.126	2.23	.97	.45	.39	.16	.10	130.	52.	112.	20.	35.	145.	307.	2 PLA
56	.148	2.22	1.20	.58	.28	.23	.17	164.	90.	203.	42.	36.	90.	243.	2 FOR
57	.128	2.23	.86	.53	.24	.18	.09	68.	36.	125.	23.	26.	83.	168.	2 FOR
58	.143	2.32	.94	.56	.14	.18	.12	130.	48.	183.	31.	25.	76.	208.	2 FOR
59	.144	2.35	.95	.51	.04	.14	.08	63.	55.	115.	24.	29.	96.	122.	2 FOR
60	.150	1.32	.40	.52	.66	.15	.10	125.	17.	149.	35.	26.	73.	253.	1 PLA
61	.152	2.92	.87	.57	.09	.17	.14	100.	60.	155.	30.	29.	110.	177.	3 FOR
62	.062	2.44	1.17	.44	.37	.10	.08	146.	45.	69.	16.	384.	174.	82.	2 SAW
63	.068	2.26	.82	.60	.35	.06	.02	126.	40.	81.	62.	318.	215.	115.	2 SMA
64	.141	2.90	.96	.53	.06	.10	.06	107.	71.	94.	20.	30.	93.	68.	3 PLA
65	.057	3.16	1.13	.80	.35	.09	.09	152.	62.	52.	29.	379.	291.	29.	3 SAW
66	.105	2.82	1.02	.52	.40	.07	.02	98.	63.	63.	63.	485.	199.	45.	3 SMA
67	.047	2.20	.99	.71	.35	.04	.02	116.	240.	46.	8.	543.	107.	50.	2 SMA
68	.067	2.18	1.08	.65	.36	.04	.02	52.	160.	48.	4.	466.	81.	39.	2 SMA
69	.100	2.13	.95	.53	.26	.04	.02	96.	172.	50.	5.	491.	143.	48.	2 SMA
70	.110	2.11	.95	.39	.24	.15	.12	58.	98.	98.	24.	57.	73.	68.	2 PLA
71	.131	2.25	.97	.43	.25	.14	.19	92.	196.	213.	40.	65.	84.	100.	2 PLA
72	.123	2.22	.90	.47	.30	.10	.13	70.	180.	120.	20.	67.	68.	67.	2 PLA
74	.103	2.28	1.00	.41	.21	.15	.15	73.	162.	151.	33.	59.	74.	103.	2 PLA
75	.139	2.19	.86	.51	.47	.14	.09	175.	50.	124.	28.	30.	140.	387.	2 PLA
76	.118	2.26	.78	.46	.18	.23	.13	106.	164.	116.	19.	112.	95.	84.	2 PLA
77	.140	1.34	.45	.51	.60	.18	.17	108.	173.	145.	22.	23.	78.	90.	1 FOR
78	.126	2.16	.98	.45	.26	.16	.14	83.	152.	257.	29.	19.	98.	77.	2 FOR

Table 3. Data Derived from Charpy Impact Tests for Samples Evaluated in Phase I. Data for samples indicated by an asterisk was supplied by material originator and was tested with the Phase II orientation. See Fig. 45

Sample Number	Key	FATT[a]	FATT[b]	ΔFATT[c]	40 ft-lb TT[d] U[e]	40 ft-lb TT[d] E[f]	40 ft-lb TT[d] ΔT(40)[g]	Upper Shelf[h]	Upper Shelf[i]
		(Degrees Fahrenheit)			(Degrees Fahrenheit)			(foot-pounds)	
1	2 PLA	65.	80.	15.	30.	40.	10.	88.	88.
2	1 PLA	20.	60.	40.	- 35.	- 50.	- 15.	155.	140.
4	1 SAW	100	100	0	190.	140.	- 50.	49.	48.
7	2 PLA	5.	30.	25.	- 30.	- 25.	5.	138.	140.
8	2 ESW	50.	75.	25.	40.	50.	10.	110.	108.
9	2 PLA	- 25.	35.	60.	-150.	- 20.	130.	160.	152.
10	2 FOR	10.	- 10.	- 20.	-110.	- 5.	105.	116.	112.
12	2 PLA	-105.	- 35.	70.	-110.	- 70.	40.	160.	160.
13	2 PLA	- 80.	- 15.	65.	-145.	- 40.	105.	120.	132.
14	2 PLA	- 75.	- 30.	45.	-110.	- 60.	50.	170.	156.
15	2 FOR	- 80	35.	115.	-130.	- 50.	80.	166.	156.
16	2 ESW	- 40.	0.	40.	- 65.	- 50.	15.	105.	100.
18*	2 SAW	90.	232.	142.	40.	192.	152.	90.	
19*	2 SAW	54.	64.	10.	23.	42.	19.	114.	114.
20*	2 SAW	30.	44.	14.	6.	16.	10.	118.	114.
21*	2 SAW	60.	90.	30.	74.	94.	20.	100.	90.
22*	2 SAW	60.	90.	30.	74.	94.	20.	100.	90.
23*	2 SAW	42.	80.	38.	0.	60.	60.	110.	100.
24*	2 SAW	72.	140.	68.	58.	120.	62.	96.	80.
25*	2 SAW	16.	92.	76.	6.	68.	62.	86.	78.
26*	2 ESW	- 80.	- 4.	76.	- 92.	- 32.	60.	96.	85.
27*	2 ESW	- 48.	- 24.	24.	- 56.	- 40.	16.	140.	130.
33	2 PLA	5.	- 15.	- 20.	- 50.	- 40.	10.	120.	120.
34	2 SAW	- 30.	35.	65.	- 25.	40.	65.	70.	67.
35	2 SAW	- 40.	80.	100.	- 30.	35.	65.	80.	80.
36	2 PLA	20.	65.	55.	- 50.	40.	90.	135.	122.
37	2 SAW	50.	190.	140.	10.	135.	125.	110.	80.
38	2 SAW	75.	110.	35.	55.	90.	35.	100.	95.
39	2 SAW	20.	85.	65.	- 45.	5.	50.	110.	116.
40	2 SAW	- 10.	50.	60.	- 50.	- 25.	25.	135.	120.
41	2 SAW	- 20.	125.	105.	- 70.	55.	125.	120.	120.
42	2 SAW	- 20.	98.	118.	- 70.	- 10.	60.	110.	112.
43	2 SAW	- 50.	87.	137.	- 80.	35.	115.	125.	124.
44	2 SAW	10.	110.	120.	- 40.	17.	57.	125.	112.

Continued.

Table 3. (Continued)

Sample Number	Key	FATT[a]	FATT[b]	ΔFATT[c]	40 ft-lb TT[d] U[e]	40 ft-lb TT[d] E[f]	40 ft-lb TT[d] ΔT(40)[g]	Upper Shelf[h]	Upper Shelf[i]
		(Degrees Fahrenheit)			(Degrees Fahrenheit)			(foot-pounds)	
45	2 PLA	- 50.	- 17.	33.	- 70.	- 80.	- 10.	220.	240.
46	2 PLA	- 40.	- 5.	35.	- 75.	- 65.	10.	230.	240.
47	2 PLA	-130.	- 70.	60.	-195.	-100.	95.	235.	230.
48	2 PLA	-140	-130	10	-140	-135	5.	235.	210.
50	1 PLA	70.	85.	15.	30.	- 25.	- 55.	120.	145.
52	1 PLA	80.	95.	15.	0.	40.	40.	120.	125.
54	2 PLA	- 25	- 5.	20.	-115.	- 85.	30.	200.	180.
55	2 PLA	10	30.	20.	- 70.	- 40.	30.	180.	175.
56*	2 FOR	0.	122.	122.	- 44.	68.	112.	120.	120.
57*	2 FOR	- 87.	- 78.	9.	-110.	- 90.	20.	210.	203.
58*	2 FOR	- 64.	- 24.	40.	-104.	- 88.	16.	203.	218.
59*	2 FOR	- 73.	- 66.	7.	-133.	-119.	14.	160.	160.
60*	1 PLA	30.	52.	22.	- 36.	- 2.	34.	203.	181.
61*	3 FOR	- 77.	- 58.	19.	-101.	- 92.	9.	189.	167.
62*	2 SAW	43.	59.	16.	21.	34.	13.	131.	131.
63*	2 SMA	- 8.	19.	27.	- 27.	7.	34.	152.	131.
64*	3 PLA	- 83.	- 80.	3.	- 96.	- 96.	0.	167.	167.
65*	3 SAW	25.	63.	38.	3.	35.	32.	116.	109.
66*	3 SMA	- 35.	30.	65.	- 47.	- 4.	43.	116.	116.
67	2 SMA	5.	60.	55.	- 60.	15.	75.	120.	115.
68	2 SMA	30.	45.	15.	10.	- 25.	- 35.	115.	110.
69	2 SMA	- 5.	15.	20.	- 50.	- 30.	20.	140.	130.
70	2 PLA	0.	50.	50.	- 10	15.	25.	140.	145.
71	2 PLA	- 10.	45.	55.	- 15.	20.	35.	100.	100.
72	2 PLA	- 65.	- 5.	60.	- 80.	- 90.	- 10.	145.	165.
74	2 PLA	- 70.	- 20	50.	- 80.	- 55.	25.	165.	165.
75	2 PLA	- 25.	30.	55.	-120.	- 40.	80.	180.	160.
76	2 PLA	70.	85.	15.	50.	35.	- 15.	115.	120.
77	1 FOR	65.	80.	15.	35.	20.	- 15.	150.	110.
78	2 FOR	50.	80.	30.	15.	- 25.	- 40.	115.	115.

[a] Fracture Appearance Transition Temperature in the unembrittled condition
[b] Fracture Appearance Transition Temperature in the step-cooled embrittled condition
[c] Change in Fracture Appearance Transition Temperature due to temper embrittlement
[d] 40 foot/pound Transition Temperature
[e] Unembrittled
[f] Step-cooled embrittled
[g] Change in 40 foot/pound Transition Temperature due to temper embrittlement
[h] Unembrittled condition
[i] Step-cooled embrittled condition

TABLE 4 Comparison of FATT Data After Isothermal Embrittlement of 1000 hr in °F

Phase II orientation, Fig. 45

Sample No.	Furnace Temperature				
	650°F	725°F	800°F	875°F	950°F
1	75	75	90	110	110
4	145	125	150	175	130
9	-25	10	15	-30	35
16	-15	5	-30	0	30
19	55	70	70	60	85
20	30	25	25	35	40
26	60	50	65	70	135
27	-10	-15	25	45	30
33	30	0	10	20	5
36	60	30	45	60	20
37	70	90	50	90	80
43	20	10	50	50	75
44	20	35	55	80	90
46	-30	-15	0	-10	-10
47	-70	-85	-60	-50	-55
54	-25	-15	0	25	25
56	40	40	90	125	150
59	-15	-10	40	25	-5
62	45	55	80	75	90
63	20	25	70	35	75
65	60	90	100	90	70
67	25	15	45	50	75
68	40	30	50	60	50
69	45	30	50	50	30
78	60	80	75	85	60

Table 5 Comparison of 40 ft-lb TT After Isothermal Embrittlement of 1000 hr in °F

Phase II orientation, Fig. 45

Sample No.	Furnace Temperature				
	650°F	725°F	800°F	875°F	950°F
1	40	25	65	85	85
4*	160	110	150	190	135
9	-85	-90	-65	-60	-40
16	-50	-15	-75	-45	-20
19	35	35	45	20	50
20	-15	-5	5	10	20
26	5	20	40	50	55
27	-35	-20	5	15	10
33	-10	-20	-10	-5	-15
36	45	-5	10	15	-20
37	40	65	40	40	25
43	-85	-65	-65	-20	15
44	-70	-5	-10	0	10
46	-55	-50	-25	-45	-55
47	-100	-105	-115	-100	-95
54	-100	-85	-110	-100	-70
56	-30	-40	30	-10	60
59	-80	-125	-75	-75	-90
62	20	15	35	40	55
63	5	5	5	20	40
65	50	70	75	60	25
67	-40	-10	0	-10	10
68	-10	0	35	-20	25
69	15	-5	20	0	0
78	20	20	25	20	25

*Upper shelf close to 40 ft-lb.

TABLE 6 Comparison of Estimates of the Upper Shelf Impact Energy After Isothermal Embrittlement of 1000 hr in °F (> means insufficient data to accurately determine value: figure given is the highest recorded)

Phase II orientation, Fig. 45

Sample No.	Furnace Temperature				
	650°F	725°F	800°F	875°F	950°F
1	80	70	80	80	85
4	50	53	50	50	50
9	175	160	175	150	150
16	>110	>90	>120	ND	115
19	90	115	100	95	100
20	115	>110	110	115	>108
26	>120	110	105	120	90
27	110	105	>105	100	>100
33	>85	85	85	90	100
36	>120	120	>115	120	>128
37	115	110	90	ND	143
43	150	135	>110	120	>115
44	140	120	120	105	105
46	>190	240	>220	245	220
47	>217	>180	240	240	>180
54	>240	190	>190	170	>180
56	>160	140	>130	130	>115
59	>180	>195	>210	170	>170
62	>150	>110	>125	>139	145
63	>120	>110	>145	140	140
65	>161	115	125	120	140
67	120	>115	>115	>120	>110
68	100	100	>100	>110	100
69	110	90	>110	105	120
78	105	105	105	110	>120

TABLE 7 Comparison of FATT Data After Isothermal Embrittlement of 10,000 hr in °F

Phase II orientation, Fig. 45

Sample No.	Furnace Temperature				
	650°F	725°F	800°F	875°F	950°F
1	90	80	115	110	100
4	120	120	115	97	115
9	-10	-60	5	110	85
16	0	-10	10	40	20
19	55	60	75	75	60
20	25	40	55	45	10
26	60	40	80	140	135
27	0	-5	60	55	35
33	10	15	30	10	25
36	50	25	25	10	15
37	55	50	140	50	110
43	30	30	85	120	75
44	30	15	105	110	130
46	-25	-15	-30	-5	-20
47	-75	-75	-25	-20	-20
54	-40	-25	10	30	50
56	45	75	180	240	175
59	-25	-10	10	0	0
62	50	45	80	90	80
63	40	40	90	90	95
65	50	100	120	165	180
67	10	40	85	120	95
68	20	35	50	85	70
69	35	30	50	30	55
78	70	65	75	60	70

TABLE 8 Comparison of 40 ft-lb TT Data After Isothermal Embrittlement of 10,000 hr in °F

Phase II orientation, Fig. 45

Sample No.	Furnace Temperature				
	650°F	725°F	800°F	875°F	950°F
1	25	40	90	95	65
4	125	175	110	110	115
9	-45	-75	-50	-20	0
16	-35	-20	-10	15	0
19	40	55	55	60	50
20	10	5	30	40	-5
26	35	10	45	75	60
27	-30	-25	30	20	-5
33	-25	-10	0	5	-5
36	-5	20	5	0	-25
37	40	50	85	50	90
43	-95	-60	0	35	35
44	-45	-25	5	40	50
46	-50	-20	-50	-40	-50
47	-125	-110	-85	-100	-110
54	-95	-100	-75	-40	-60
56	-40	-10	80	150	75
59	-80	-90	-55	-50	-80
62	15	20	35	40	45
63	15	10	30	50	50
65	15	55	50	115	110
67	-25	-20	45	75	50
68	10	10	25	70	25
69	20	0	5	15	10
78	25	10	0	25	25

TABLE 9 Comparison of Upper Shelf Impact Energies After 10,000 hr Isothermal Embrittlement (in ft-lb)

Phase II orientation, Fig. 45

Sample No.	Furnace Temperature				
	650°F	725°F	800°F	875°F	950°F
1	ND	>90	>95	>87	84
4	58	40	54	51	71
9	187	>170	>170	>185	239
16	150	>125	>106	>85	125
19	>136	>105	>110	>115	107
20	136	ND	>125	115	139
26	134	>125	>110	110	116
27	119	>110	>120	>120	126
33	>86	>80	>86	>105	85
36	140	>120	ND	ND	>123
37	>121	ND	ND	240	>123
43	>240	>105	ND	240	162
44	>150	>125	>100	>115	>143
46	>240	>240	>140	240	239
47	>240	>225	>160	ND	239
54	240	>200	>190	240	239
56	160	>156	>100	115	181
59	200	>194	>190	>195	208
62	155	ND	ND	>110	150
63	>240	>170	>136	ND	>177
65	157	ND	>115	>200	>192
67	132	>112	>112	>110	114
68	126	>115	>110	>115	110
69	>118	>125	ND	>140	>145
78	>126	>125	ND	>125	119

ND = Not Determined.

> = Greater than or highest value recorded.

TABLE 10 Comparison of FATT Data After Isothermal Embrittlement of 20,000 hr in °F

Phase II orientation, Fig. 45.

Sample No.	Furnace Temperature				
	650°F	725°F	800°F	875°F	950°F
1	95	90	125	110	100
4	130	130	135	85	75
9	5	0	25	85	90
16	25	5	20	50	25
19	50	50	75	70	65
20	40	45	65	75	50
26	55	55	120	145	170
27	-15	-10	30	50	20
33	-10	0	15	25	30
36	30	25	50	45	40
37	50	85	60	175	60
43	35	25	75	135	95
44	30	40	75	150	135
46	-25	-10	10	10	10
47	-75	-60	-20	0	15
54	-20	-15	35	70	75
56	50	100	200	225	175
59	-60	0	15	25	5
62	50	60	125	100	100
63	50	55	90	90	90
65	60	70	150	110	100
67	40	70	110	110	100
68	50	50	65	80	50
69	30	35	50	50	60
78	45	80	60	85	90

TABLE 11 Comparison of 40 ft-lb TT Data After Isothermal Embrittlement of 20,000 hr in °F

Phase II orientation, Fig. 45

Sample No.	Furnace Temperature				
	650°F	725°F	800°F	875°F	950°F
1	65	70	105	80	65
4	145	160	120	65	75
9	-35	-40	-25	35	5
16	-5	-10	10	20	0
19	40	35	75	70	35
20	10	25	45	50	30
26	15	45	70	95	100
27	-45	-60	30	40	0
33	-20	-10	0	20	20
36	0	-5	-10	0	0
37	35	60	50	140	55
43	0	-20	0	30	40
44	-40	-50	10	25	60
46	-50	-50	-30	-30	-25
47	-115	-100	-75	-75	-55
54	-75	-75	-50	0	-10
56	-25	0	100	125	75
59	-85	-75	-15	-15	-50
62	35	25	50	45	45
63	10	30	45	55	40
65	55	40	70	70	50
67	-20	10	60	20	50
68	25	25	40	50	45
69	40	0	30	0	15
78	0	10	15	10	30

TABLE 12 Comparison of Upper Shelf Impact Energies After 20,000 hr Isothermal Embrittlement (in ft-lb)

Phase II orientation, Fig. 45

Sample No.	Furnace Temperature				
	650°F	725°F	800°F	875°F	950°F
1	90	90	85	90	90
4	50	50	60	65	75
9	205	160	160	180	155
16	105	115	115	100	110
19	100	110	110	105	>85
20	125	90	110	130	130
26	110	115	110	95	115
27	110	115	105	105	115
33	100	100	85	90	95
36	130	140	130	110	>95
37	160	120	120	115	145
43	135	135	130	155	220
44	130	120	120	130	120
46	240	240	240	240	240
47	240	240	240	240	>180
54	220	200	180	230	160
56	160	160	145	135	150
59	190	230	225	240	230
62	150	160	165	130	150
63	175	180	160	165	150
65	155	>130	160	140	135
67	135	130	125	120	120
68	110	110	105	120	100
69	125	120	115	110	150
78	125	120	115	100	95

TABLE 13 Comparison of FATT in De-Embrittled (D), Unembrittled (U) and Step-Cooled Embrittled (E) Conditions in °F

Phase I orientation, Fig. 45

Sample No.	Type	D	U	E
1	2 PLA	80	65	80
4	1 SAW	125	100	100
8	2 ESW	70	50	75
9	2 PLA	-50	-25	35
16	2 ESW	-10	-40	0
18	2 SAW	50	90*	232*
19	2 SAW	30	54*	64*
20	2 SAW	0	30*	44*
24	2 SAW	70	72*	140*
26	2 ESW	40	-80*	-4*
27	2 ESW	-60	-48*	-24*
33	2 PLA	-35	5	-15
36	2 PLA	5	20	65
37	2 SAW	40	50	190
38	2 SAW	50	75	110
44	2 SAW	0	-10	110
46	2 PLA	-55	-40	-5
47	2 PLA	-90	-130	-70
52	1 PLA	50	80	95
54	2 PLA	-60	-25	-5
56	2 FOR	25	0*	122*
61	3 FOR	-45	-77*	-58*
66	3 SMA	-10	-35*	30*
67	2 SMA	-15	5	60
68	2 SMA	25	30	45
69	2 SMA	20	-5	15
78	2 FOR	35	50	80

KEY		
	1, 1¼Cr - ½Mo	FOR, Forging
	2, 2¼Cr - ½Mo	PLA, Plate
	3, 3Cr - 1Mo	SAW, Submerged arc weld
		ESW, Electroslag weld
		SMA, Shielded metal arc weld

*Data reported by material originator.

TABLE 14 Comparison of 40 ft-lb TT in De-Embrittled (D), Unembrittled (U) and Step-Cooled Embrittled (E) Conditions in °F

Phase I orientation, Fig. 45

Sample No.	Type	D	U	E
1	2 PLA	50	30	40
4	1 SAW	150	190	140
8	2 ESW	40	40	50
9	2 PLA	-70	-150	-20
16	2 ESW	-25	-65	-50
18	2 SAW	35	40*	192*
19	2 SAW	30	23*	42*
20	2 SAW	-50	6*	16*
24	2 SAW	50	58*	120*
26	2 ESW	0	-92*	-32*
27	2 ESW	-70	-56*	-40
33	2 PLA	-40	-50	-40
36	2 PLA	-10	-50	40
37	2 SAW	10	10	135
38	2 SAW	45	55	90
44	2 SAW	-75	-40	17
46	2 PLA	-70	-75	-65
47	2 PLA	-140	-195	-100
52	1 PLA	-45	0	40
54	2 PLA	-120	-115	-85
56	2 FOR	-45	-44*	68*
61	3 FOR	-105	-101*	-92*
66	3 SMA	-60	-47*	-4*
67	2 SMA	-50	-60	15
68	2 SMA	-10	10	-25
69	2 SMA	5	-50	-30
78	2 FOR	-15	15	-35

KEY
1, 1¼Cr - ½Mo
2, 2¼Cr - ½Mo
3, 3Cr - 1Mo
FOR, Forging
PLA, Plate
SAW, Submerged arc weld
ESW, Electroslag weld
SMA, Shielded metal arc weld

*Data reported by material originator.

TABLE 15 Comparison of Upper Shelf Energies in De-Embrittled (D), Unembrittled (U) and Step-Cooled Embrittled (E) Conditions in ft-lb

Phase I orientation, Fig. 45

Sample No.	Type	D	U	E
1	2 PLA	100	88	88
4	1 SAW	65	49	48
8	2 ESW	120	110	108
9	2 PLA	180	160	152
16	2 ESW	105	105	100
18	2 SAW	>75	90*	—*
19	2 SAW	140	114*	114*
20	2 SAW	145	118*	114*
24	2 SAW	88	96*	80*
26	2 ESW	130	96*	85*
27	2 ESW	130	140*	130*
33	2 PLA	110	120	120
36	2 PLA	150	135	122
37	2 SAW	>120	110	80
38	2 SAW	100	100	95
44	2 SAW	—	125	112
46	2 PLA	>240	230	240
47	2 PLA	>220	235	230
52	1 PLA	120	120	125
54	2 PLA	>240	200	180
56	2 FOR	>180	120*	120
61	3 FOR	200	189*	167*
66	3 SMA	140	116*	116*
67	2 SMA	>125	120	115
68	2 SMA	>125	115	110
69	2 SMA	160	140	130
78	2 FOR	140	115	115

KEY		
	1, 1¼Cr - ½Mo	FOR, Forging
	2, 2¼Cr - ½Mo	PLA, Plate
	3, 3Cr - 1Mo	SAW, Submerged arc weld
		ESW, Electroslag weld
		SMA, Shielded metal arc weld

>Upper shelf not accurately determined due to lack of data. The figure given is the highest impact energy observed.

*Data reported by material originator.

TABLE 16 Comparison of FATT and 40 ft-lb TT in the Unembrittled (U) and Step-Cooled Embrittled (E) Conditions for Phase I Orientation (L-S and T-S) and Phase II Orientation (L-T and T-L) See Fig. 45.

Sample No.	FATT, U		FATT, E		40 ft-lb U		40 ft-lb E	
	I	II	I	II	I	II	I	II
1	65	60	80	95	30	55	40	40
4	100	90	100	95	190*	80*	140*	75*
8	50	70	75	80	40	40	50	50
33	5	- 5	-15	20	(-50)	-15	(- 40)	- 10
36	20	25	65	25	- 50	10	40	10
46	- 40	- 15	-5	-30	- 75	-60	- 65	- 40
47	-130	-150	-70	-75	-195	-170	(-100)	- 75
52	80	100	95	110	0	0	40	(-10)
54	- 25	- 40	-5	45	-115	-110	- 85	- 75
67	5	20	60	25	- 60	- 5	15	20
69	- 5	30	15	70	- 50	10	- 30	25
78	50	70	80	85	15	10	(- 35)	0

*40 ft-lb is close to upper shelf.

Data in brackets is ±50°F.

TABLE 17 Comparison of ΔT(40) from the Unembrittled Condition (U) to the Step-Cooled Condition (E) and the Maximum Embrittlement After 1000, 10,000 and 20,000 hr Isothermal Embrittlement

Sample No.	$\Delta T(40)_{U-E}$ °F	$\Delta T(40)_{U-1000}$ °F	$\Delta T(40)_{U-10000}$ °F	$\Delta T(40)_{U-20000}$ °F	J** —
1	-15	30	35	50	154
4*	-5	110	25	80	239
9	20	70	-30	5	133
16	10	35	70	75	135
19	19	27	37	52	115
20	10	14	34	44	198
26	60	147	167	192	240
27	16	71	86	196	111
33	5	10	20	35	173
36	0	5	10	-10	91
37	125	45	70	120	242
43	115	85	105	110	256
44	57	40	80	90	267
46	20	35	40	35	151
47	95	75	85	115	161
54	35	40	70	110	234
56	112	104	194	169	316
59	14	58	83	118	98
62	13	34	24	29	174
63	34	67	77	82	196
65	32	72	112	67	235
67	25	15	80	65	172
68	-35	25	60	40	101
69	15	10	5	20	115
78	-10	15	15	20	241

*Upper shelf is close to 40 ft-lb.

** $J = (Mn + Si)(P + Sn) \times 10^4$.

TABLE 18

Thermal Cycles and Transition Temperatures from Charpy Specimens Tested at Each Stage of the repeated de-embrittlement experiment

Thermal Cycle Stage	Sample 18		Sample 38	
	FATT, °F	40 ft-lb TT, °F	FATT, °F	40 ft-lb TT, °F
1 Age 5000 hr at 875°F De-embrittle 1100°F 1 hr Water quench	60	50	30	50
+				
2 Age 1000 hr at 875°F	140	145	105	115
+				
3 Age 4000 hr more at 875°F		No tests		
+				
4 De-embrittle 1100°F 1 hr Water quench	40	40	30	60
+				
5 Age 5000 hr at 875°F	175	180	115	100
+				
6 De-embrittle 1100°F 1 hr Water quench		No tests		
+				
7 Age 1000 hr at 875°F	120	140	110	100
+				
8 Age 4000 hr more at 875°F	100	110	100	90

TABLE 19 Heat Treatments Used on 2¼Cr - 1Mo Ingot No. 75 to Produce Three Structures and Three Strength Levels

Structure	Rockwell B Hardness	Nominal UTS (ksi)	Heat Treatment
Ferrite-Pearlite	87	(85)	1700°F for 1 hr, Furnace cool to 1200°F, hold 2 hr, Water Quench
Bainite/Martensite	87	(85)	1700°F for 1 hr, Water Quench 1275°F for 24 hr, Water Quench
Bainite	87	(85)	As-received material, de-embrittled 1100°F for hr, Water Quench
Bainite	98	(113)	1700°F for 1 hr, forced air cool to 950°F, Hold for 1 hr, Air cool 1275°F for 4 hr, Water Quench
Bainite	108	(150)	1700°F for 1 hr, forced air cool to 950°F, hold for 1 hr, Air cool, 1100°F, ½ hr, Water Quench
As-received condition	87	(85)	1750°F for 3 hr, Water Quench, 1225°F for 4½ hr, Air cool. 1100°F for 15 hr 1200°F for 30 hr 1275°F for 16 hr

TABLE 20

Basic data for sample no. 75 reheat-treated to give three structures and three strength levels. The 40 ft-lb transition temperatures and fracture appearance transition temperatures (FATT) for the de-embrittled condition (0 hr) and after 1,000, 10,000 and 20,000 hr at 875°F are given along with changes (Δ) due to the isothermal exposure. A minus sign in the Δ columns indicates that the steel is de-embrittling.

Structure	Initial Hardness R_B	Time @ 875°F (hr)	40 ft-lb TT (°F)	Δ40 ft-lb TT (°F)	FATT (°F)	ΔFATT (°F)
QBM	87	0	-130	—	- 55	—
		1,000	-115	15	- 50	5
		10,000	20	150	80	135
		20,000	20	150	90	145
F-P	87	0	75	—	125	—
		1,000	45	- 30	95	- 30
		10,000	40	- 35	80	- 45
		20,000	35	- 40	90	- 35
B	87	0	- 85	—	- 10	—
		1,000	- 40	45	40	50
		10,000	0	85	110	120
		20,000	- 25	60	80	90
B	98	0	-110	—	- 35	—
		1,000	- 90	20	- 5	30
		10,000	10	120	60	95
		20,000	20	130	80	115
B	108	0	170	—	205	—
		1,000	220	50	250	45
		10,000	150	- 20	190	- 15
		20,000	110	- 60	160	- 45

KEY:

QBM — Quenched Bainite-Martensite Structure

F-P — Ferrite—Pearlite Structure

B — Bainite Structure

TABLE 21

Analytical Chemistries in wt % and ppm of Samples Chosen
for Preliminary Auger Analyses

Sample No.	wt %							ppm						
	C	Cr	Mo	Mn	Si	Ni	Cu	P	Sn	Sb	As	S	O	N
20	.121	1.97	.86	.52	.28	.13	.21	100	147	20	100	121	337	123
26	.146	2.25	.93	.61	.25	.15	.10	91	188	25	47	127	144	127
27	.168	2.22	.92	.59	.21	.13	.08	64	75	15	92	135	93	121
37	.067	2.15	.77	.96	.54	.12	.02	118	43	11	34	110	653	125
43	.058	2.41	.97	.67	.32	.10	.16	190	69	21	200	77	412	137
56	.148	2.22	1.20	.58	.28	.23	.17	164	203	42	243	90	36	90
63	.068	2.26	.82	.60	.35	.06	.02	126	81	62	115	40	318	215

TABLE 22

Highest Levels of Elements at or Adjacent to the Grain Boundaries in wt %
(the readings given in brackets are on the limit of resolution)

Sample No.	Element						
	C	Cr	Mo	Ni	Cu	P	Sn
20	3.0	6.0	3.0	(.5)	1.3	3.0	—
26	2.5	7.1	5.3	(.5)	1.3	4.2	(.5)
43	2.5	6.5	4.5	(.5)	(1.1)	3.8	(.2)
56	7.8	7.0	5.0	1.2	1.8	4.0	.8
63	2.0	8.6	8.1	—	—	4.6	—

TABLE 23 J_{Ic} Values Determined as a Function of the Test Temperature for Sample No. 75 in the Unembrittled Condition

Test Temperature (°F)	J_{Ic}
50	>1500
100	>1500*
150	>1500
200	1050
250	927
300	700

*Insufficient data

Table 24

The Fracture Appearance Transition Temperatures, 40 ft-lb Transition Temperatures (FATT, 40 ft-lb TT) and Upper Shelf Energy Values for Isothermal Embrittlement in the Hydrogen-Environment and Air Compared

Sample No.	Environment	Isothermal Temp., °F	FATT °F	40 ft-lb TT °F	Upper Shelf† ft-lb
46	Air	650	- 30	- 55	> 190
46	H_2	650	- 25	- 25	> 240
46	Air	875	- 10	- 45	> 240
46	H_2	875	40	- *	25
56	Air	650	40	- 30	> 160
56	H_2	650	125	10	> 140
56	Air	875	125	- 10	130
56	H_2	875	75	- 10	105
59	Air	650	- 15	- 80	> 180
59	H_2	650	- 10	- 75	220
59	Air	875	25	- 75	170
59	H_2	875	- 10	- 75	180

*Upper shelf lower than 40 ft-lb.

†Upper shelf values indicated by > means that insufficient specimens were available for the accurate determination of the upper shelf.

Table 25

Comparison of the Analytical Chemistries
from Various Specimens Taken from Sample No. 46

Element	As-received	1,000 hr exposure in air @ 875°F	1,000 hr exposure in H_2 @ 650°F	1,000 hr exposure in H_2 @ 875°F
C	.11	.12	.12	.12
Cr	2.34	2.35	2.35	2.36
Mo	1.08	.98	.96	1.00
Mn	.43	.45	.44	.46
Si	.17	.14	.15	.16
Ni	.19	.19	.18	.20
Cu	.25	.27	.27	.27
P	.010	.017	.018	.015
S	.003	.006	.006	.006
Sn	.015	.014	.015	.013

Table 26

Rockwell B Hardness Measurements from Specimens in the
"As-Received" Condition and After Exposure in Air and H_2

Condition	Sample No.		
	46	56	59
As-received or unexposed	81	85.5	86
875°F for 1,000 hr in air	81.5	91.5	91
650°F for 1,000 hr in 3500 psig H_2	82.5	93	91
875°F for 1,000 hr in 3500 psig H_2	72.5	88	83.5

TABLE 27 Comparison of the FATT, 40 ft-lb TT and Upper Shelf Energy for samples in the de-embrittled (D), Unembrittled (U), step-cooled embrittled (E) and isothermally embrittled at 875°F for 1,000 hr, 10,000 hr and 20,000 hr conditions.

Sample No.	Condition	FATT °F	40 ft-lb TT °F	Upper Shelf ft-lb
52 (1 PLA)	D	50	- 45	120
	U	80	0	120
	E	95	40	125
	1,000	100	10	130
	10,000	95	- 10	145
	20,000	115	70	110
61 (3 FOR)	D	-45	-105	200
	U	-77*	- 60*	189*
	E	-58*	- 50*	167*
	1,000	0	- 55	200
	10,000	10	- 50	200
	20,000	20	- 25	170
66 (35 SMA)	D	-10	- 60	140
	U	-35*	- 47*	116*
	E	-30*	- 4*	116*
	1,000	55	0	150
	10,000	50	10	>100
	20,000	70	25	120

> Upper shelf not accurately determined due to lack of data. The figure given is the highest impact energy observed.

* Data reported by material originator.

TABLE 28 Comparison of Step-Cooled Embrittlement $\Delta T(40)_{U-E}$ with isothermal embrittlement after 1,000, 10,000 and 20,000 hr at 875°F. Predictions of isothermal embrittlement based upon Eqs. (4) are included.

Sample No.	$\Delta T(40)_{U-E}$ °F	$\Delta T(40)_{U-1000}$ °F	$\Delta T(40)_{U-10000}$ °F	$\Delta T(40)_{U-20000}$ °F
52 (measured)	40	10	-10	70
52 (predicted)		56	80	92
61 (measured	10	5	10	35
61 (predicted)		14	20	23
66 (measured)	43	47	57	72
66 (predicted)		60	86	99

Table 29(a) - Review of Samples Exhibiting 40 ft-lb Transition Temperature Higher Than 50°F (from Tables 5, 8, and 11)

		Isothermally Aged Samples With 40 ft-lb Transition Temperature Higher Than +50°F															
		Time: 1,000 hours					Time: 10,000 hours					Time: 20,000 hours					
Sample No.	Key	650	725	800	875	950	650	725	800	875	950	650	725	800	875	950	Unembrittled Samples
		(Temperature °F)					(Temperature °F)					(Temperature °F)					
4[a]	1 SAW	X	X	X	X	X	X	X	X	X	X	X	X	X	X	X	X
65	3 SAW		X	X	X			X	X	X	X	X		X	X	X	
1	2 PLA			X	X	X			X	X	X	X	X	X	X	X	
26	2 ESW					X				X	X			X	X	X	
37	2 SAW		X						X	X	X		X	X	X	X	
56	2 FOR					X			X	X	X			X	X	X	
62	2 SAW					X											
19	2 SAW							X	X	X	X			X	X		
67	2 SMA									X				X			
68	2 SMA									X							
44	2 SAW															X	
63	2 SMA														X		
Total Samples:	12	1	3	3	3	5	1	3	6	9	7	3	3	8	8	7	1

Table 29(b) - Summary of Isothermally-Induced Temper Embrittlement Data Giving Percentages of Samples with 40 ft-lb Transition Temperature Above +50°F

Type of Sample Isothermally Exposed in Phase II:	2 PLA	2 FOR	2 SAW	2 ESW	2 SMA	1 SAW	3 SMA	TOTAL
Number of Samples Tested in Each Category:	7	3	6	3	4	1	1	25
Number of Samples With 40 ft-lb Transition Temperature > +50°F from above:	1	1	4	1	3	1	1	12
Percentage of Samples With 40 ft-lb Transition Temperature > +50°F:	14	33	67	33	75	100	100	
Percentage of all Plate and Forging Samples With 40 ft-lb Transition Temperature > +50°F:	20							
Percentage of all 2¼Cr-1Mo Welds With 40 ft-lb Transition Temperature > +50°F:			62					

[a] Upper shelf close to 40 ft-lb Transition Temperature.

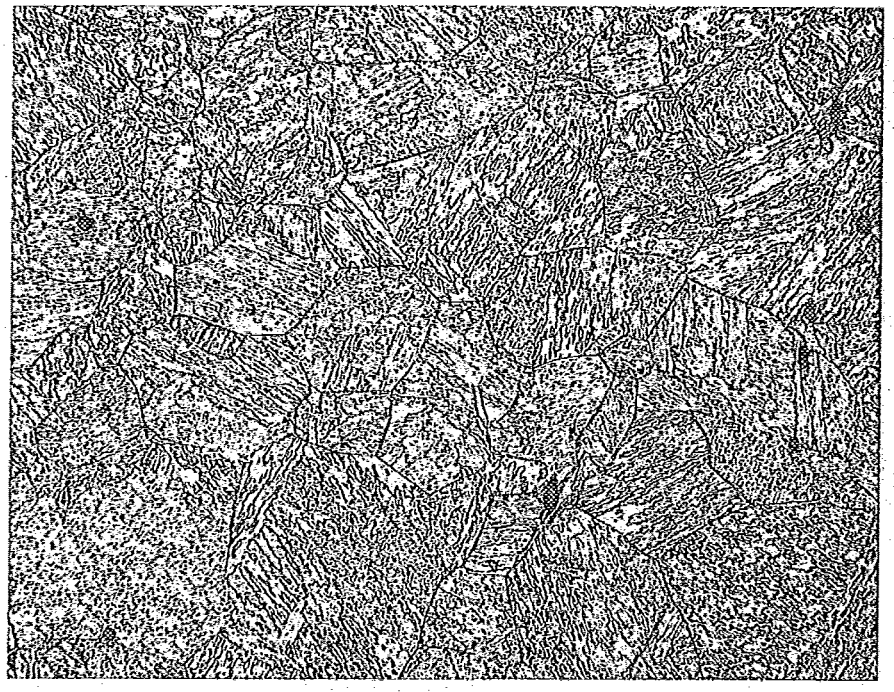

Mag. 200X

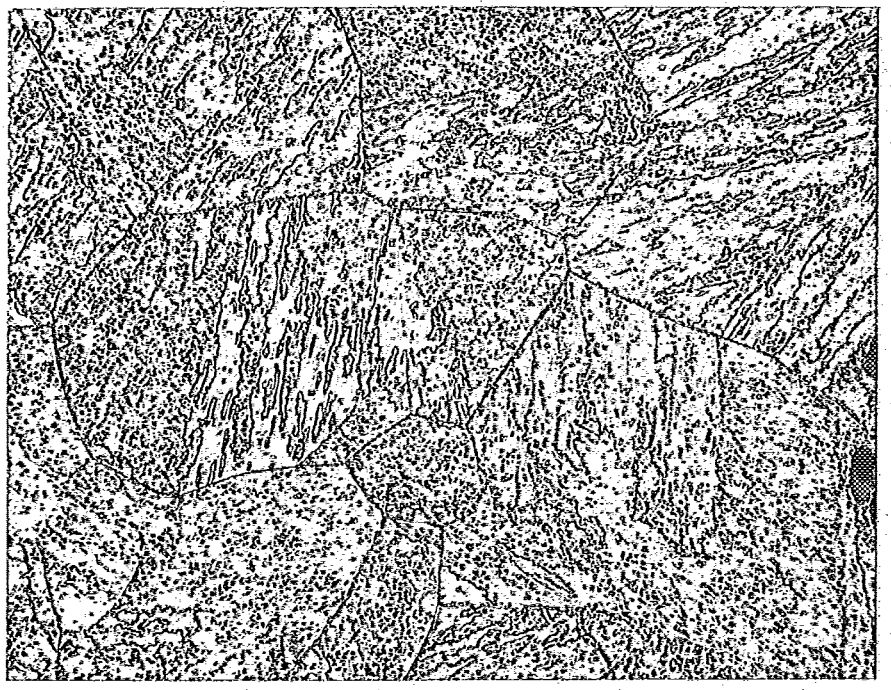

Mag. 500X

Sample No. 1 Material Key: 2 PIA

Fig. 1. Metallographic sections of sample No. 1 showing typical bainitic structure

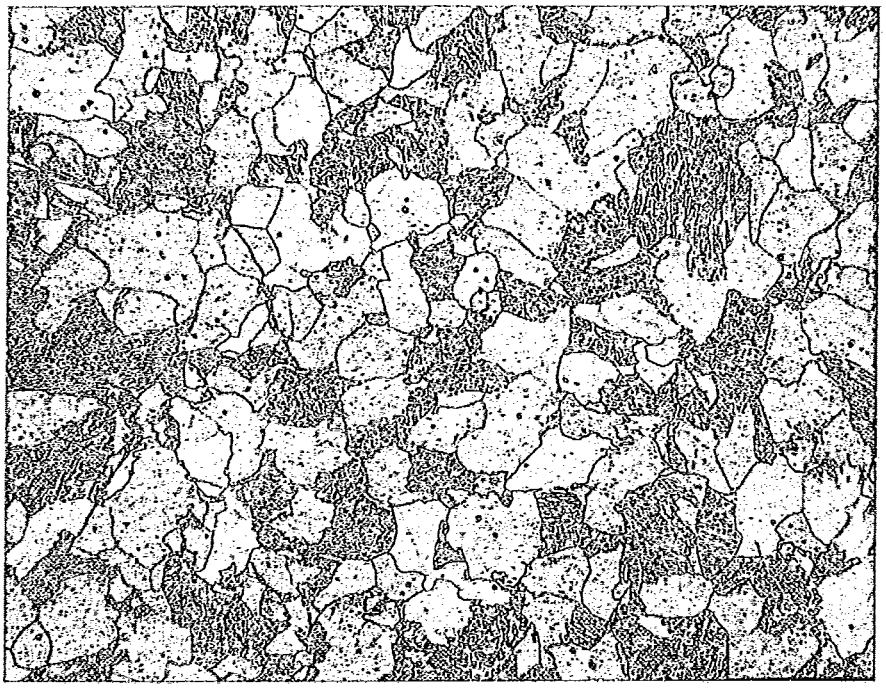

Mag. 200X

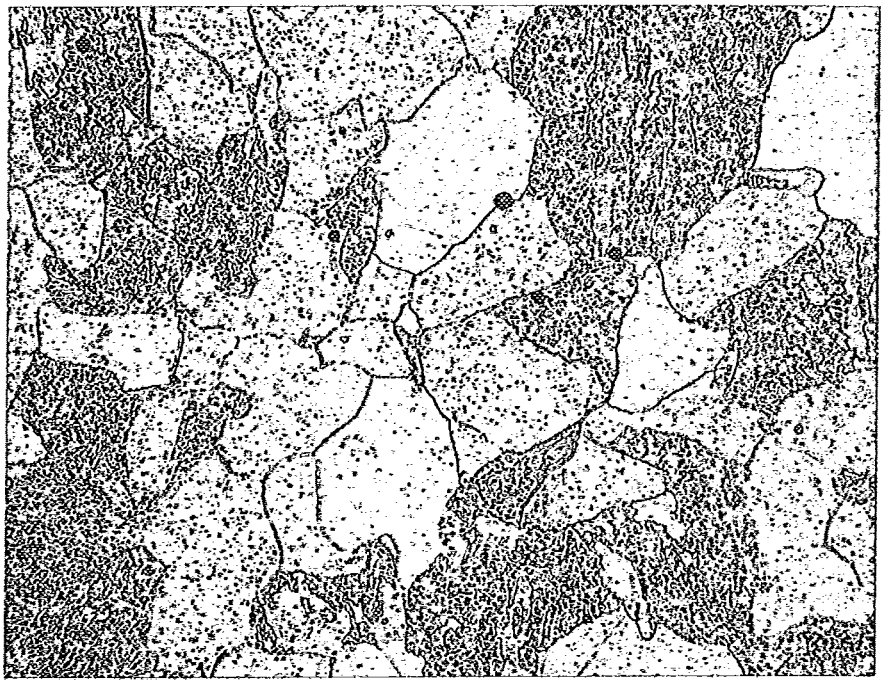

Mag. 500X

Sample No. 8 Material Key: 2PIA

Fig. 2. Metallographic sections of sample No. 8 showing typical ferrite-pearlite structure

It	L	A	B	C	R	D_a *	Thd.
1	5.00	1.37	1.12	2.25	.25	.505	.75-10
2	4.25	1.00	.87	2.25	.12	.357	.50-20
3	2.75	.75	.87	1.25	.12	.252	.38-16
4	4.25	1.00	.87	2.25	.12	.375	.62-11

* Tolerance .001

Do not undercut at D_a & DT

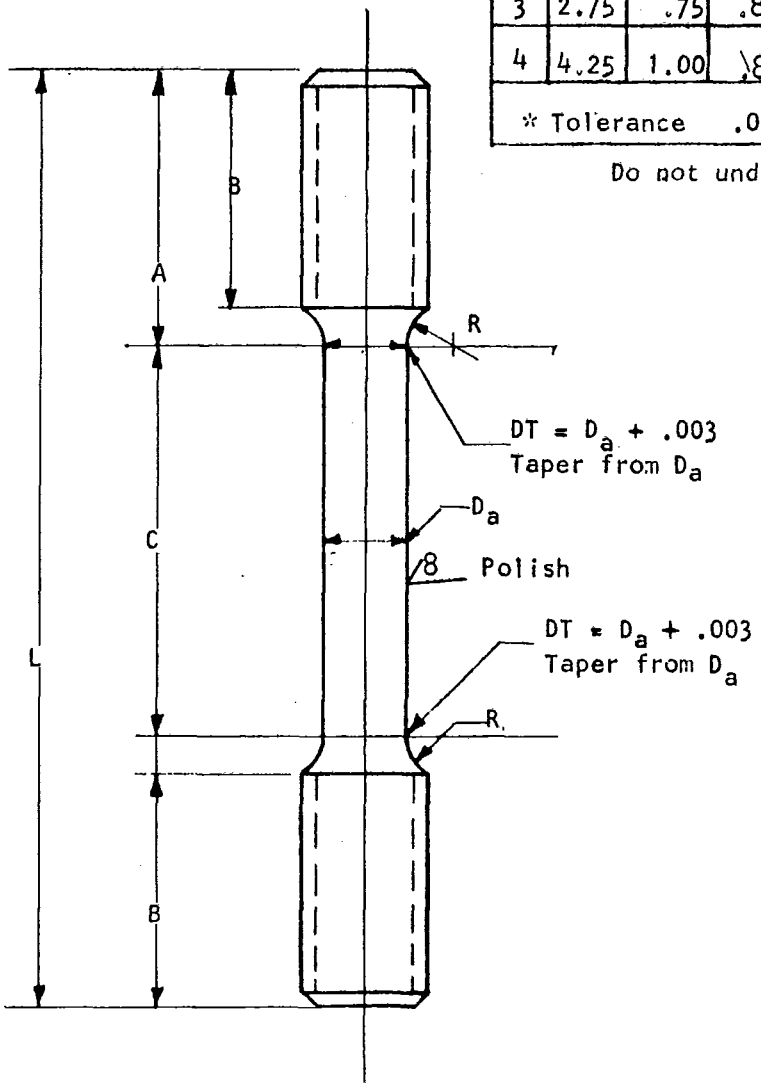

FIG. 3. STANDARD TENSILE TEST SPECIMEN

32 FINISH UNLESS OTHERWISE SPECIFIED	TOLERANCES		
Westinghouse Research Laboratories	UNLESS OTHERWISE SPECIFIED		
	2 PL. DEC.	3 PL. DEC.	ANGLES
	±.02	±.005	±0.5°

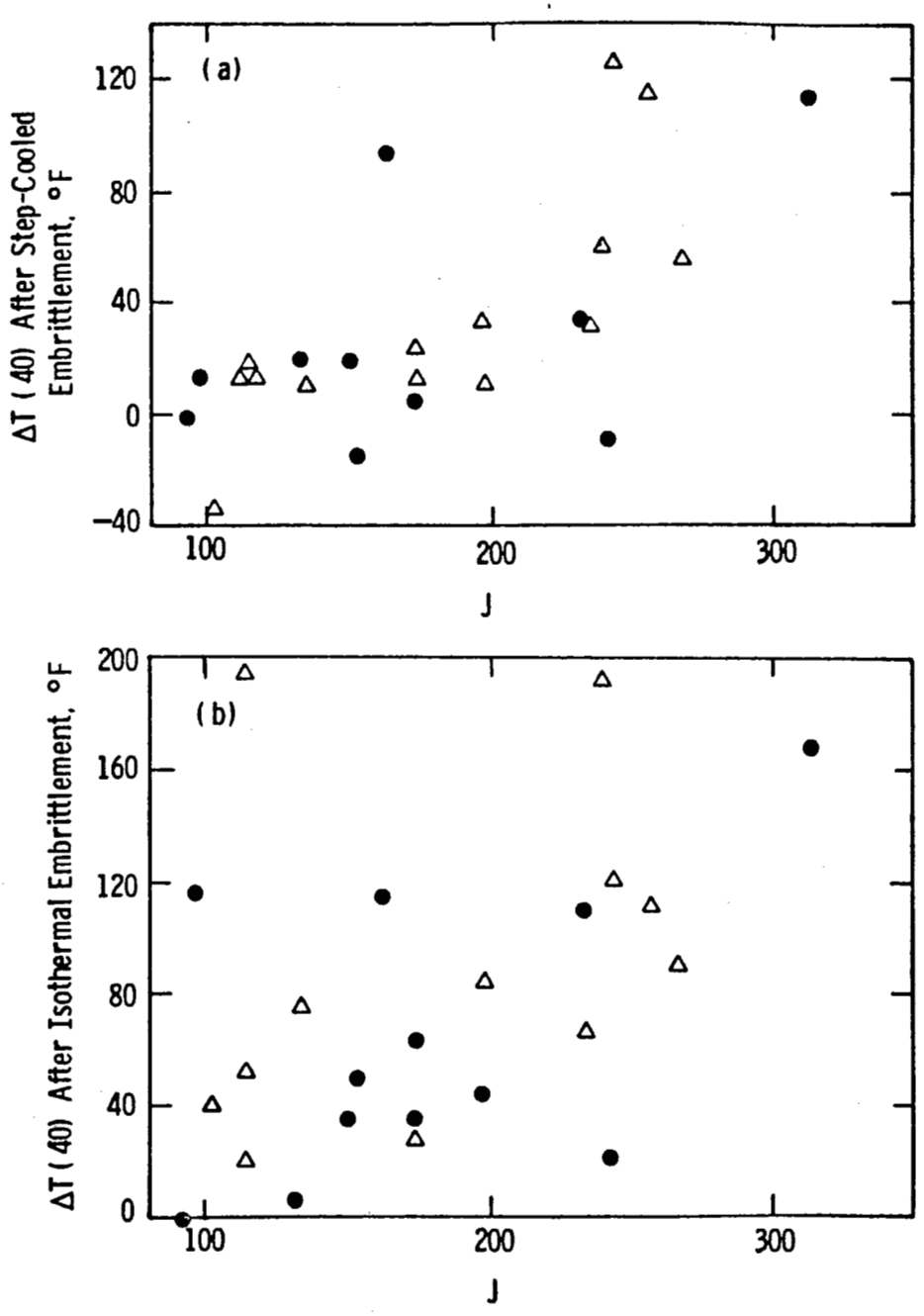

Fig. 4. Shift in the 40 ft-lb Transition Temperature plotted as a function of J - (Mn + Si)(P + Sn) x 10^4
(a) After step-cooled embrittlement
(b) After 20,000 hr isothermal embrittlement
See Table 10. Δ Weld O Plate and Forging

Curve 730339-B

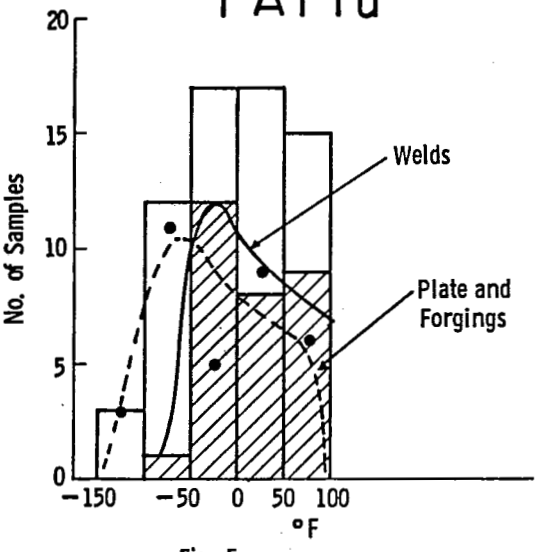

Fig. 5

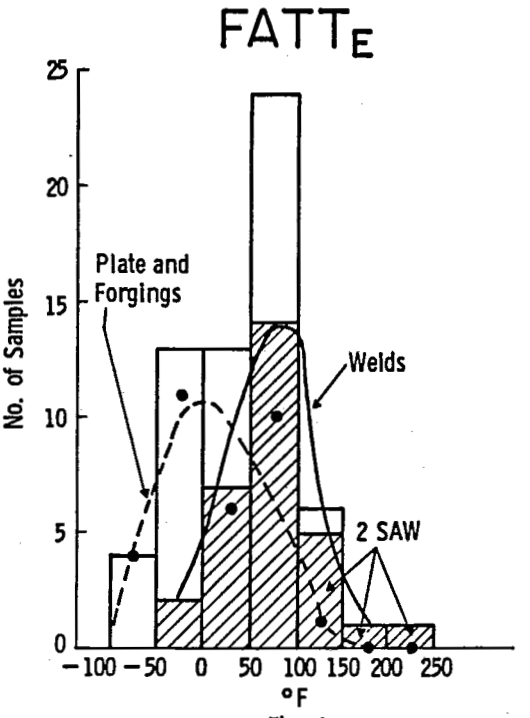

Fig. 6

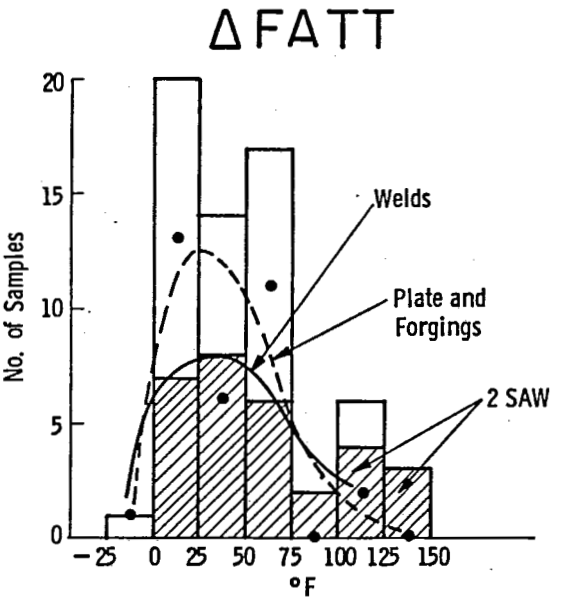

Fig. 7

Figs. 5, 6, 7. Historgrams of fracture appearance transition temperatures in the "as received" ($FATT_U$), step cooled embrittled ($FATT_E$) and charge in transition temperature $\Delta FATT_{E-U}$ respectively for all samples. Welds are depicted by hatched areas. The dots represent plate and forgings.

B. Shaw
d.m.s. - e.s.

Curve 730338-B

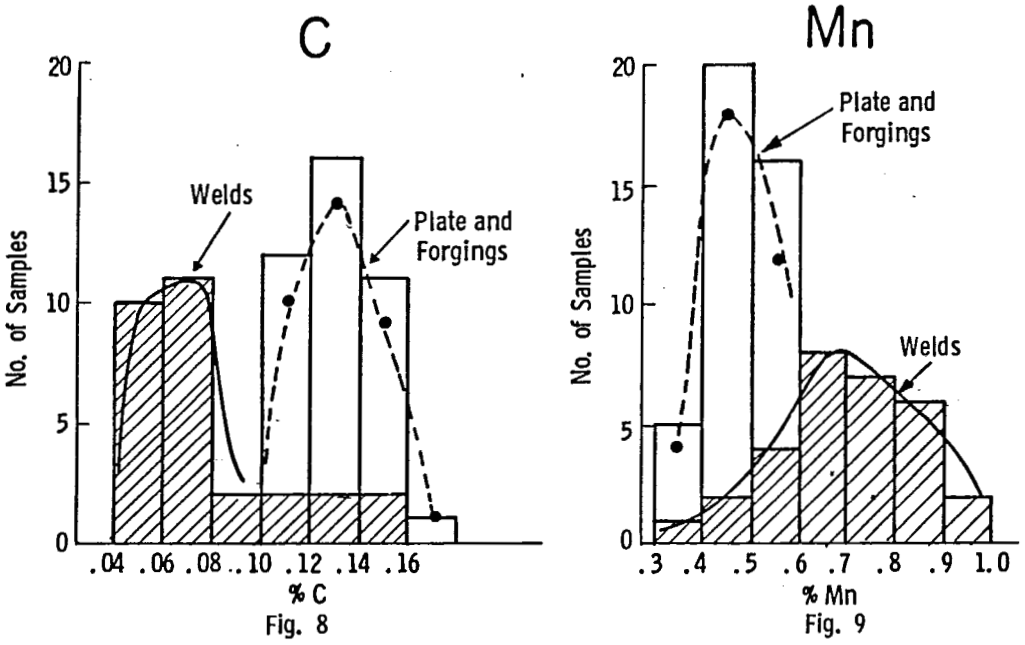

Fig. 8

Fig. 9

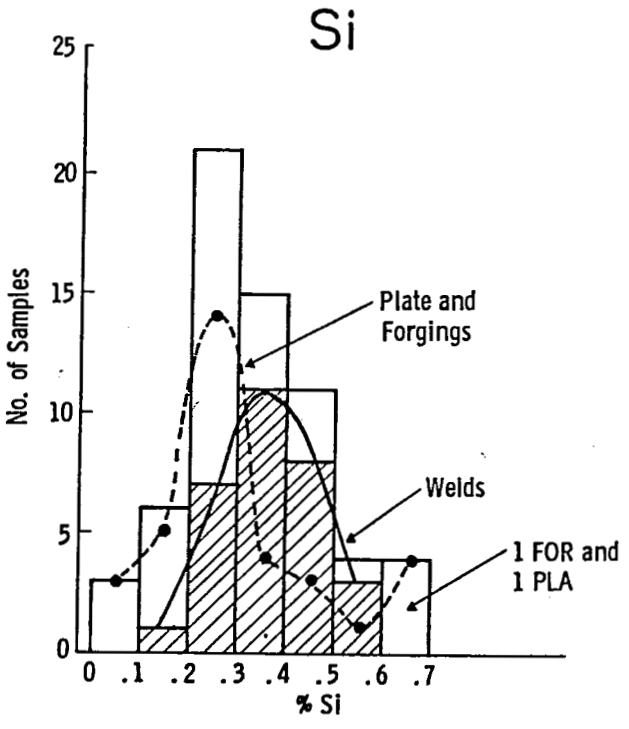

Fig. 10

Figs. 8, 9, 10. Histograms of carbon manganese and silicon for all samples respectively for all samples. Welds are depicted by hatched areas and the dots represent plate and forgings.

B. Shaw
d.m.s.

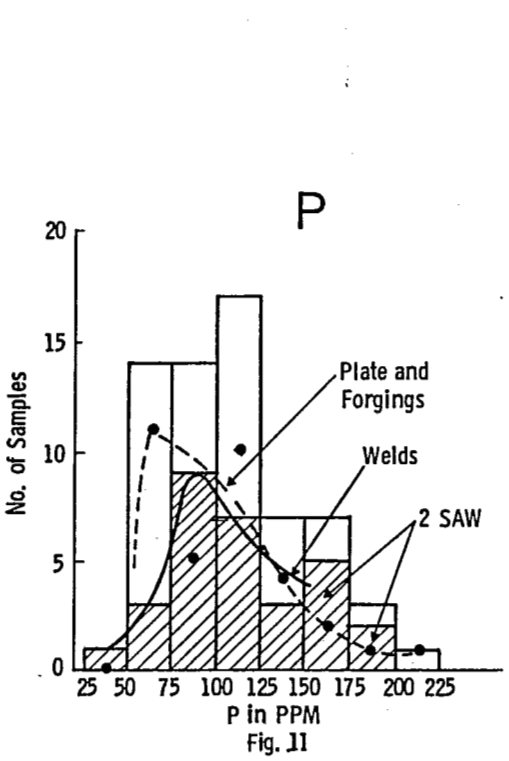

Fig. 11

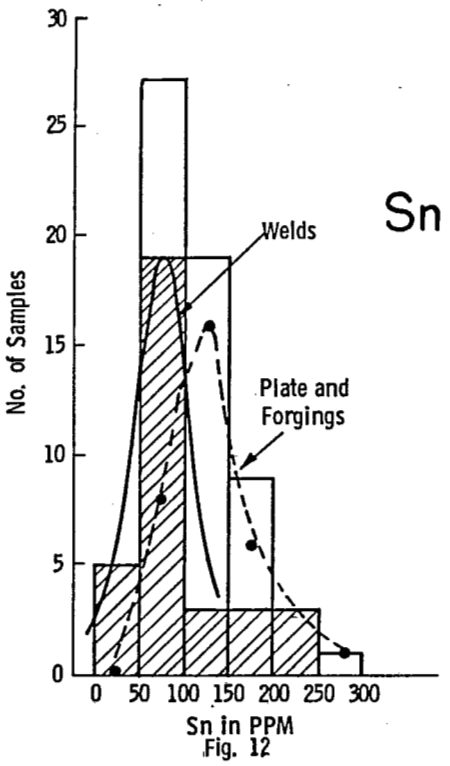

Fig. 12

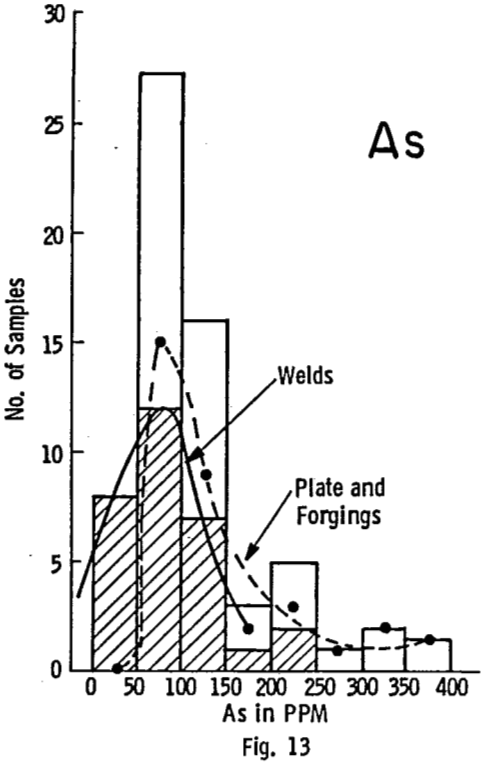

Fig. 13

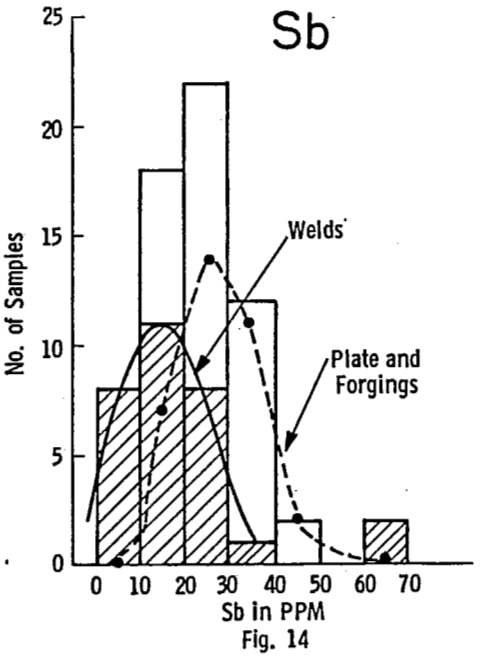

Fig. 14

Figs. 11, 12, 13 and 14. Histograms of the tramp elements P, Sn, As and Sb respectively for all samples. Welds are depicted by hatched areas and the dots represent the plate and forgings.

Curve 730341-C

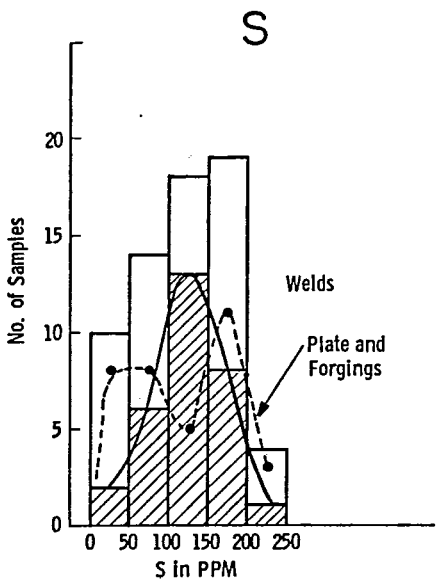

Fig. 15

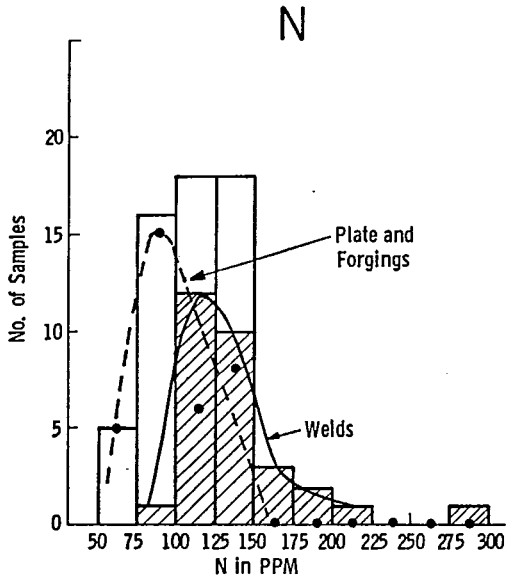

Fig. 16

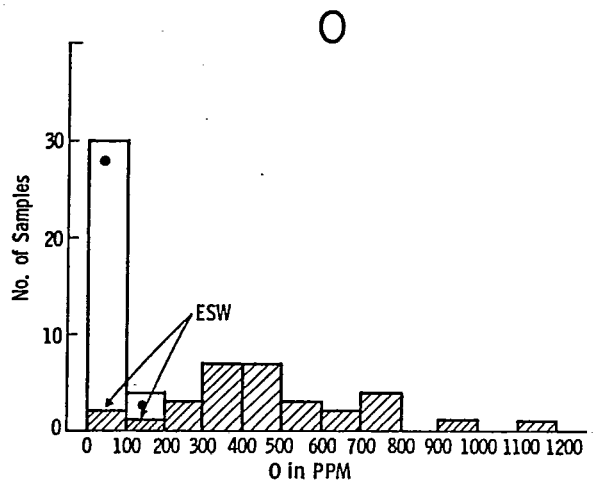

Fig. 17

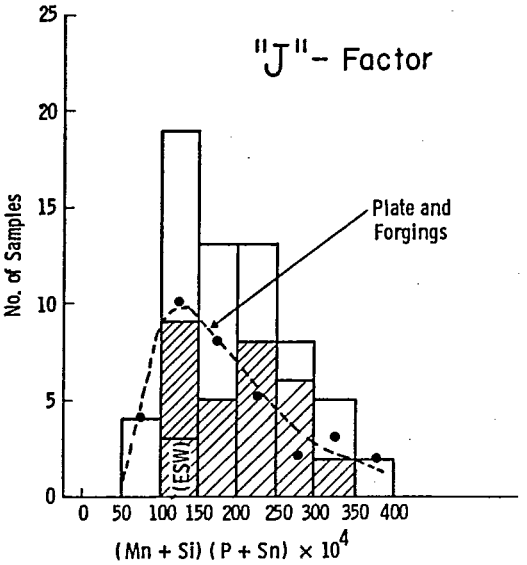

Fig. 18

Figs. 15, 16, 17, 18. Histograms of the elements S, N and O and the embrittlement factor J respectively for all samples. The welds are depicted by the hatched areas and the dots represent the plate and forgings.

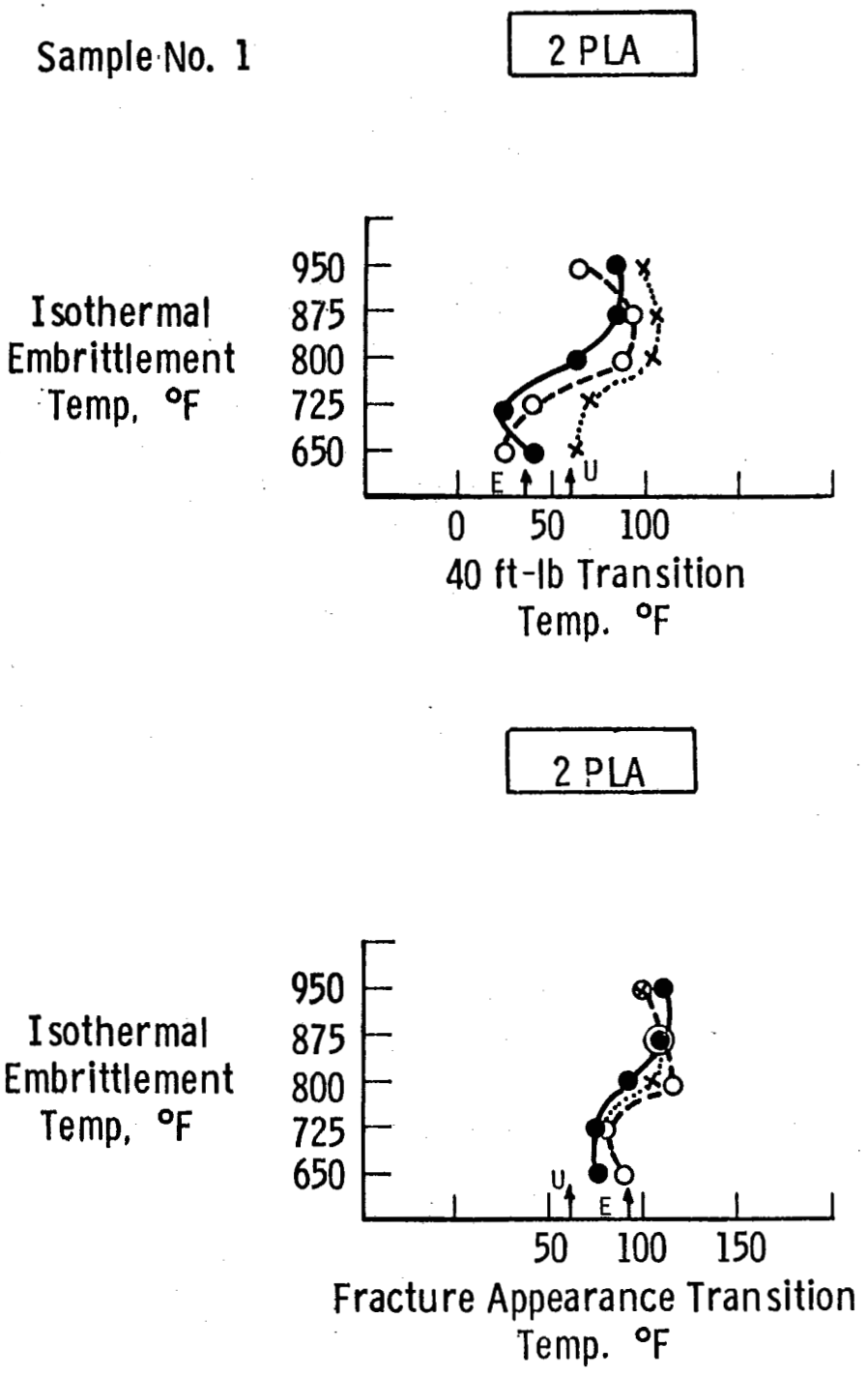

Fig. 19 The 40 ft-lb transition temperature and fracture appearance transition temperature plotted as a function of the isothermal annealing temperature after 1,000 ●, 10,000 ○, and 20,000 hr X. The bench mark ↑ U represents the starting condition and ↑ E the step-cooled embrittled condition.

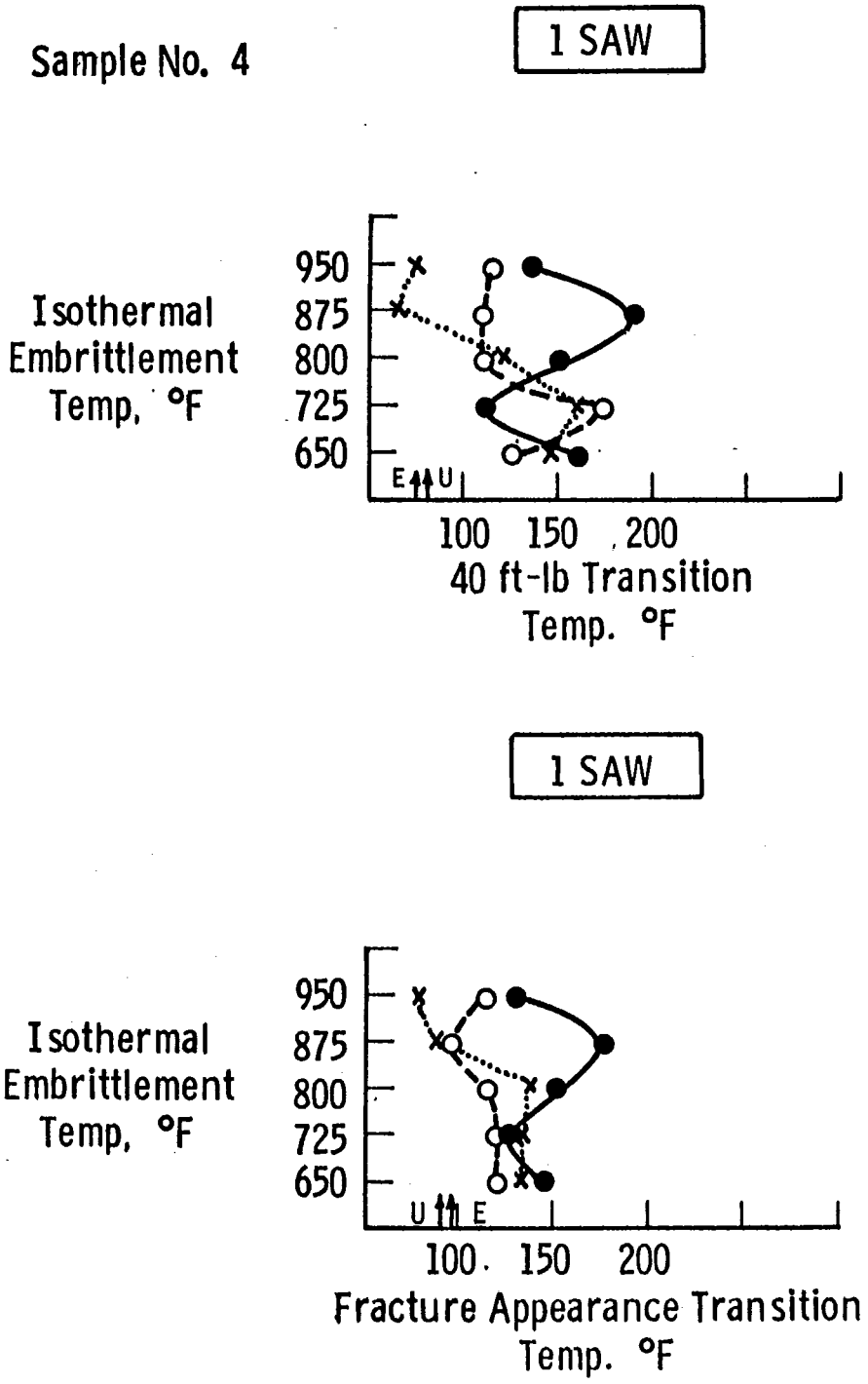

Fig. 20 The 40 ft-lb transition temperature and fracture appearance transition temperature plotted as a function of the isothermal annealing temperature after 1,000 ●, 10,000 ○, and 20,000 hr X. The bench mark ↑ U represents the starting condition and ↑ E the step-cooled embrittled condition.

Sample No. 9

2 PLA

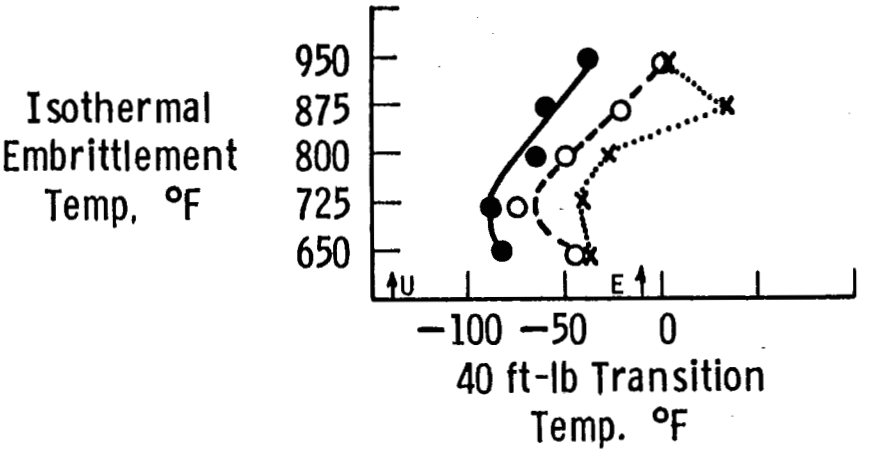

2 PLA

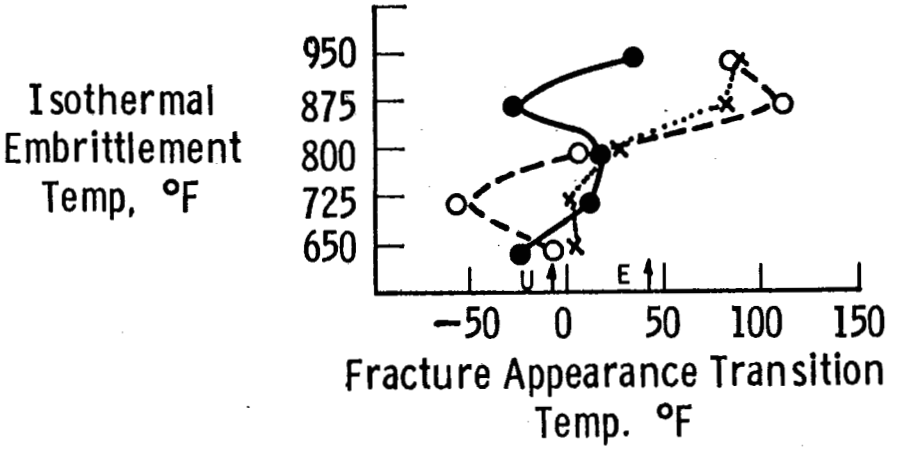

Fig. 21 The 40 ft-lb transition temperature and fracture appearance transition temperature plotted as a function of the isothermal annealing temperature after 1,000 ●, 10,000 ○, and 20,000 hr X. The bench mark ↑ U represents the starting condition and ↑ E the step-cooled embrittled condition.

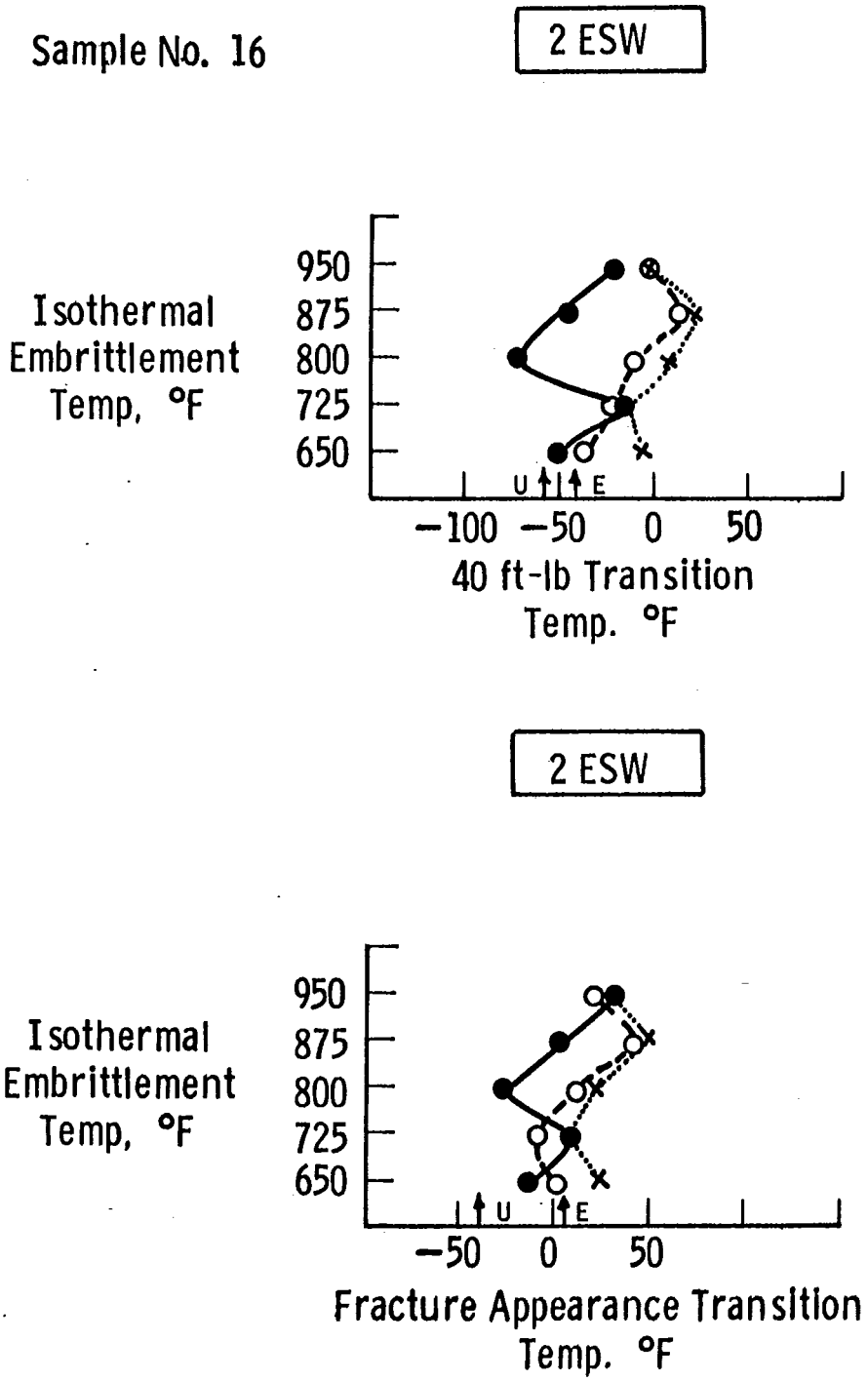

Fig. 22 The 40 ft-lb transition temperature and fracture appearance transition temperature plotted as a function of the isothermal annealing temperature after 1,000 ●, 10,000 ○, and 20,000 hr X. The bench mark ↑ U represents the starting condition and ↑ E the step-cooled embrittled condition.

Sample No. 19

2 SAW

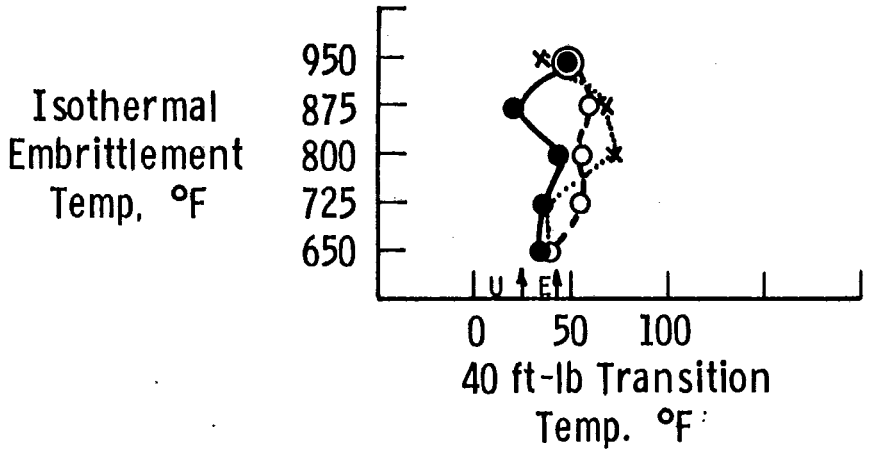

2 SAW

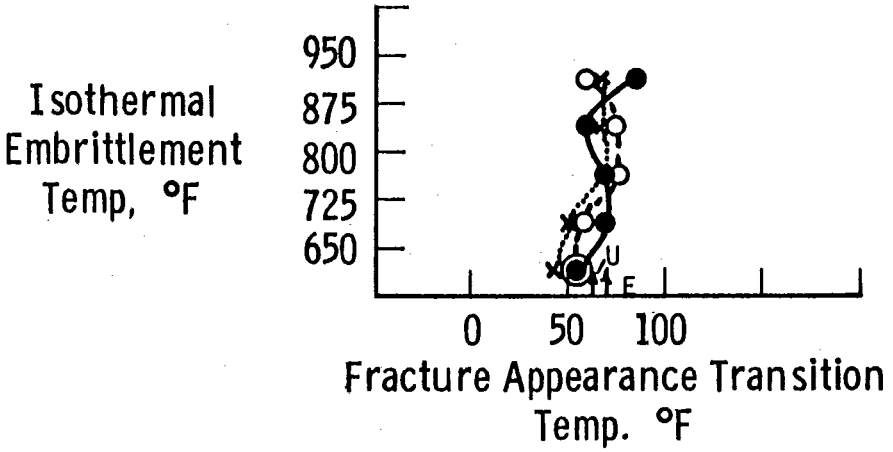

Fig. 23 The 40 ft-lb transition temperature and fracture appearance transition temperature plotted as a function of the isothermal annealing temperature after 1,000 ●, 10,000 ○, and 20,000 hr X. The bench mark ↑ U represents the starting condition and ↑ E the step-cooled embrittled condition.

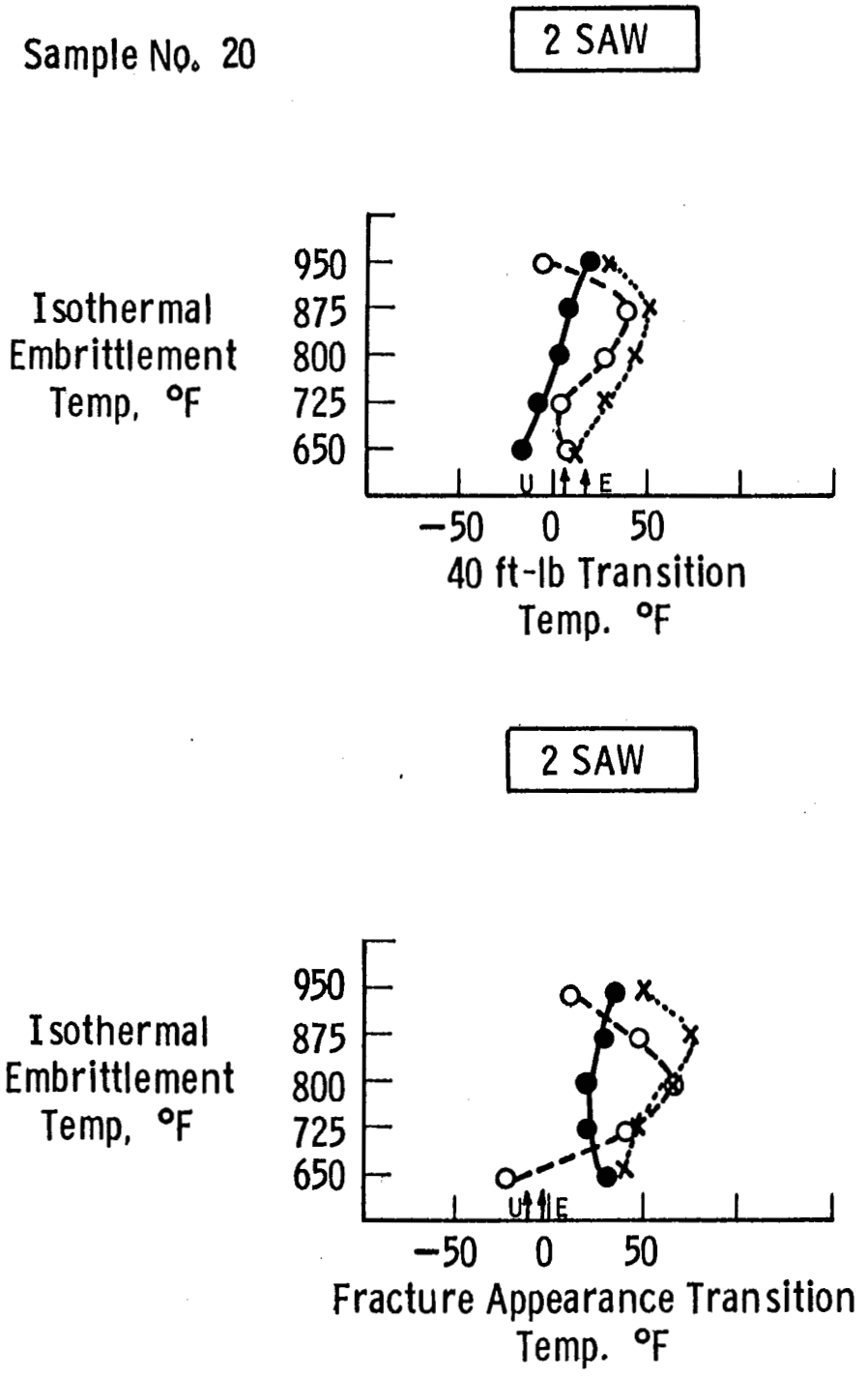

Fig. 24 The 40 ft-lb transition temperature and fracture appearance transition temperature plotted as a function of the isothermal annealing temperature after 1,000 ●, 10,000 ○, and 20,000 hr X. The bench mark ↑ U represents the starting condition and ↑ E the step-cooled embrittled condition.

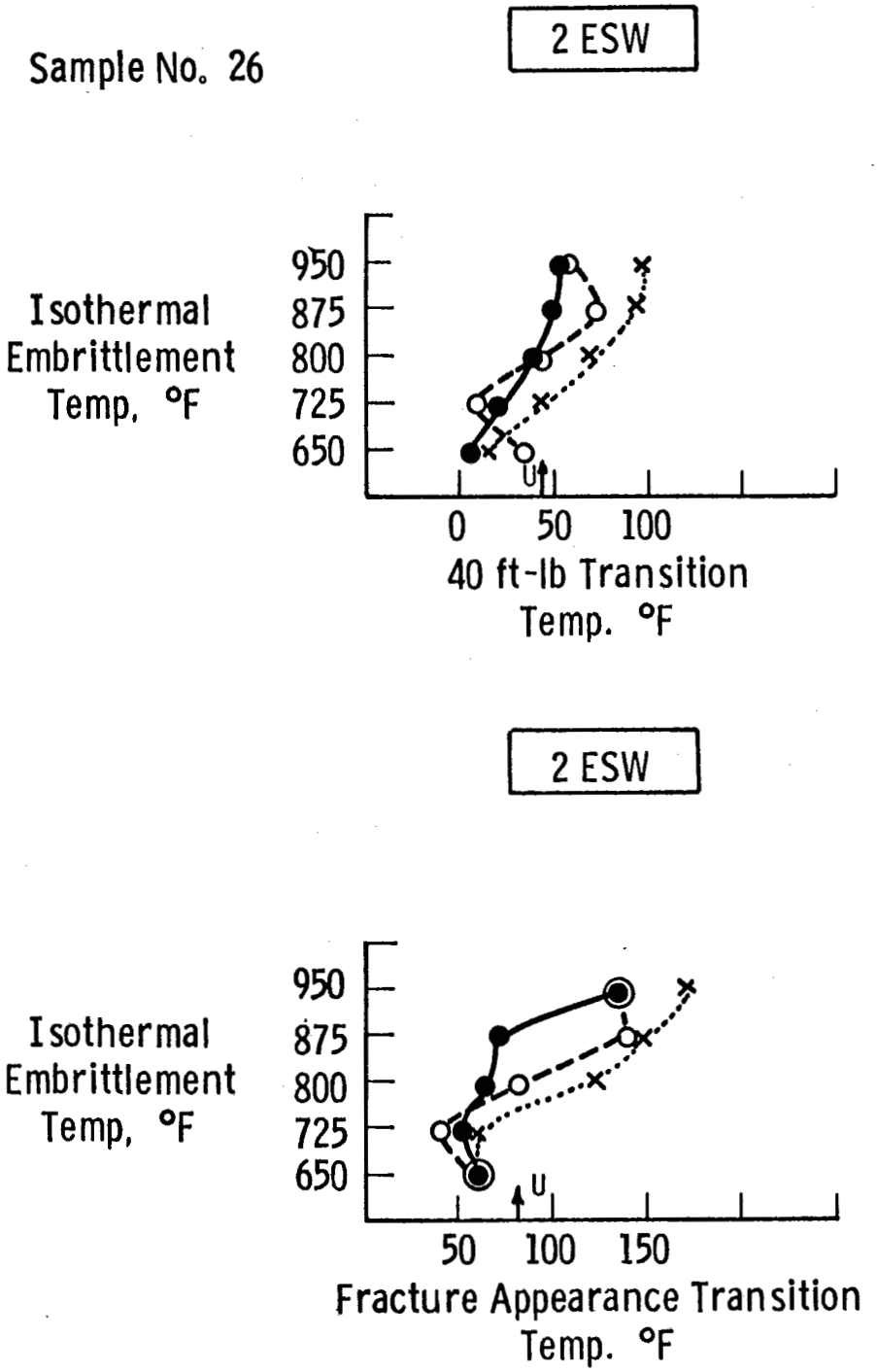

Fig. 25 The 40 ft-lb transition temperature and fracture appearance transition temperature plotted as a function of the isothermal annealing temperature after 1,000 ●, 10,000 ○, and 20,000 hr X. The bench mark ↑ U represents the starting condition.

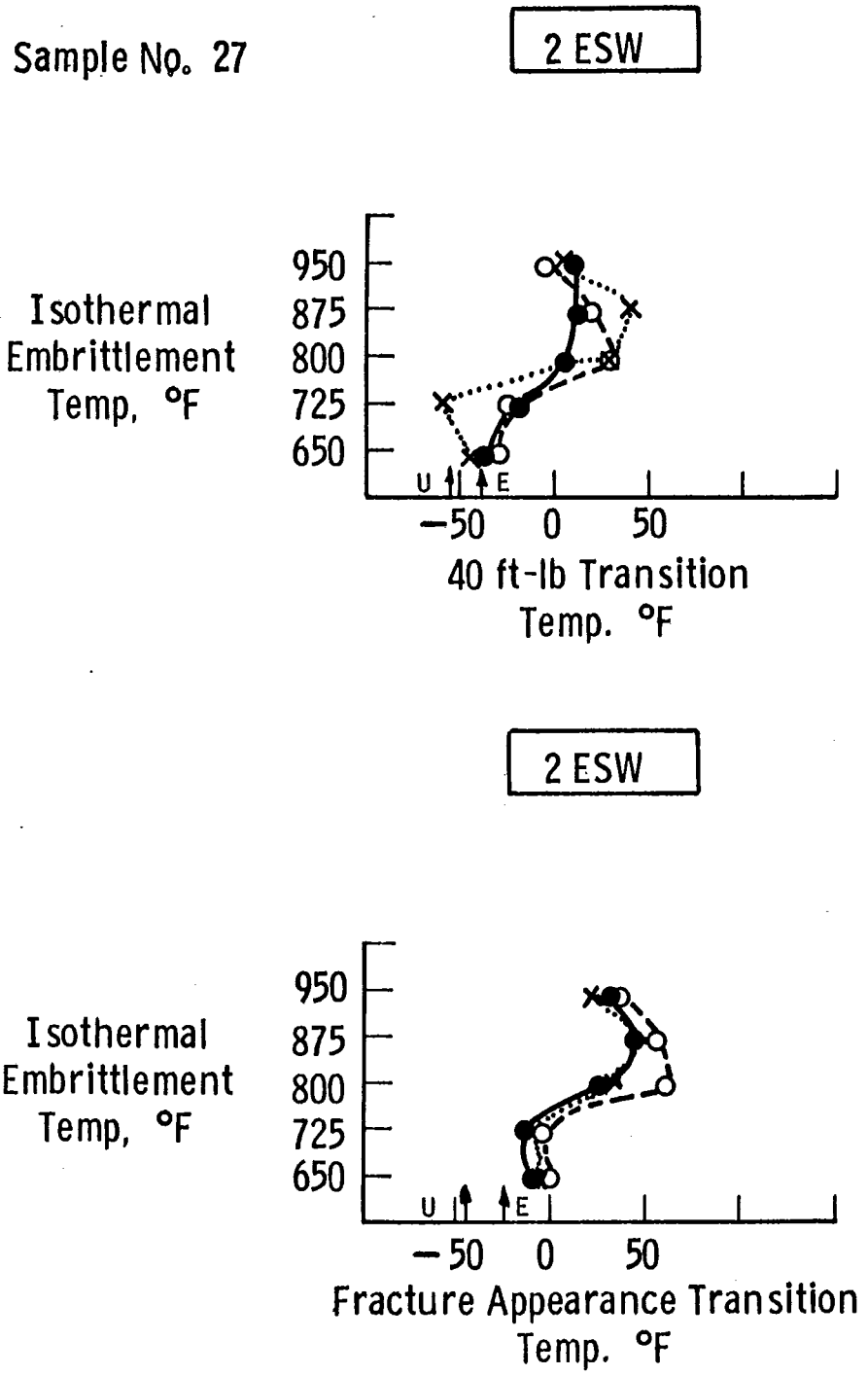

Fig. 26 The 40 ft-lb transition temperature and fracture appearance transition temperature plotted as a function of the isothermal annealing temperature after 1,000 ●, 10,000 ○, and 20,000 hr X. The bench mark ↑ U represents the starting condition and ↑ E the step-cooled embrittled condition.

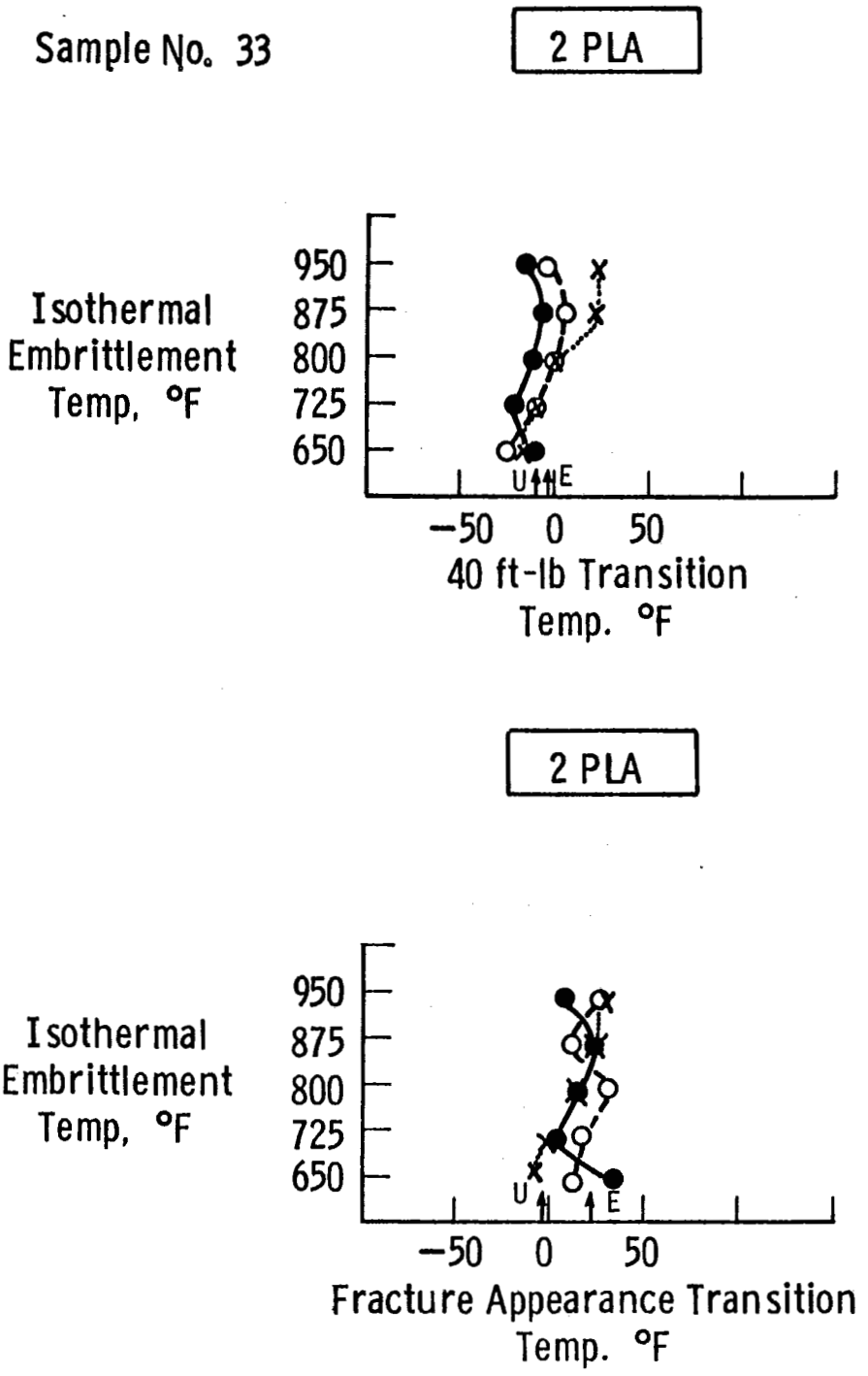

Fig. 27 The 40 ft-lb transition temperature and fracture appearance transition temperature plotted as a function of the isothermal annealing temperature after 1,000 •, 10,000 ○, and 20,000 hr X. The bench mark ↑ U represents the starting condition and ↑ E the step-cooled embrittled condition.

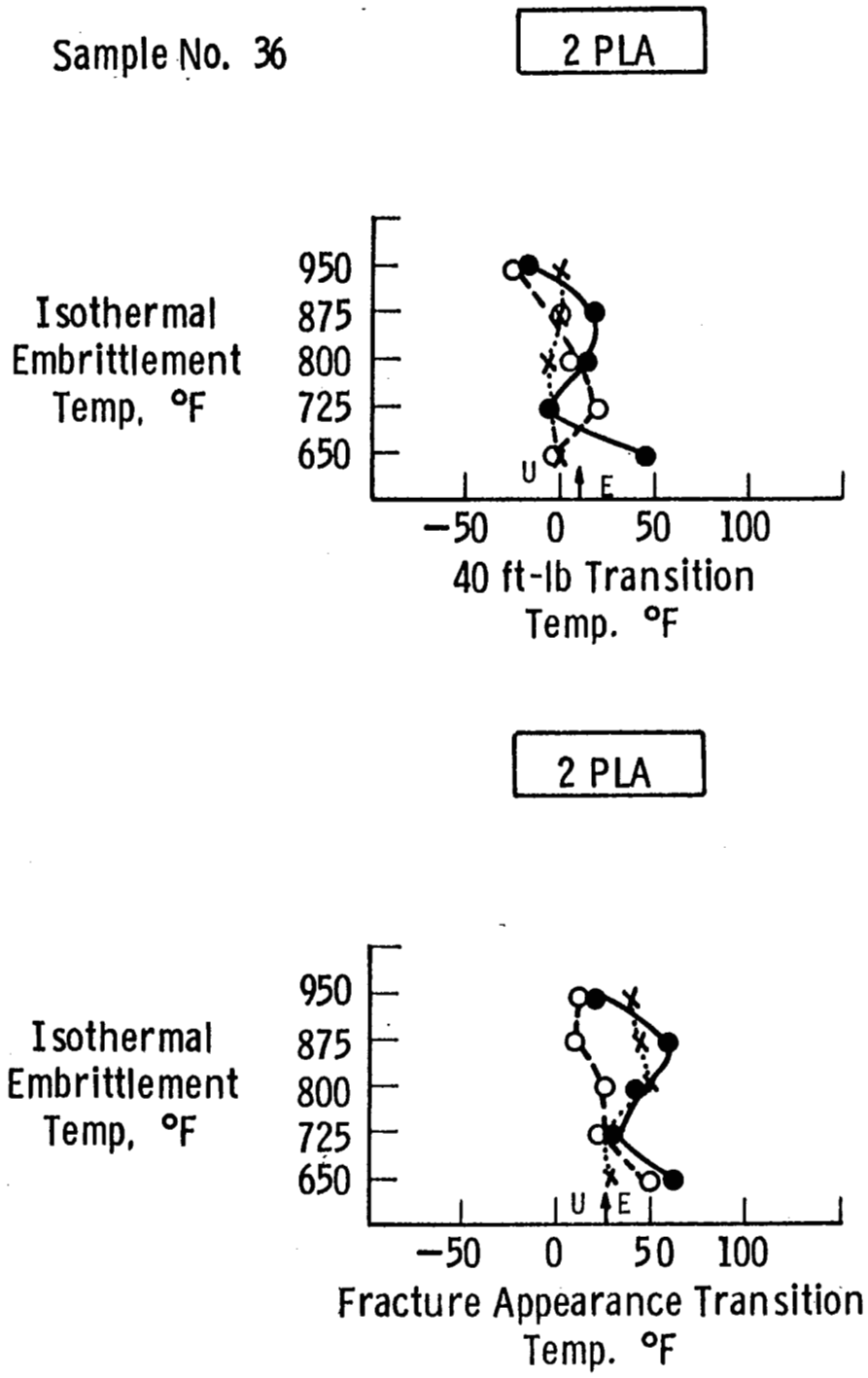

Fig. 28 The 40 ft-lb transition temperature and fracture appearance transition temperature plotted as a function of the isothermal annealing temperature after 1,000 ●, 10,000 ○, and 20,000 hr X. The bench mark ↑ U represents the starting condition and ↑ E the step-cooled embrittled condition.

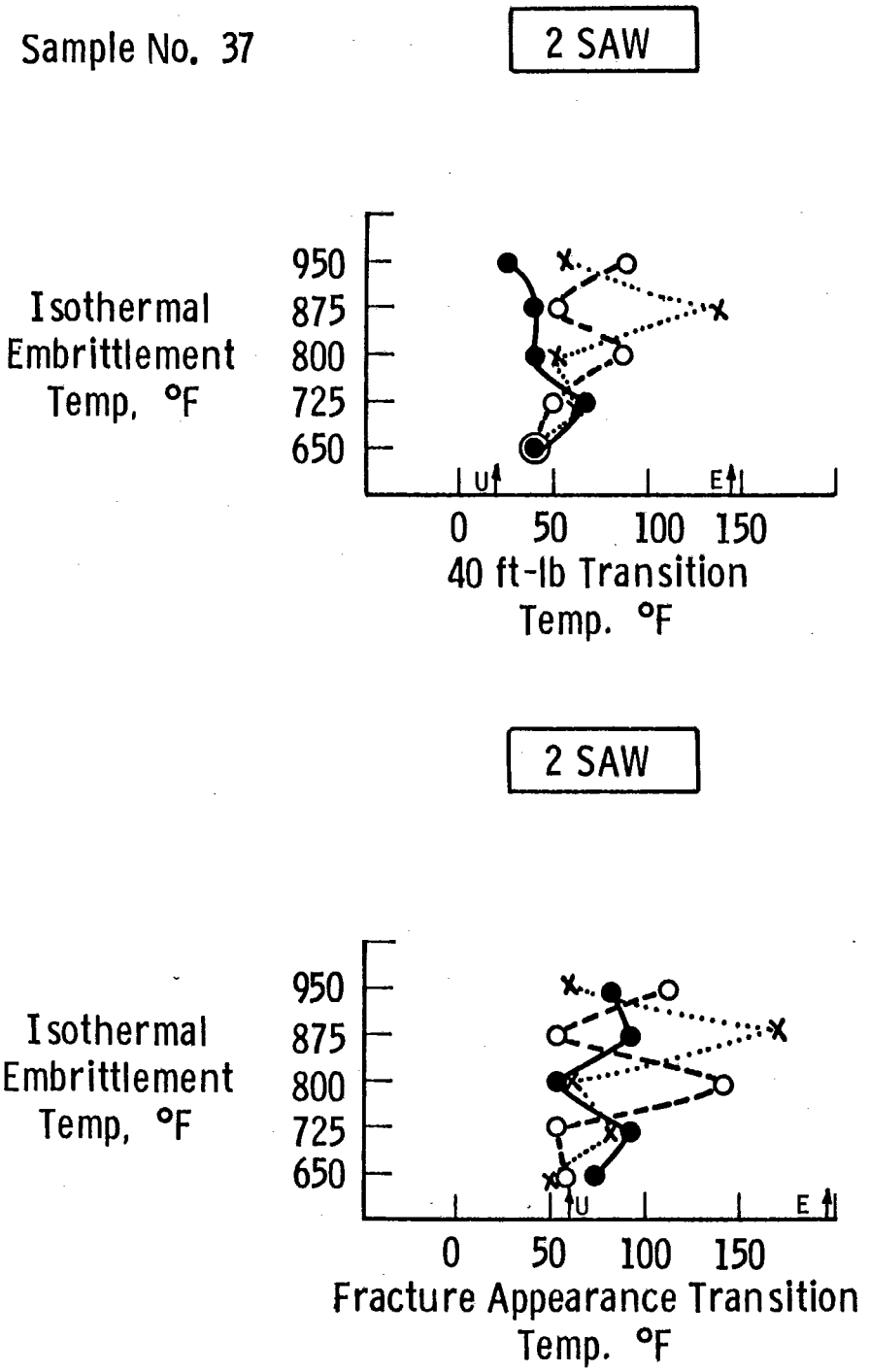

Fig. 29 The 40 ft-lb transition temperature and fracture appearance transition temperature plotted as a function of the isothermal annealing temperature after 1,000 ●, 10,000 ○, and 20,000 hr X. The bench mark ↑ U represents the starting condition and ↑ E the step-cooled embrittled condition.

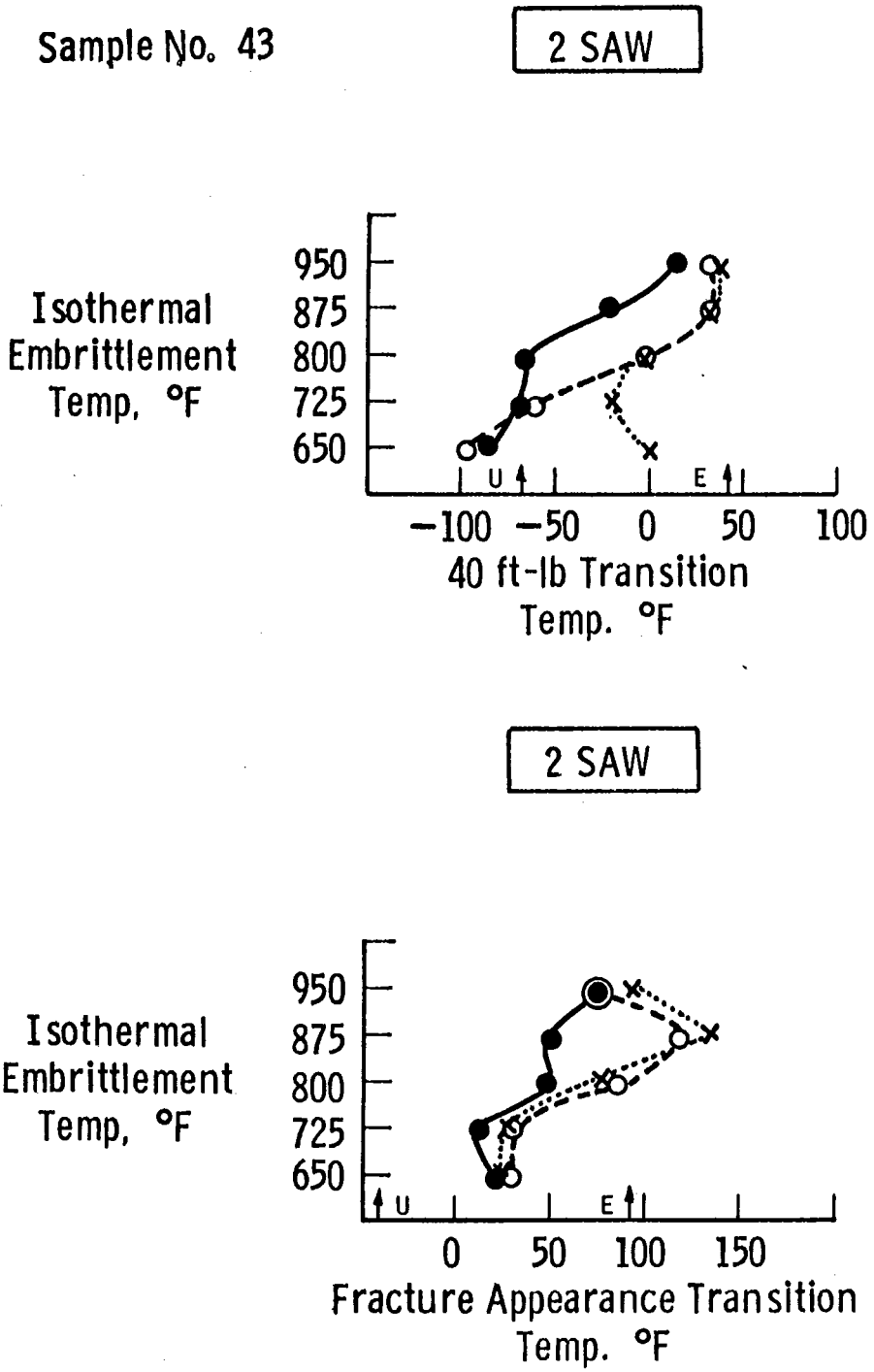

Fig. 30 The 40 ft-lb transition temperature and fracture appearance transition temperature plotted as a function of the isothermal annealing temperature after 1,000 ⊙, 10,000 ○, and 20,000 hr X. The bench mark ↑ U represents the starting condition and ↑ E the step-cooled embrittled condition.

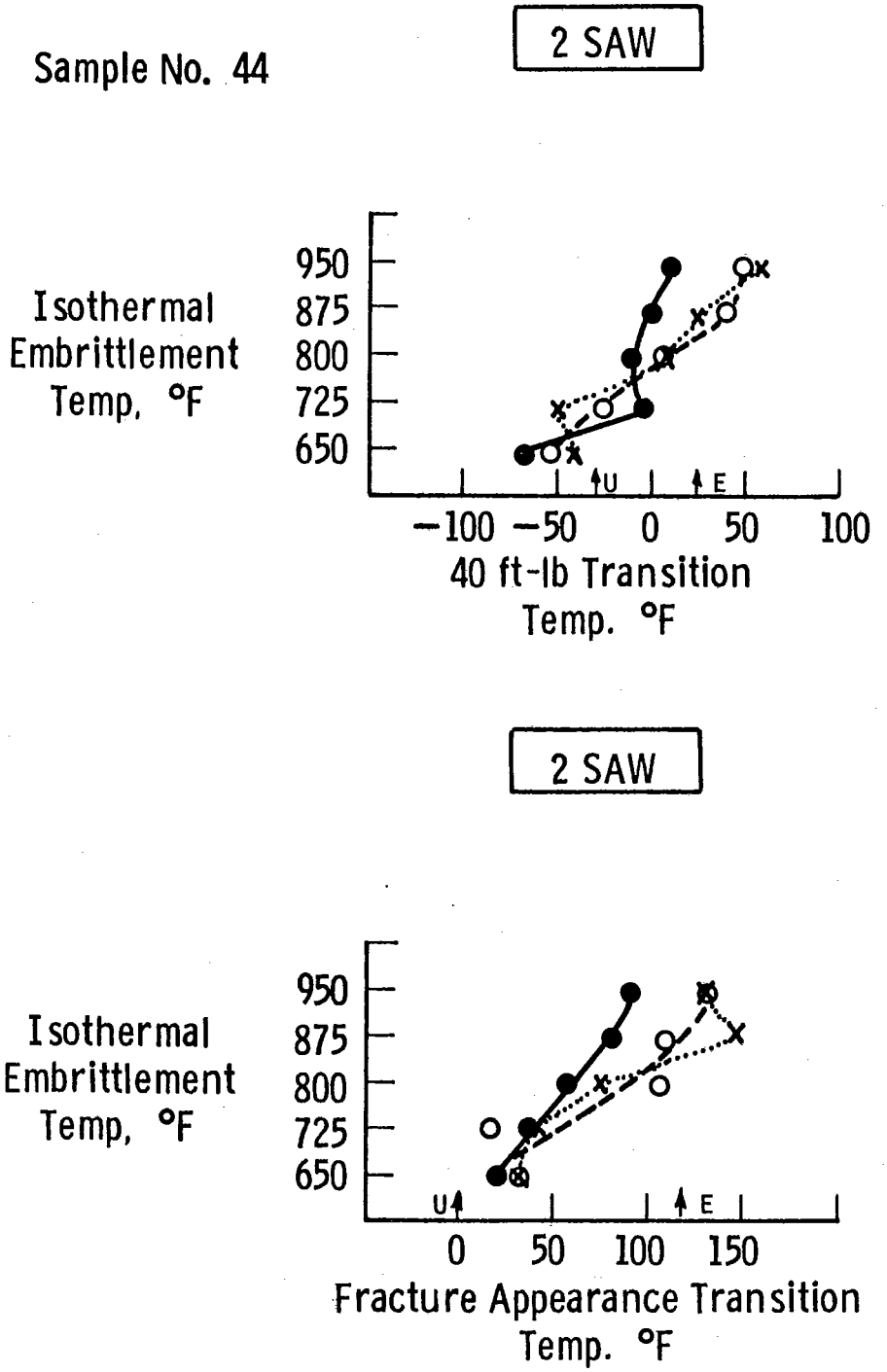

Fig. 31 The 40 ft-lb transition temperature and fracture appearance transition temperature plotted as a function of the isothermal annealing temperature after 1,000 ●, 10,000 ○, and 20,000 hr X. The bench mark ↑ U represents the starting condition and ↑ E the step-cooled embrittled condition.

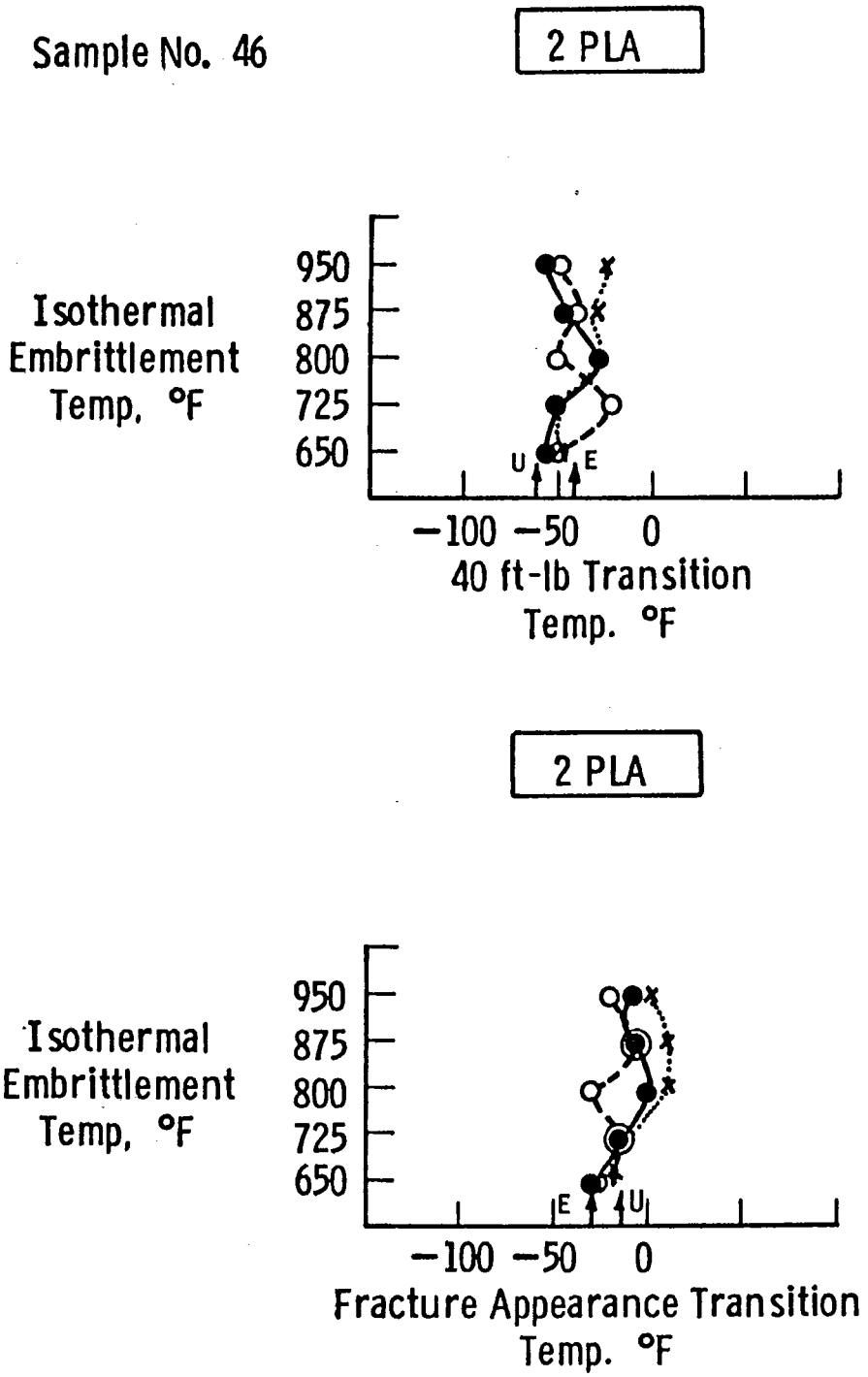

Fig. 32 The 40 ft-lb transition temperature and fracture appearance transition temperature plotted as a function of the isothermal annealing temperature after 1,000 ●, 10,000 ○, and 20,000 hr X. The bench mark ↑ U represents the starting condition and ↑ E the step-cooled embrittled condition.

Sample No. 47

2 PLA

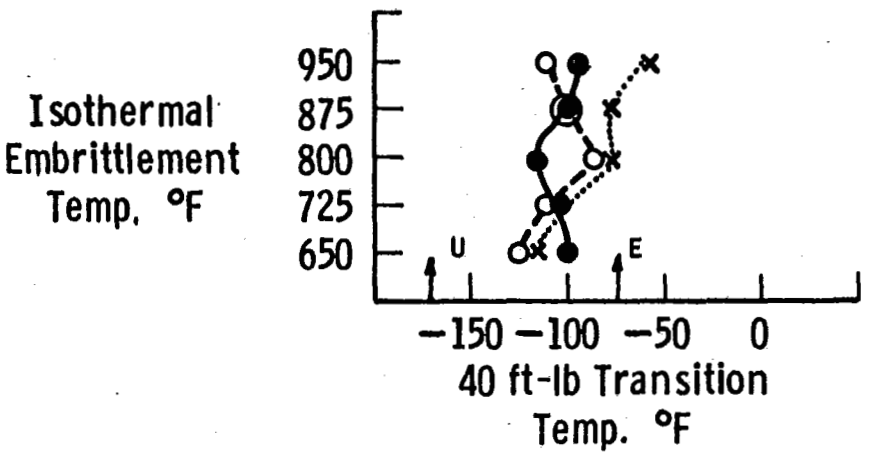

2 PLA

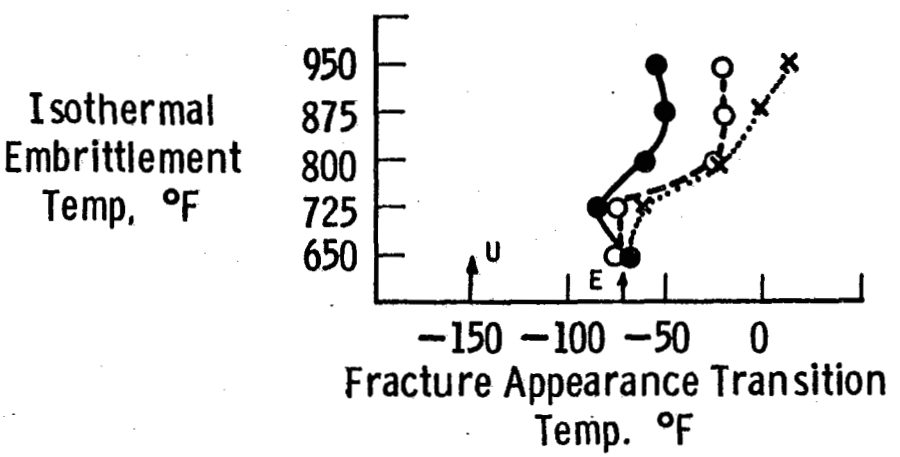

Fig. 33 The 40 ft-lb transition temperature and fracture appearance transition temperature plotted as a function of the isothermal annealing temperature after 1,000 ●, 10,000 ○, and 20,000 hr X. The bench mark ↑ U represents the starting condition and ↑ E the step-cooled embrittled condition.

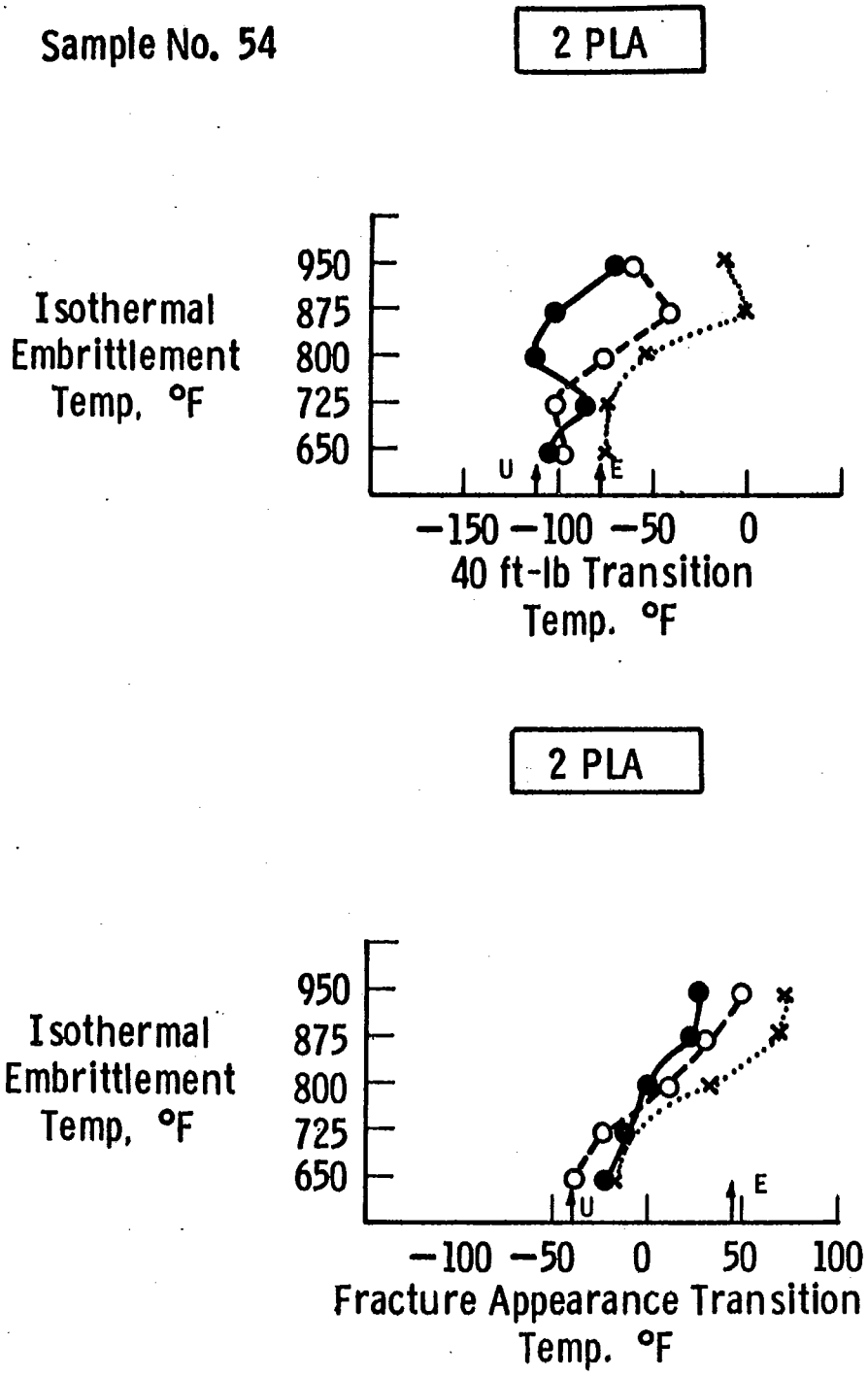

Fig. 34 The 40 ft-lb transition temperature and fracture appearance transition temperature plotted as a function of the isothermal annealing temperature after 1,000 ●, 10,000 ○, and 20,000 hr X. The bench mark ↑ U represents the starting condition and ↑ E the step-cooled embrittled condition.

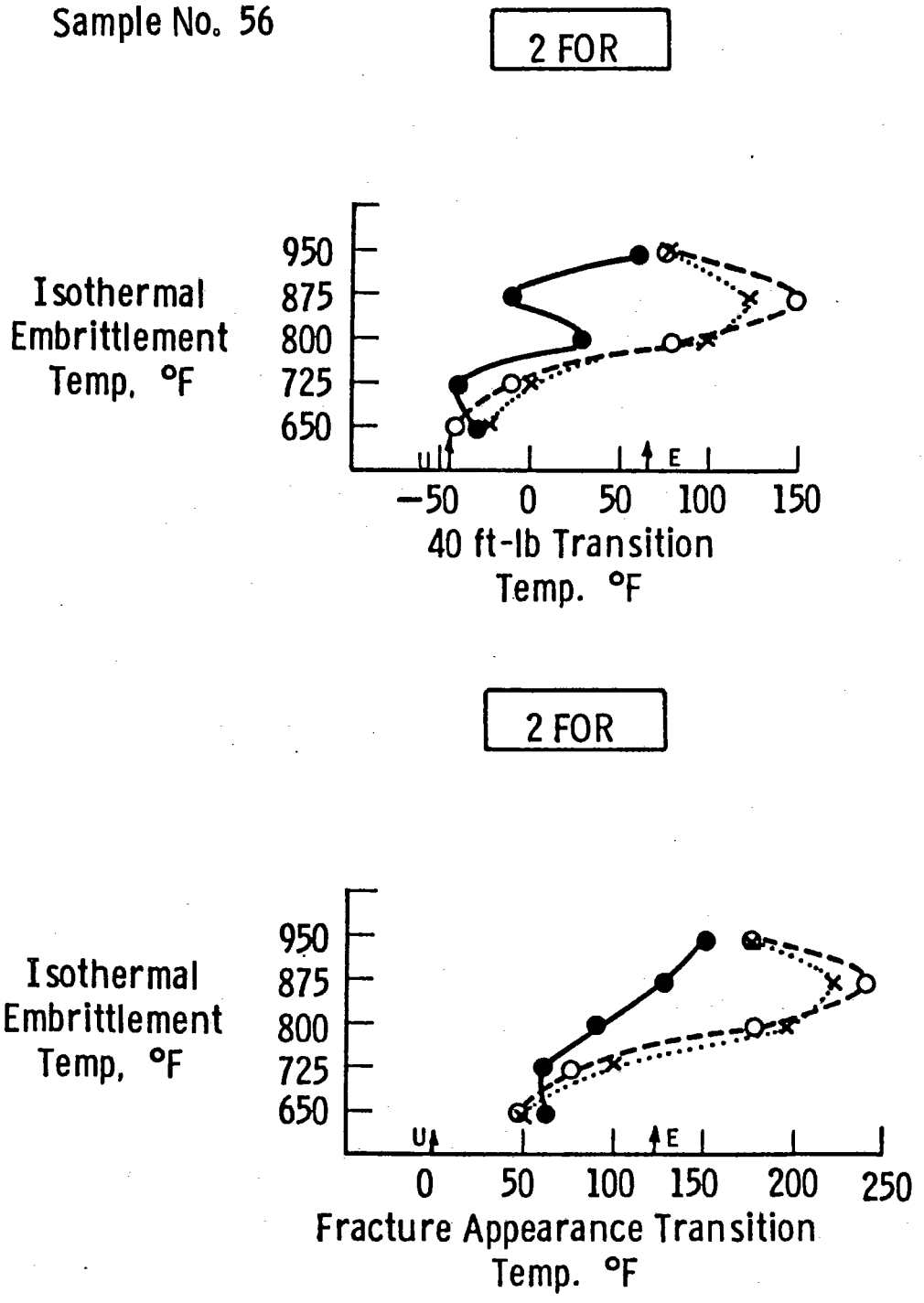

Fig. 35 The 40 ft-lb transition temperature and fracture appearance transition temperature plotted as a function of the isothermal annealing temperature after 1,000 •, 10,000 ○, and 20,000 hr X. The bench mark ↑ U represents the starting condition and ↑ E the step-cooled embrittled condition.

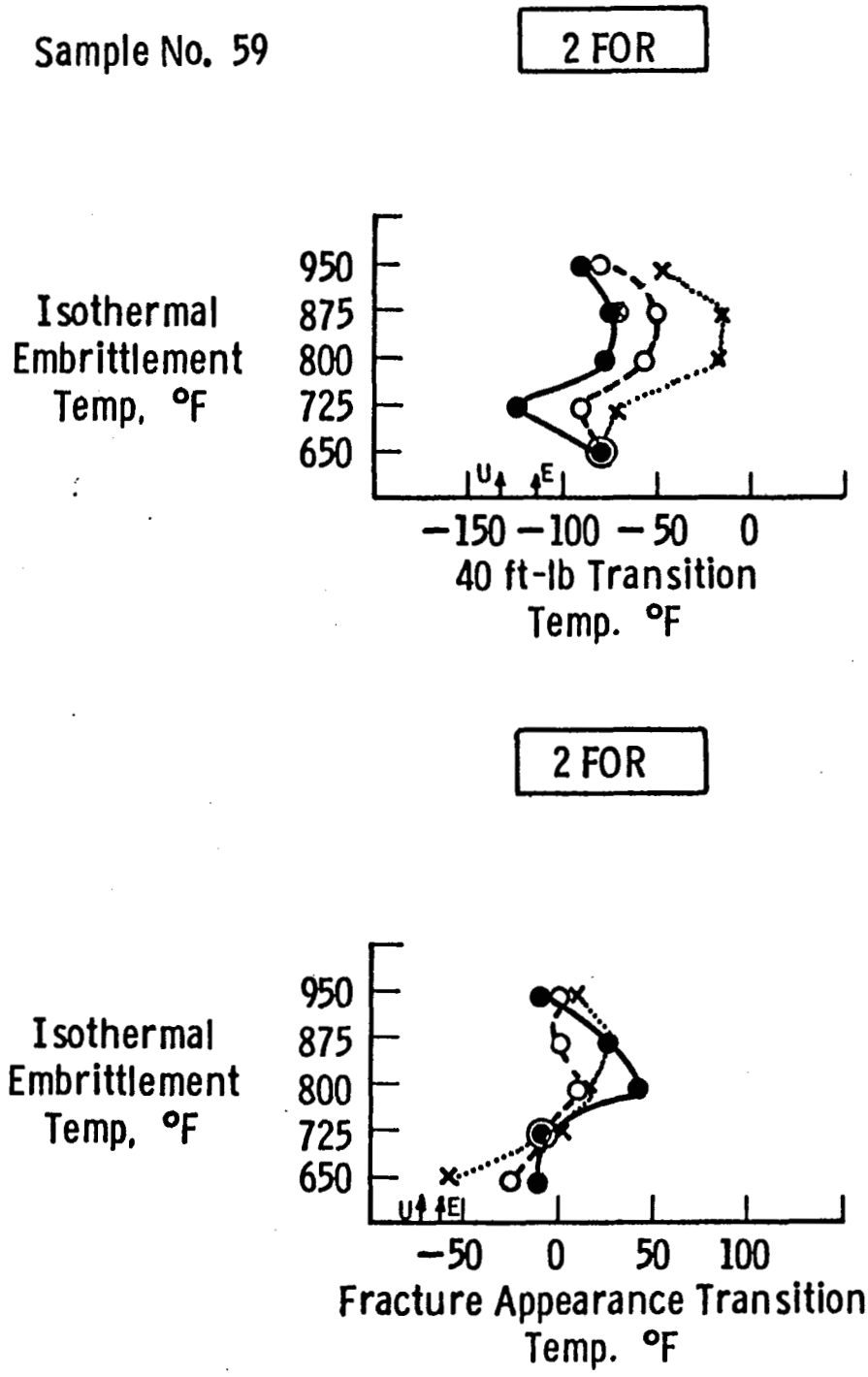

Fig. 36 The 40 ft-lb transition temperature and fracture appearance transition temperature plotted as a function of the isothermal annealing temperature after 1,000 •, 10,000 ○, and 20,000 hr X. The bench mark ↑ U represents the starting condition and ↑ E the step-cooled embrittled condition.

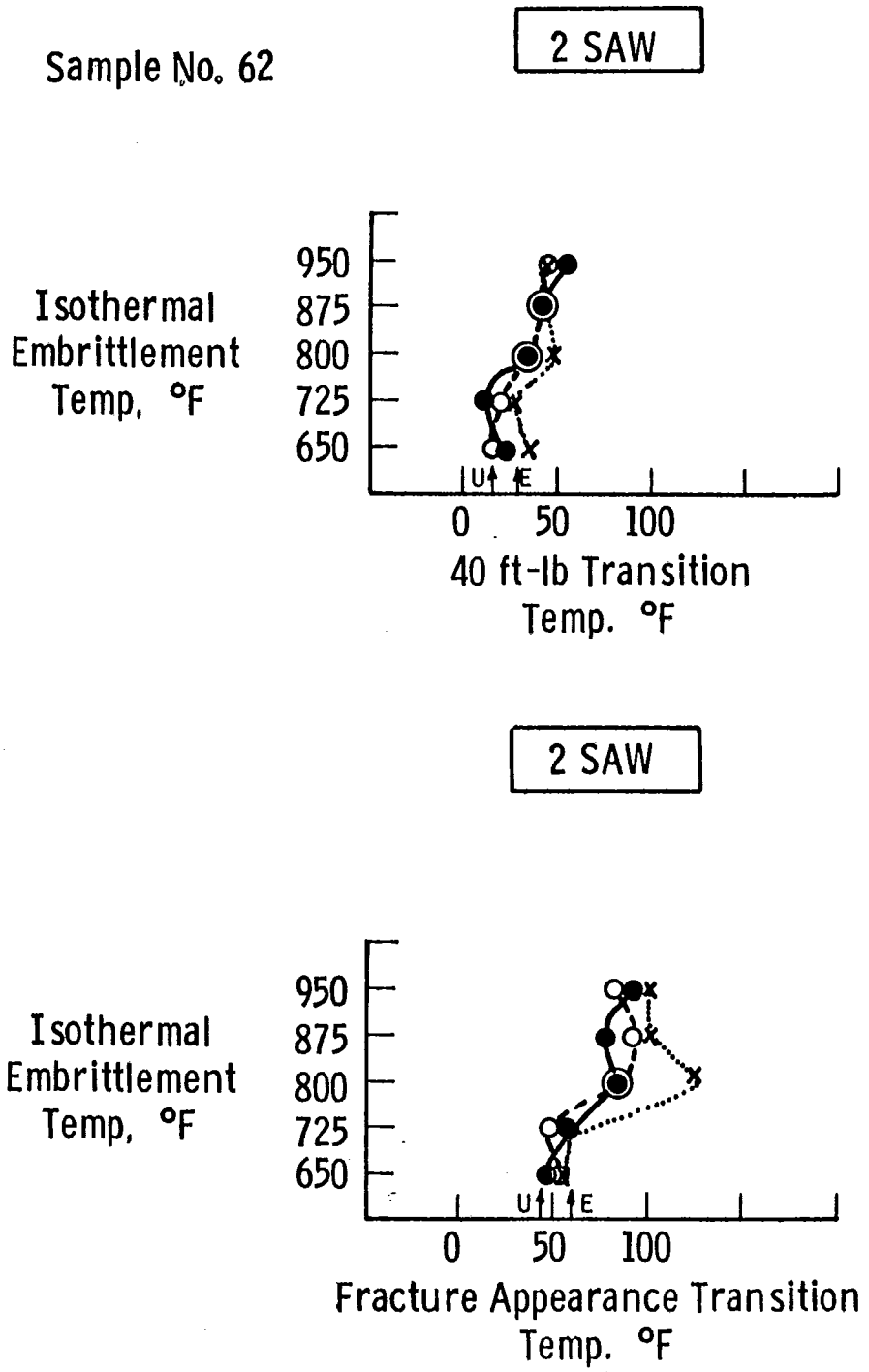

Fig. 37 The 40 ft-lb transition temperature and fracture appearance transition temperature plotted as a function of the isothermal annealing temperature after 1,000 ⊙, 10,000 ○, and 20,000 hr X. The bench mark ↑ U represents the starting condition and ↑ E the step-cooled embrittled condition.

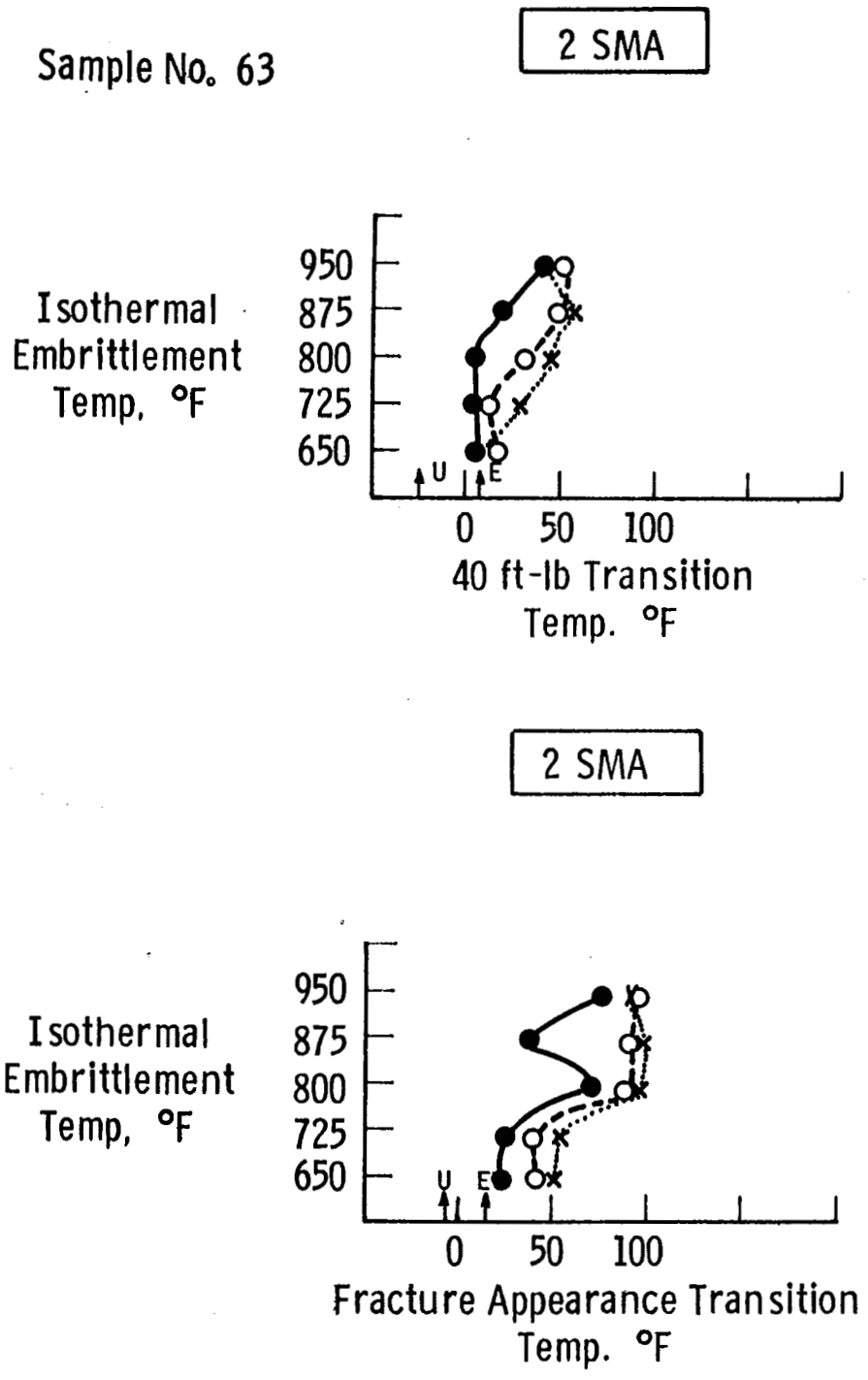

Fig. 38 The 40 ft-lb transition temperature and fracture appearance transition temperature plotted as a function of the isothermal annealing temperature after 1,000 ●, 10,000 ○, and 20,000 hr X. The bench mark ↑ U represents the starting condition and ↑ E the step-cooled embrittled condition.

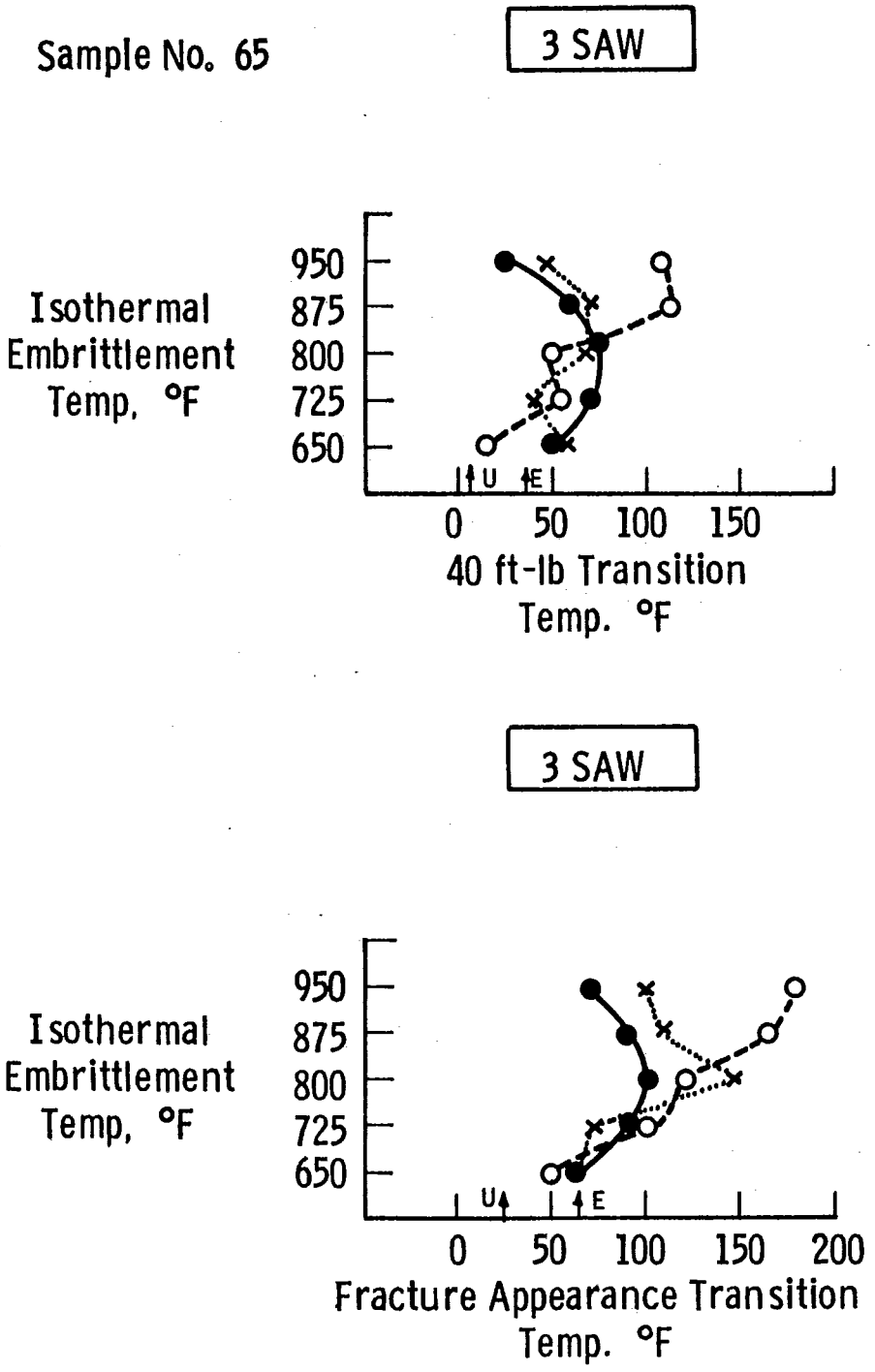

Fig. 39 The 40 ft-lb transition temperature and fracture appearance transition temperature plotted as a function of the isothermal annealing temperature after 1,000 ●, 10,000 ○, and 20,000 hr X. The bench mark ↑ U represents the starting condition and ↑ E the step-cooled embrittled condition.

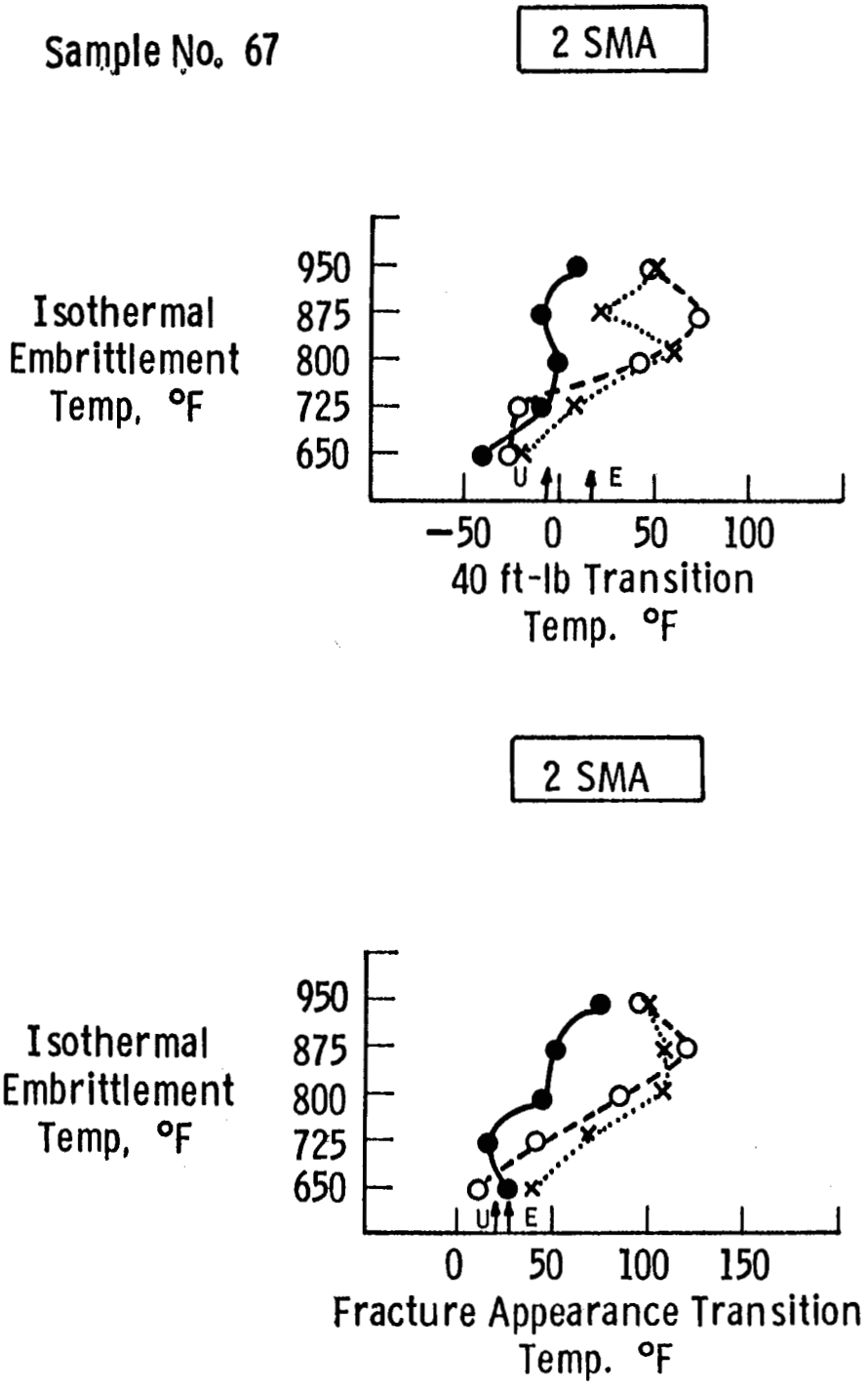

Fig. 40 The 40 ft-lb transition temperature and fracture appearance transition temperature plotted as a function of the isothermal annealing temperature after 1,000 ●, 10,000 ○, and 20,000 hr X. The bench mark ↑ U represents the starting condition and ↑ E the step-cooled embrittled condition.

Sample No. 68

2 SMA

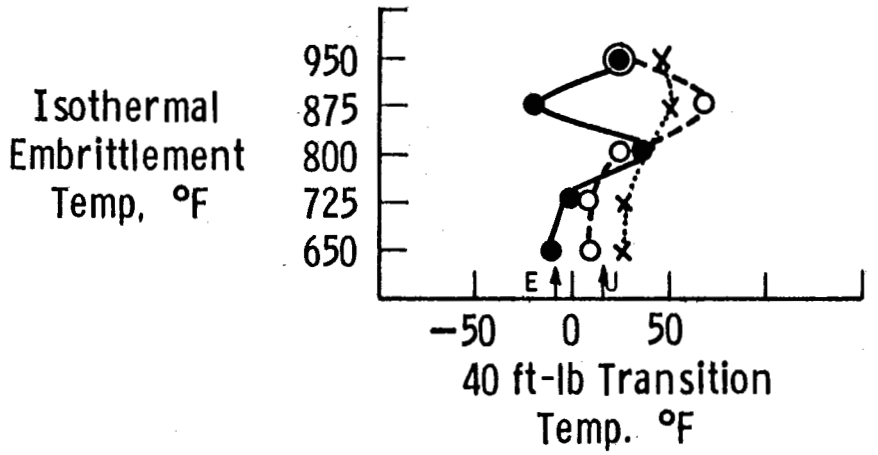

2 SMA

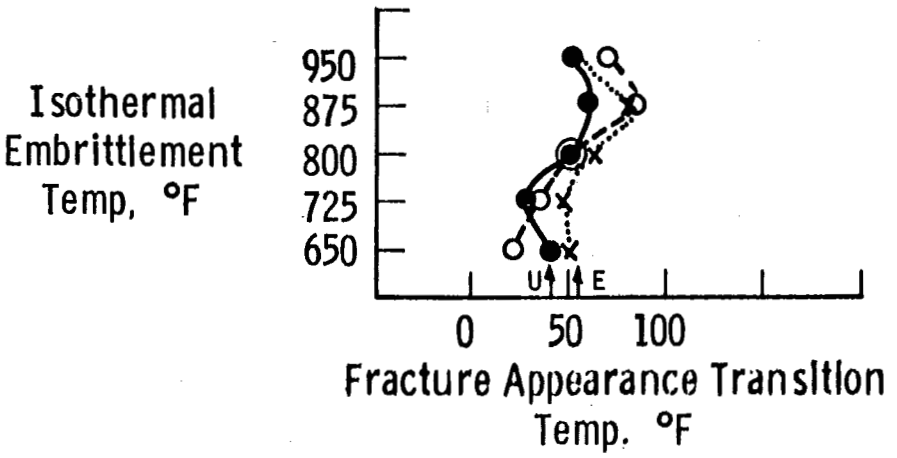

Fig. 41 The 40 ft-lb transition temperature and fracture appearance transition temperature plotted as a function of the isothermal annealing temperature after 1,000 ●, 10,000 ○, and 20,000 hr X. The bench mark ↑ U represents the starting condition and ↑ E the step-cooled embrittled condition.

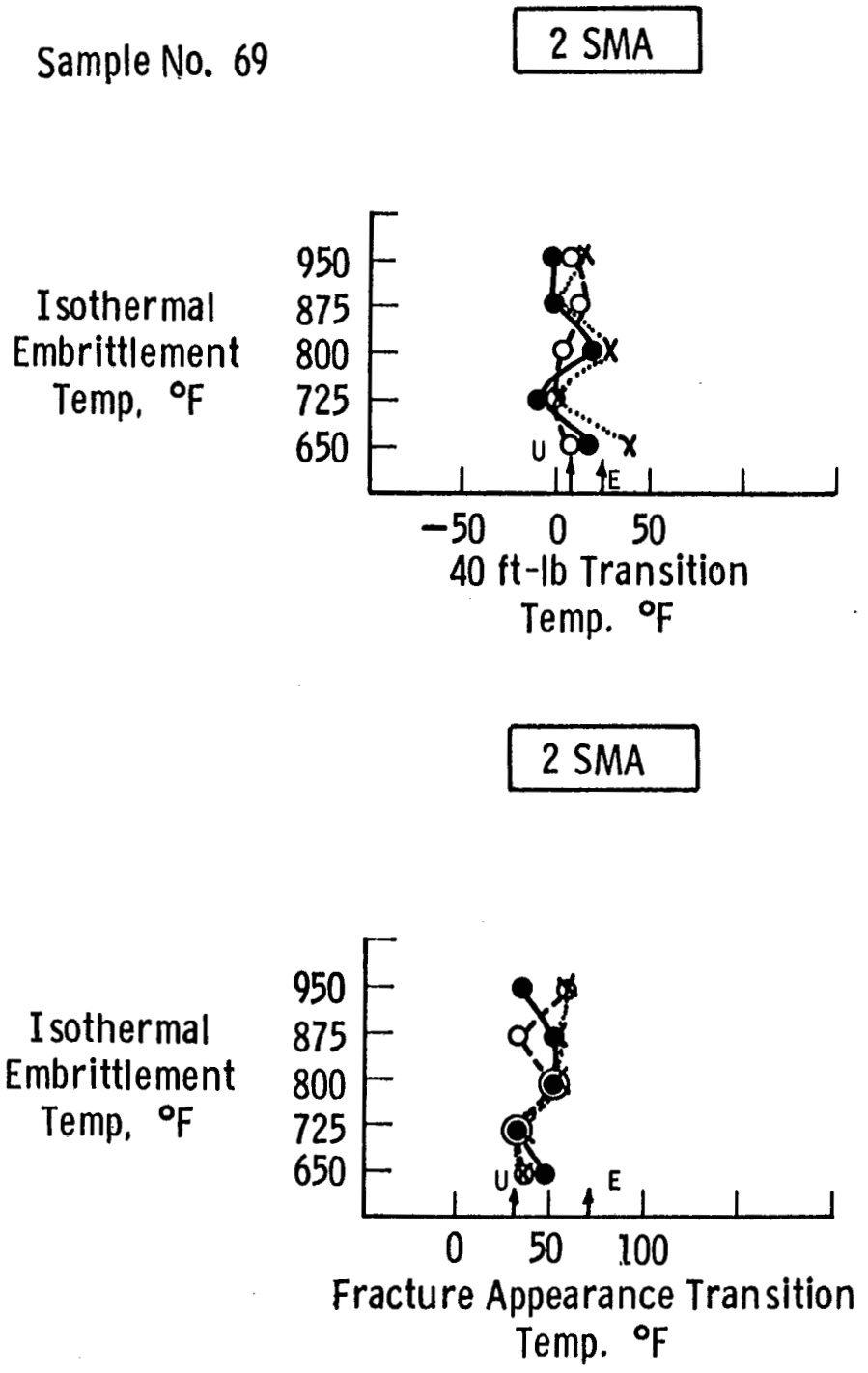

Fig. 42 The 40 ft-lb transition temperature and fracture appearance transition temperature plotted as a function of the isothermal annealing temperature after 1,000 •, 10,000 ○, and 20,000 hr X. The bench mark ↑ U represents the starting condition and ↑ E the step-cooled embrittled condition.

Sample No. 78

2 FOR

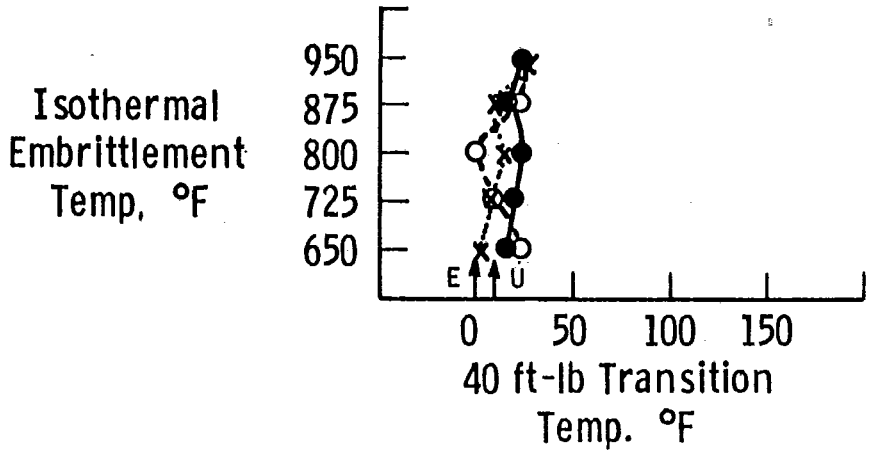

2 FOR

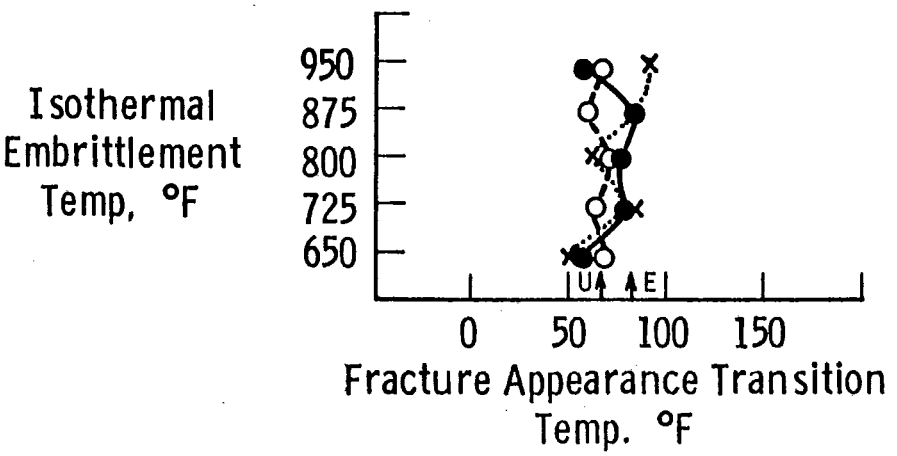

Fig. 43 The 40 ft-lb transition temperature and fracture appearance transition temperature plotted as a function of the isothermal annealing temperature after 1,000 ●, 10,000 ○, and 20,000 hr X. The bench mark ↑ U represents the starting condition and ↑ E the step-cooled embrittled condition.

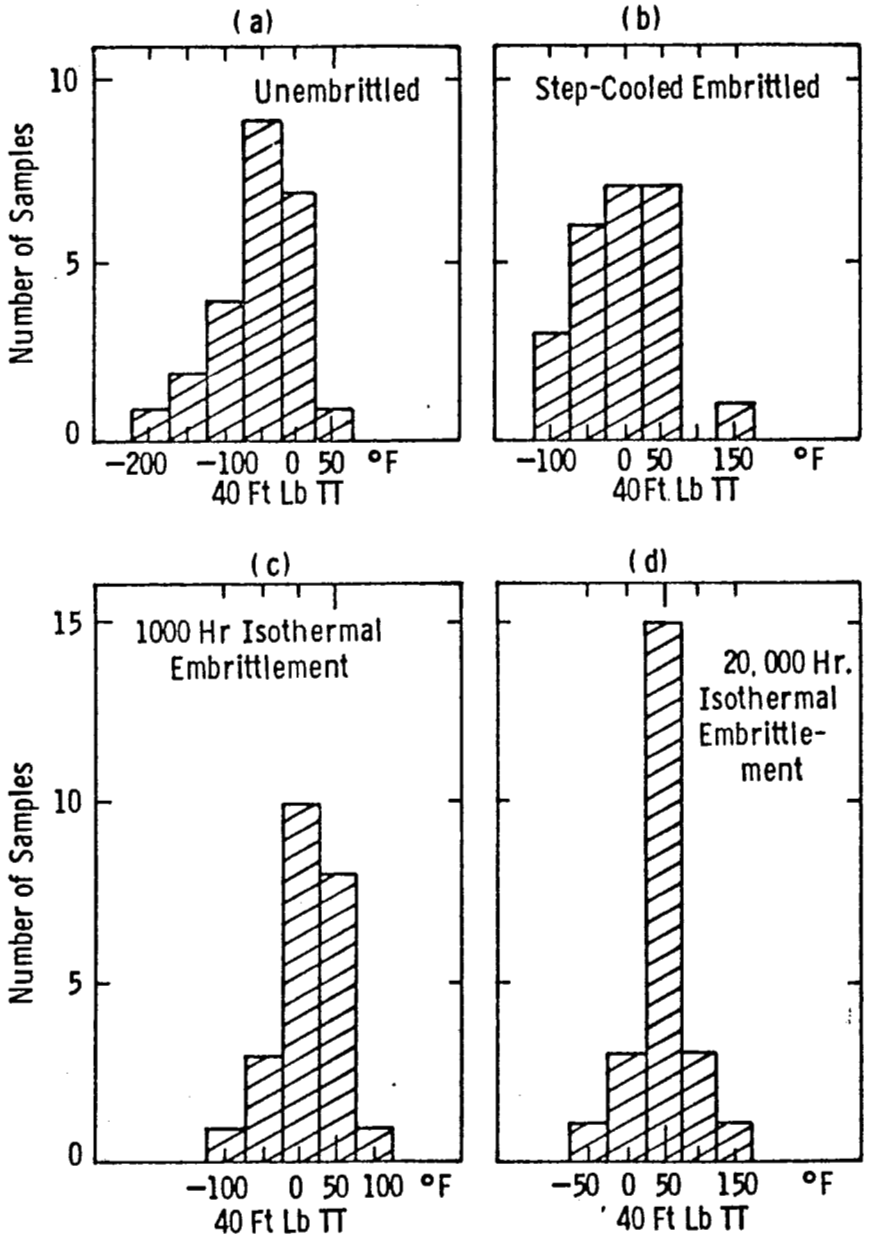

Fig. 44. Histograms of the 40 ft-lb Transition Temperature for samples evaluated in Phase I and II of the project.
(a) Unembrittled or "as received" condition
(b) Step-cooled embrittled condition
(c) After 1000 hr isothermal embrittlement
(d) After 20,000 hr isothermal embrittlement

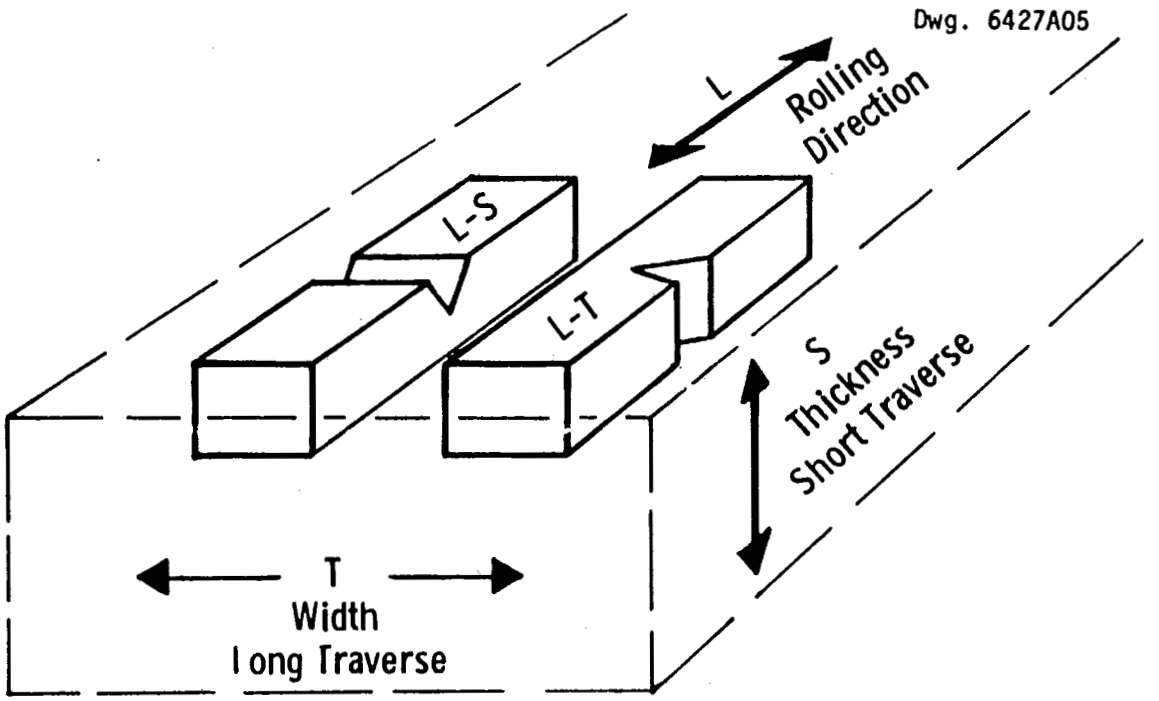

Fig. 1(a) Plate: Orientation and designation of samples

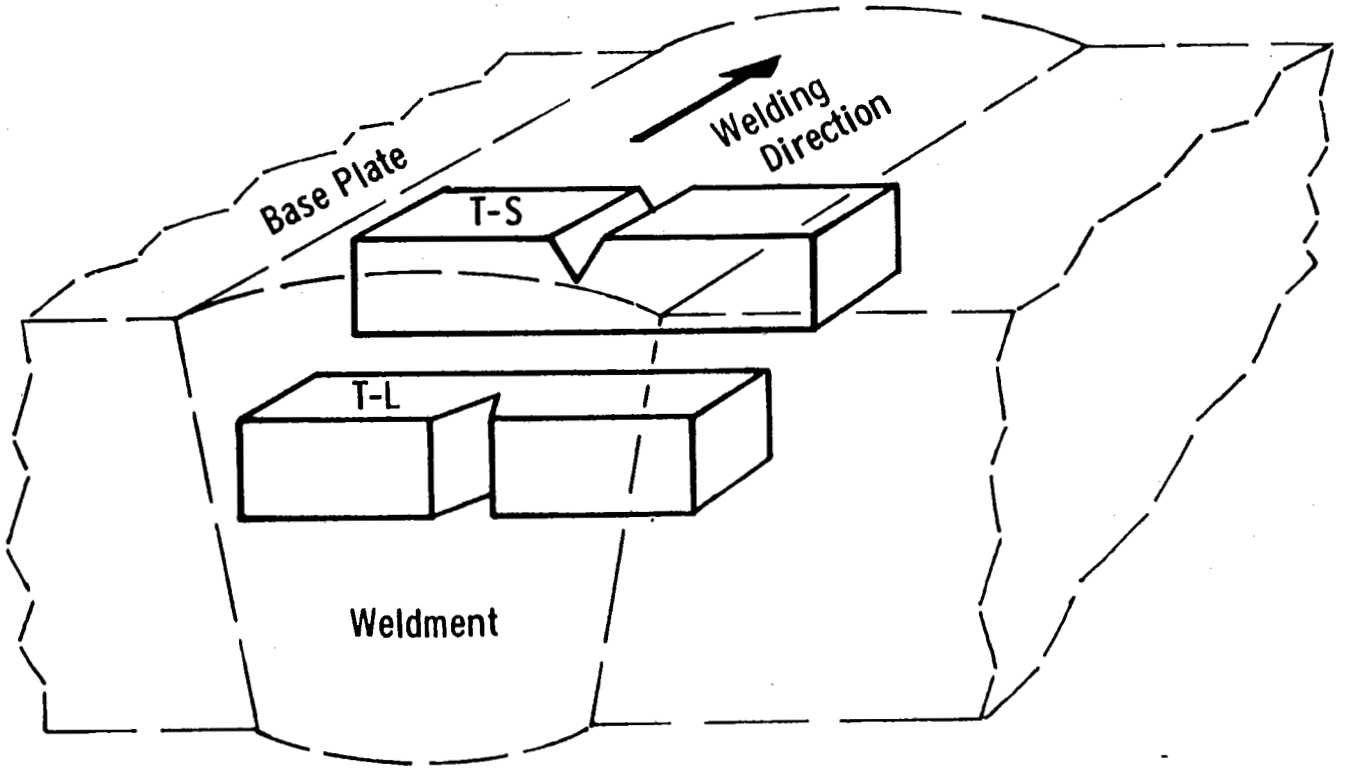

Fig. 45. Schematic of orientation of notches in Charpy specimens
Phase I: L-S and T-S
Phase II: L-T and T-L

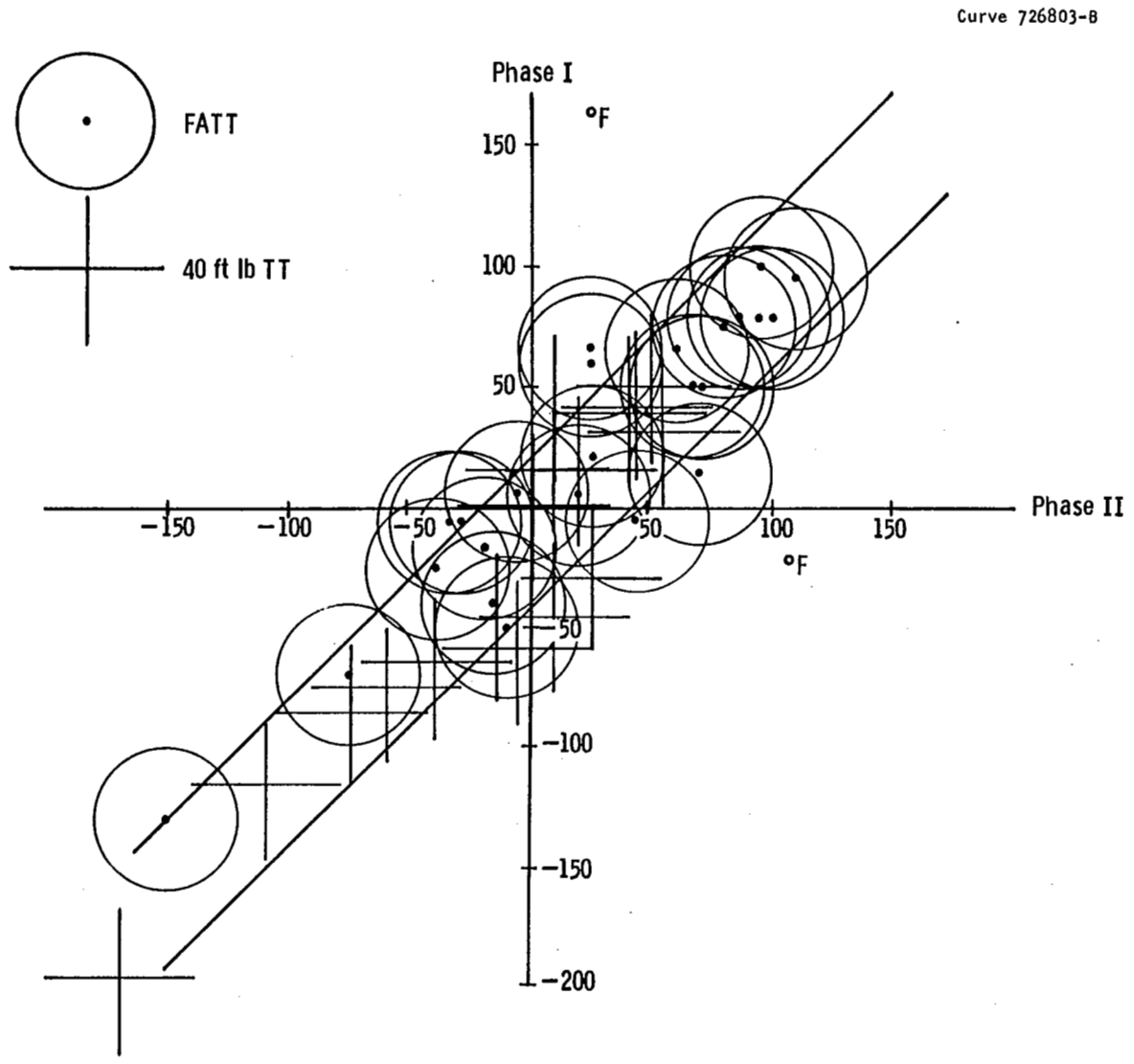

Fig. 46 FATT and 40 ft-lb TT data from unembrittled and step-cooled embrittled specimens plotted so that the relationship between Phase I and Phase II orientations can be seen.

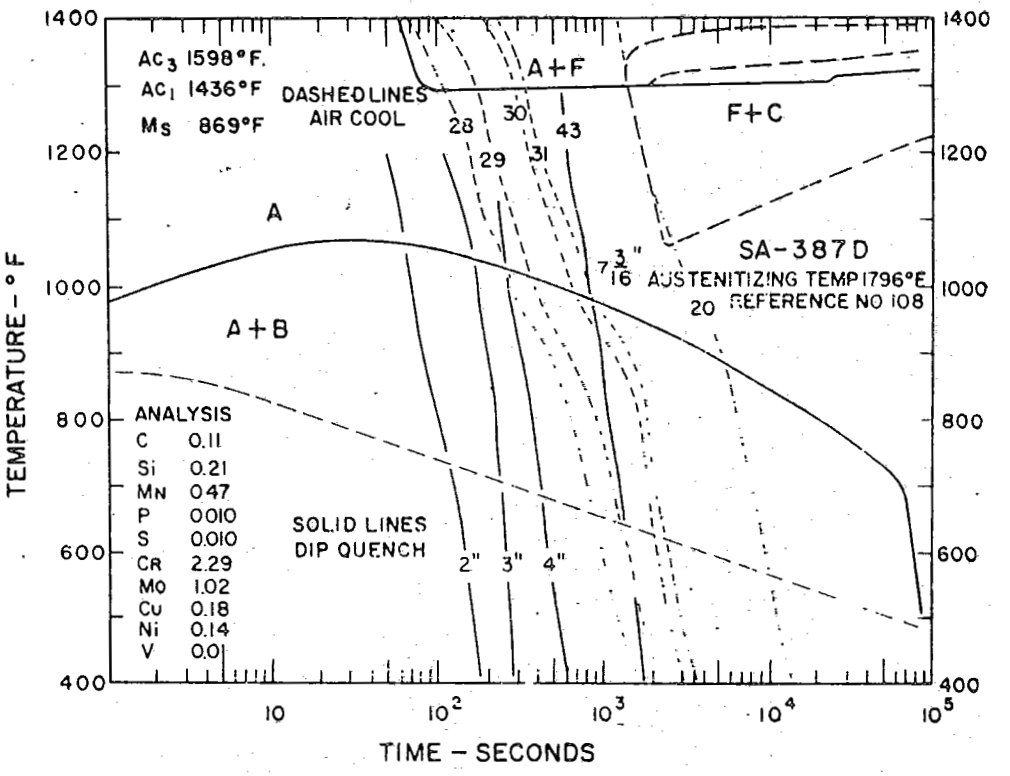

Fig. 47. Cooling rate data superimposed on A387D continuous cooling transformation diagram. (Taken from R. E. LORENTZ, Jr. Welding Jnl., 41 p 440S (1962)).

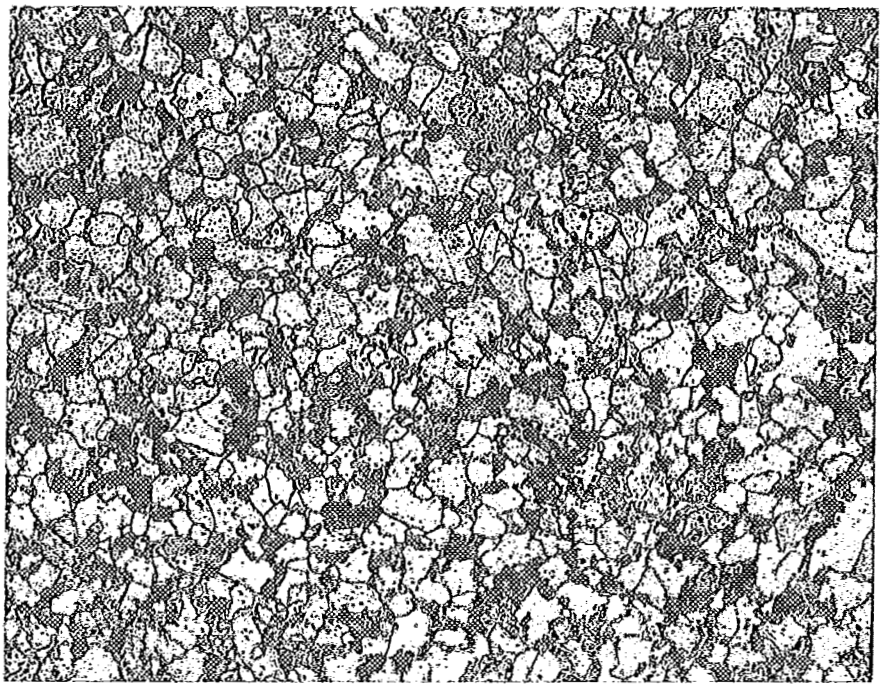

Mag. 200X

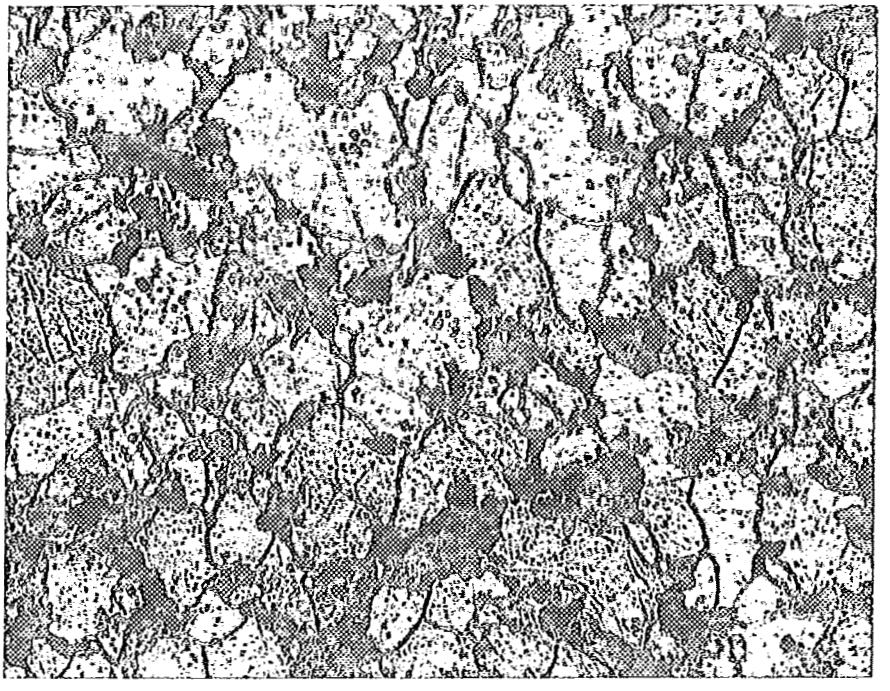

Mag. 500X

Fig. 48 Ferrite-pearlite structure produced in sample No. 75 for the structural study at a hardness of R_B = 87.

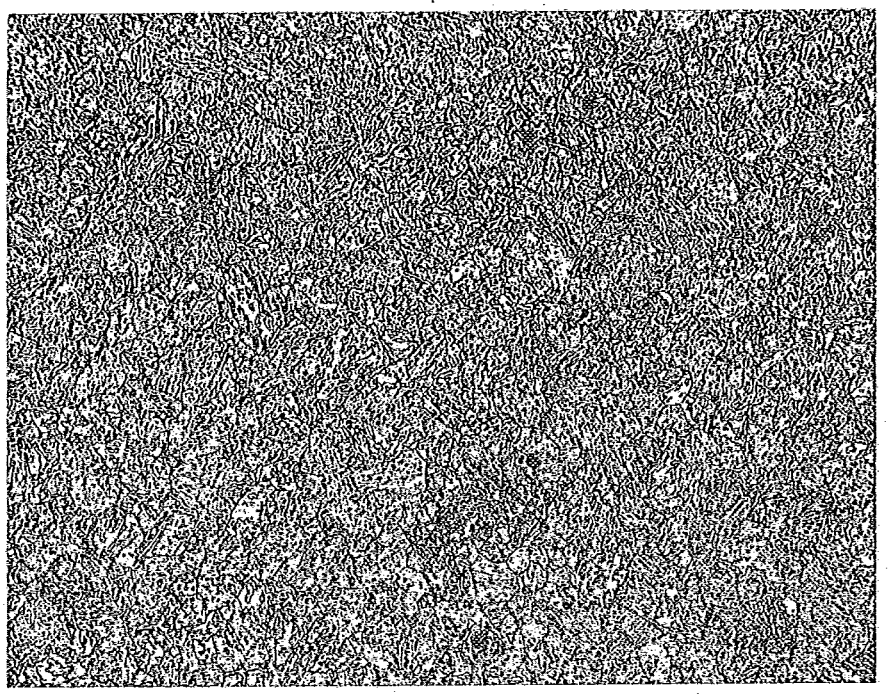

Mag. 200X

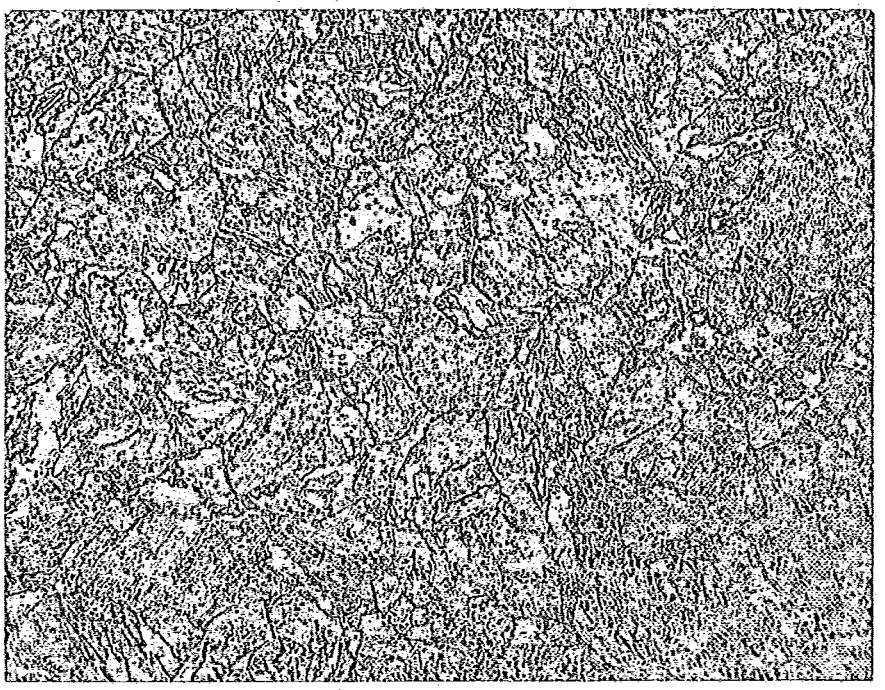

Mag. 500X

Fig. 49 Bainitic structure produced in slow cooled heat treatment. This sample was tempered to give a hardness of R_B = 98. (see Table 19)

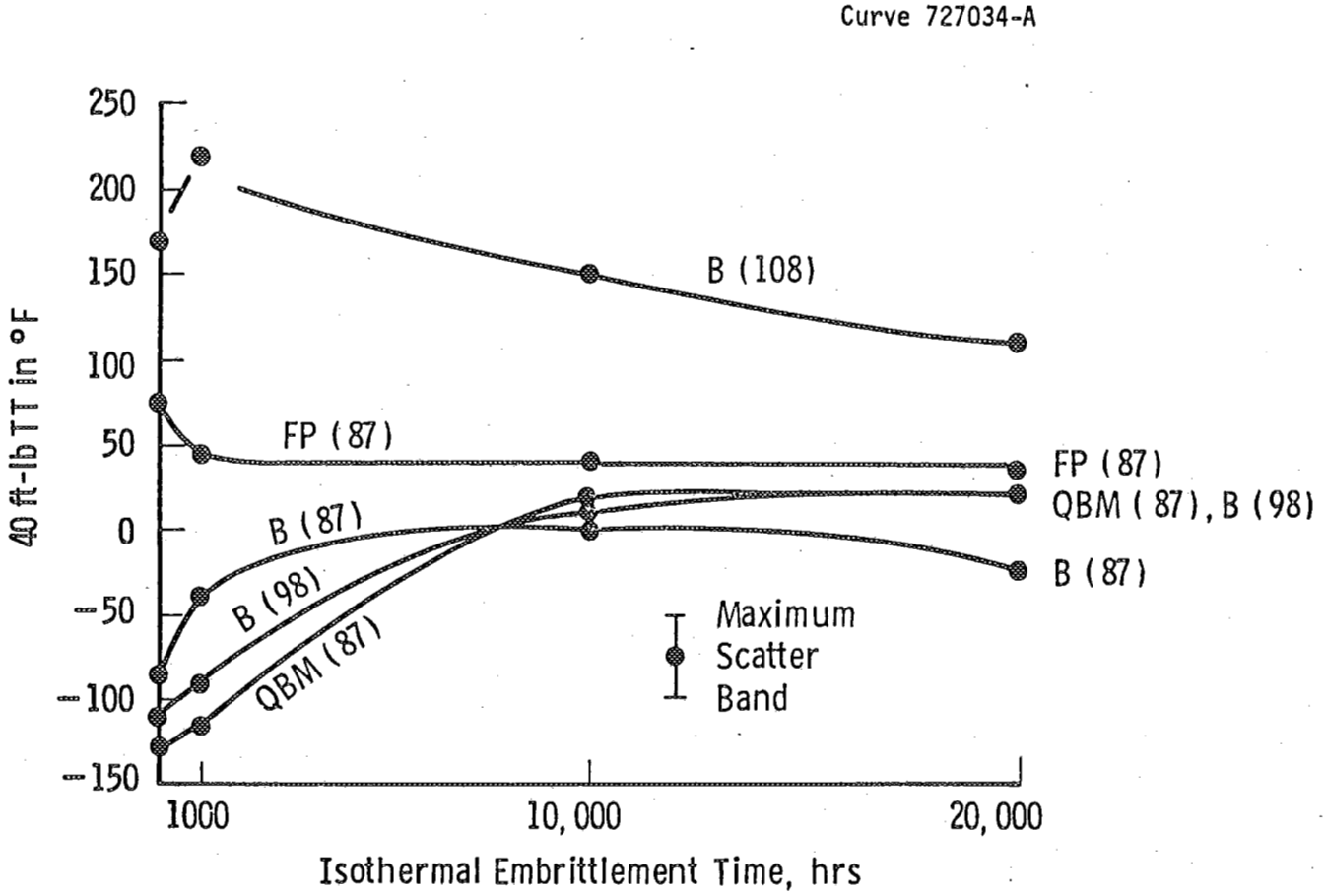

Fig. 50 The 40 ft-lb TT as a function of isothermal embrittlement time for five samples representing the effects of strength level (Rockwell B hardness) and structure

Key	Structure	R_B
QBM (87)	Quenched Bainite-Martensite	87
F-P (87)	Ferrite Pearlite	87
B (87)	Bainite	87
B (98)	Bainite	98
B (108)	Bainite	108

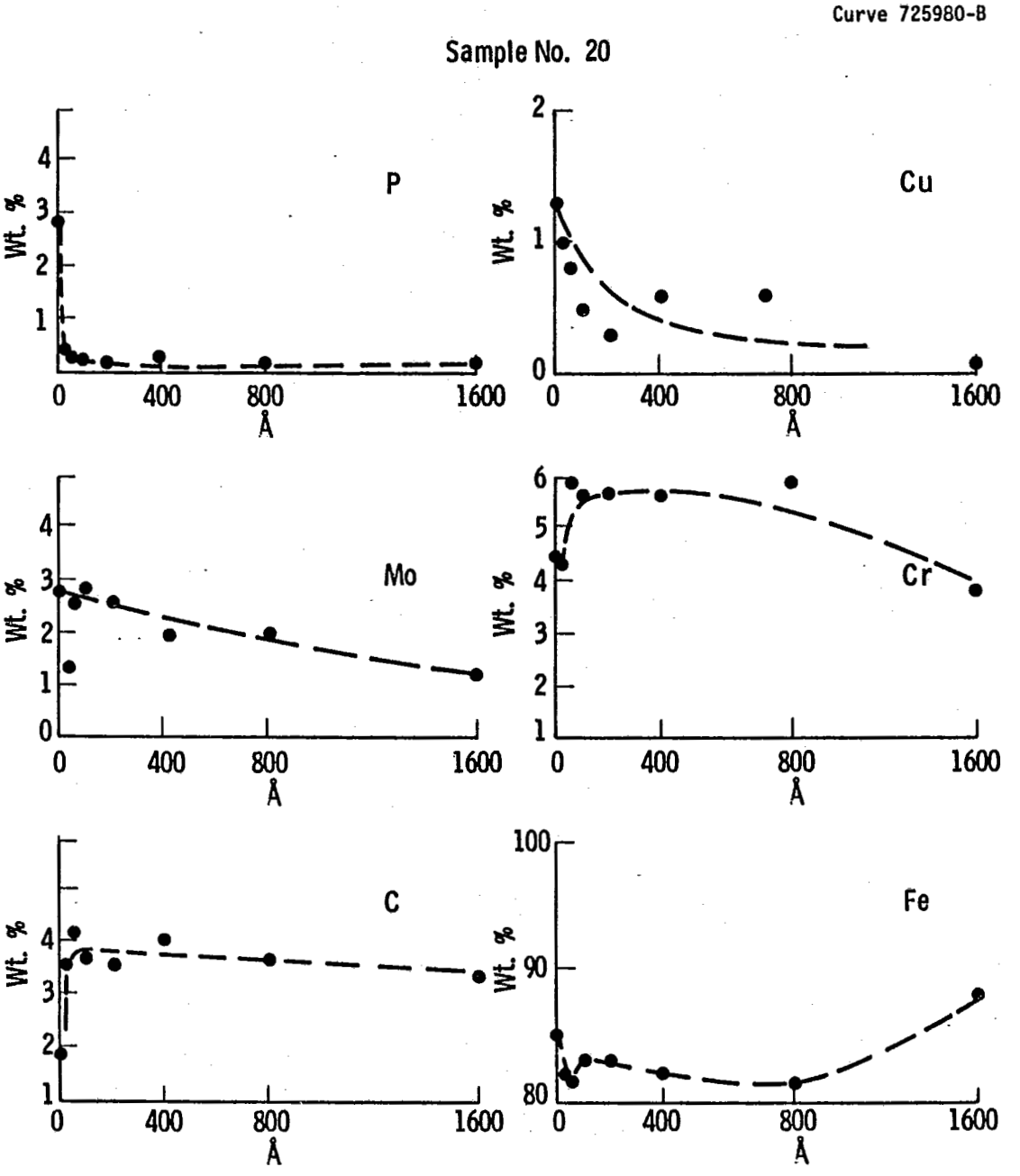

Fig. 51 The wt % of segregated elements as a function of the distance from the grain boundary derived from the Auger spectra for Sample No. 20 after 20,000 hr isothermal embrittlement.

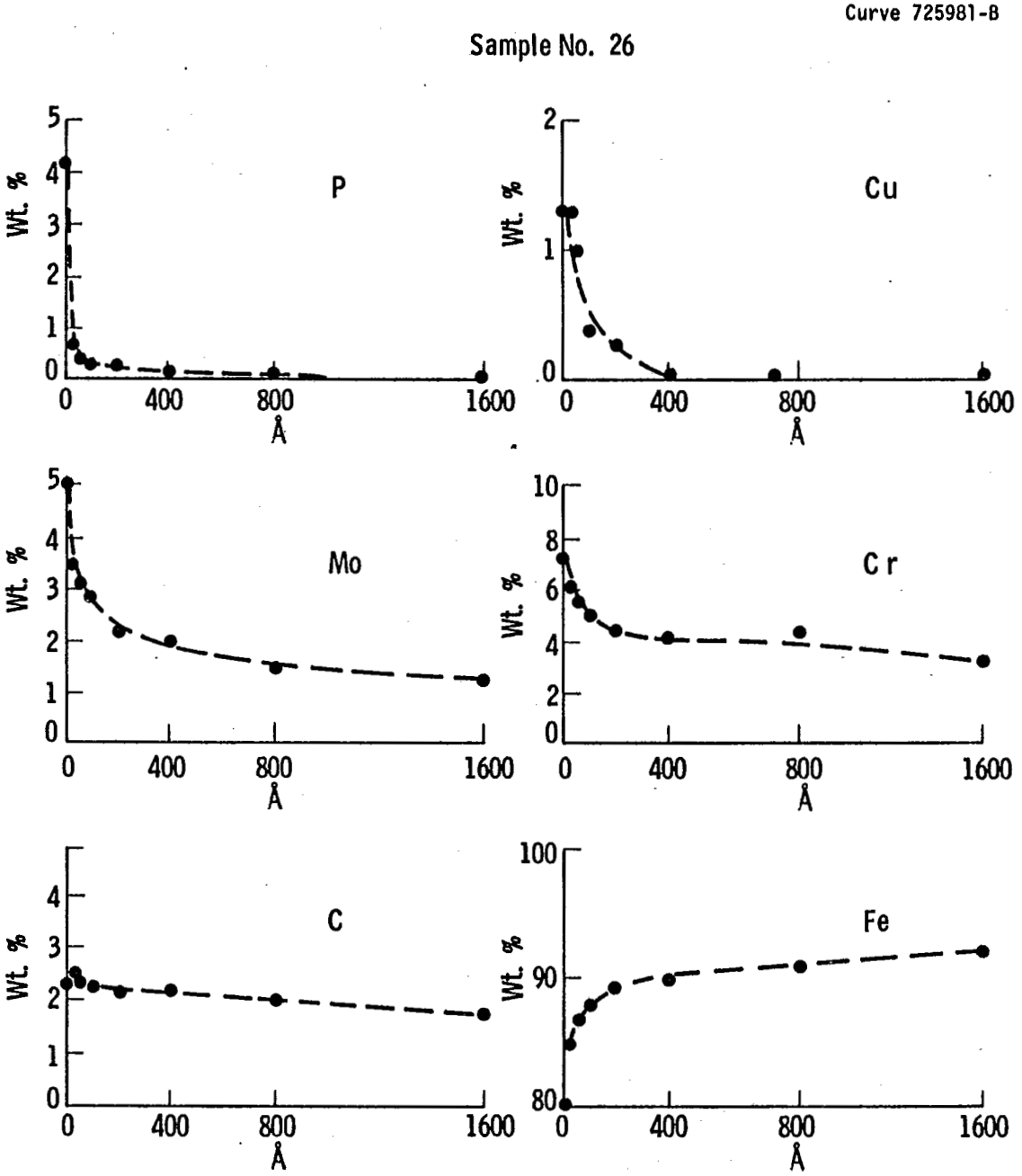

Fig. 52 The wt % of segregated elements as a function of the distance from the grain boundary derived from the Auger spectra for Sample No. 26 after 20,000 hr isothermal embrittlement.

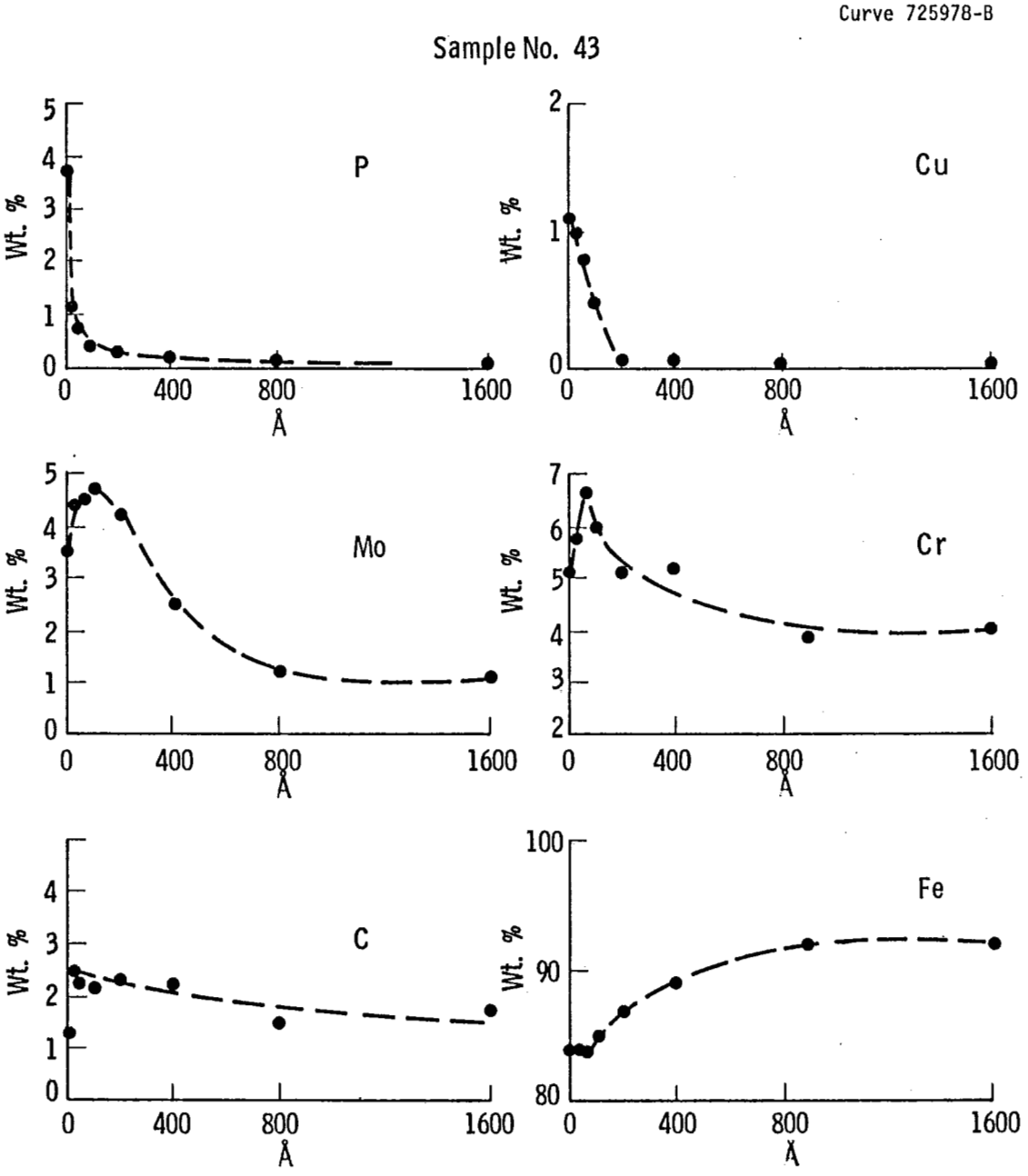

Fig. 53 The wt % of segregated elements as a function of the distance from the grain boundary derived from the Auger spectra for Sample No. 43 after 20,000 hr isothermal embrittlement.

Curve 725977-B

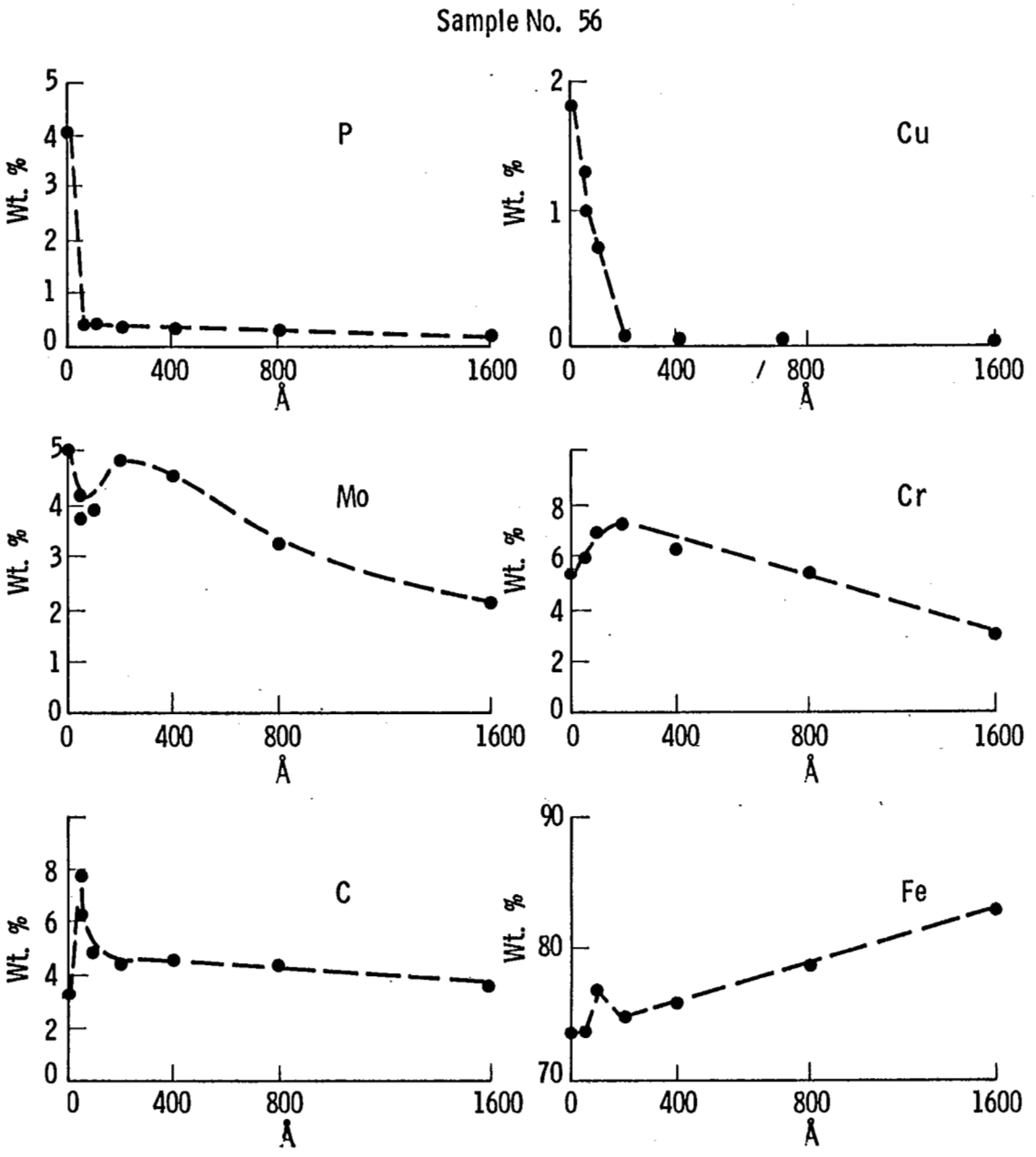

Fig. 54 The wt % of segregated elements as a function of the distance from the grain boundary derived from the Auger spectra for Sample No. 56 after 20,000 hr isothermal embrittlement.

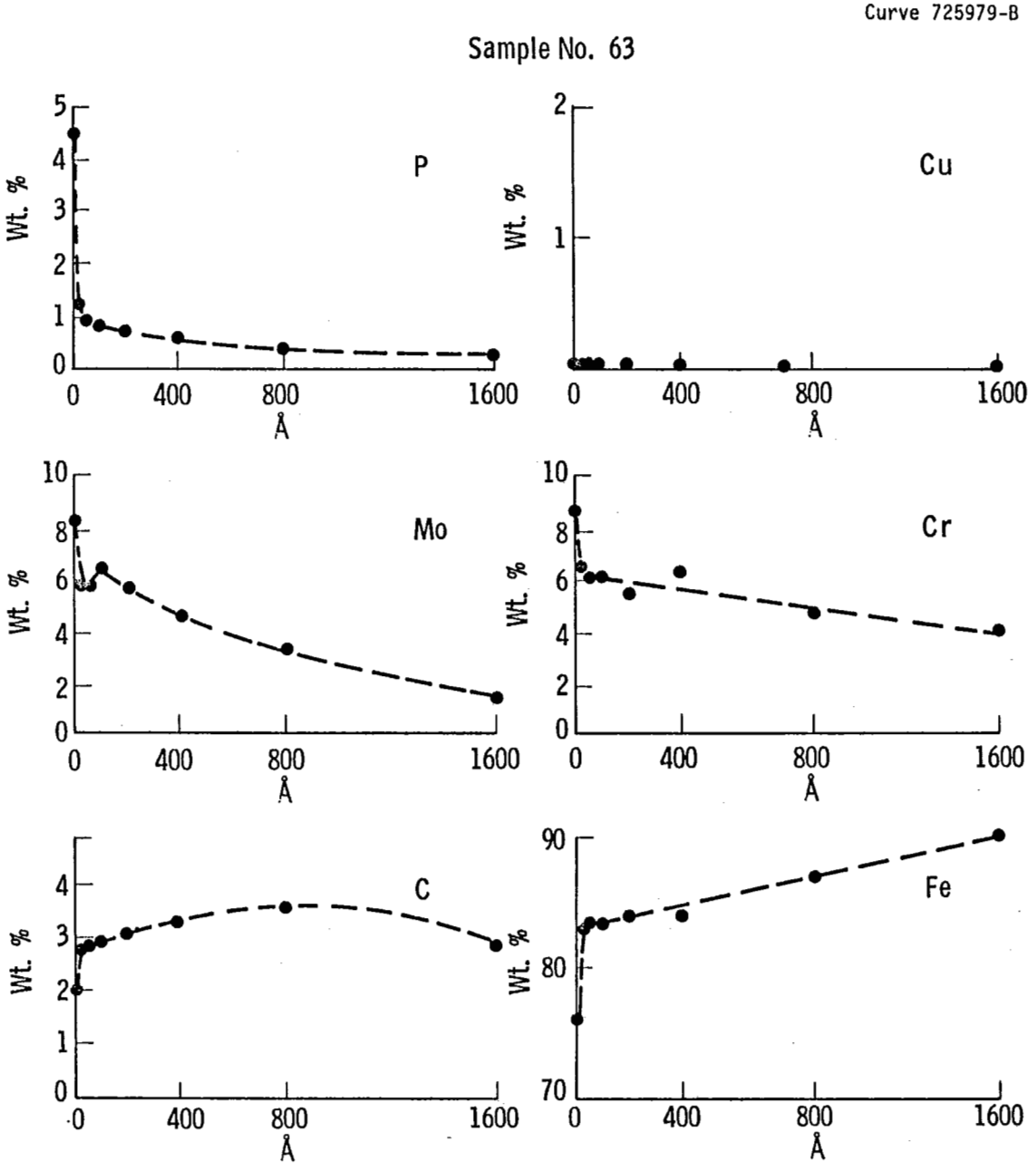

Fig. 55 The wt % of segregated elements as a function of the distance from the grain boundary derived from the Auger spectra for Sample No. 63 after 20,000 hr isothermal embrittlement.

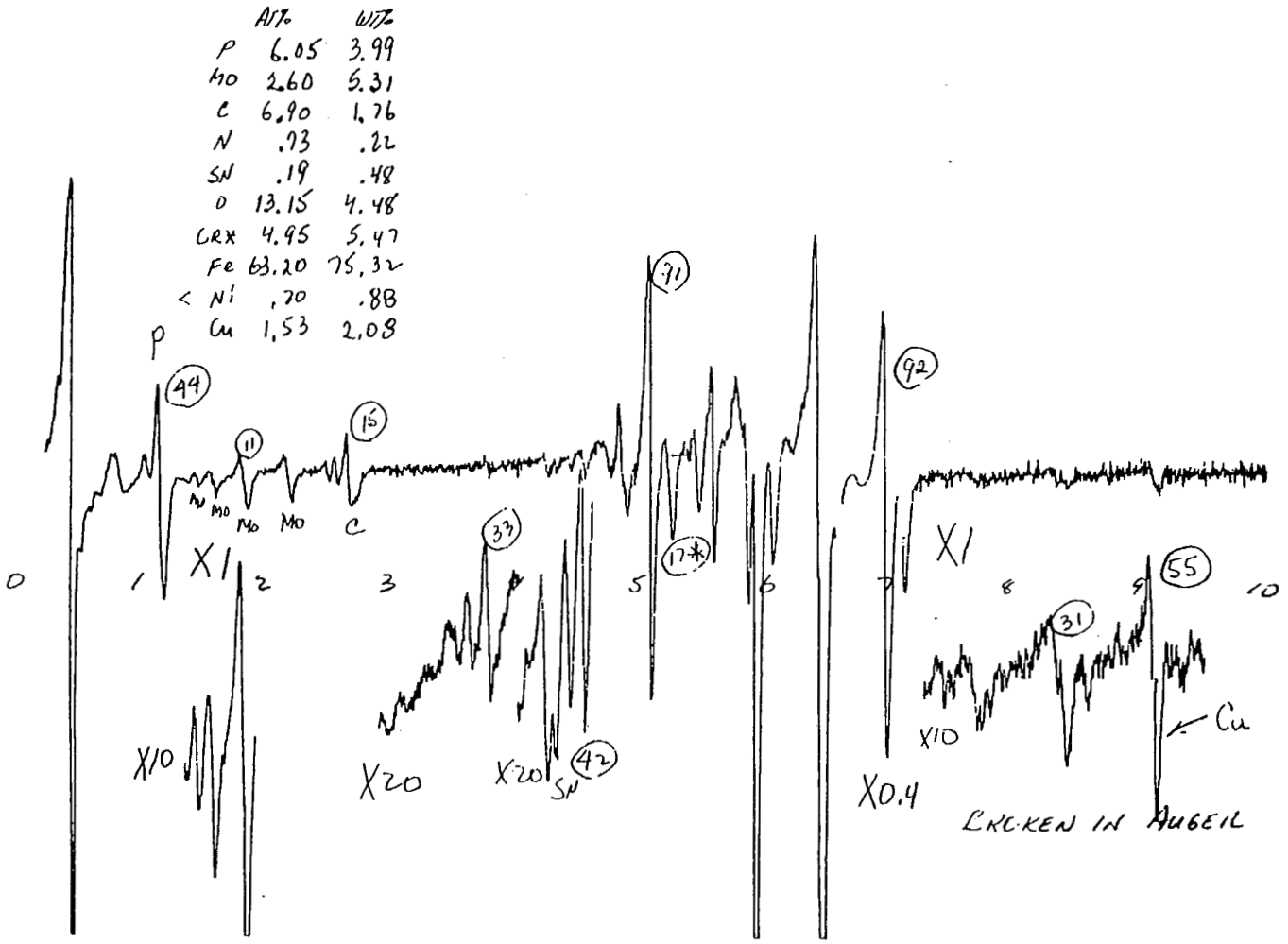

Fig. 56 Auger spectrum from Sample No. 56 which had been isothermally embrittled for 20,000 hr at 875°F. Note the very large Cu peak on the right-hand side.

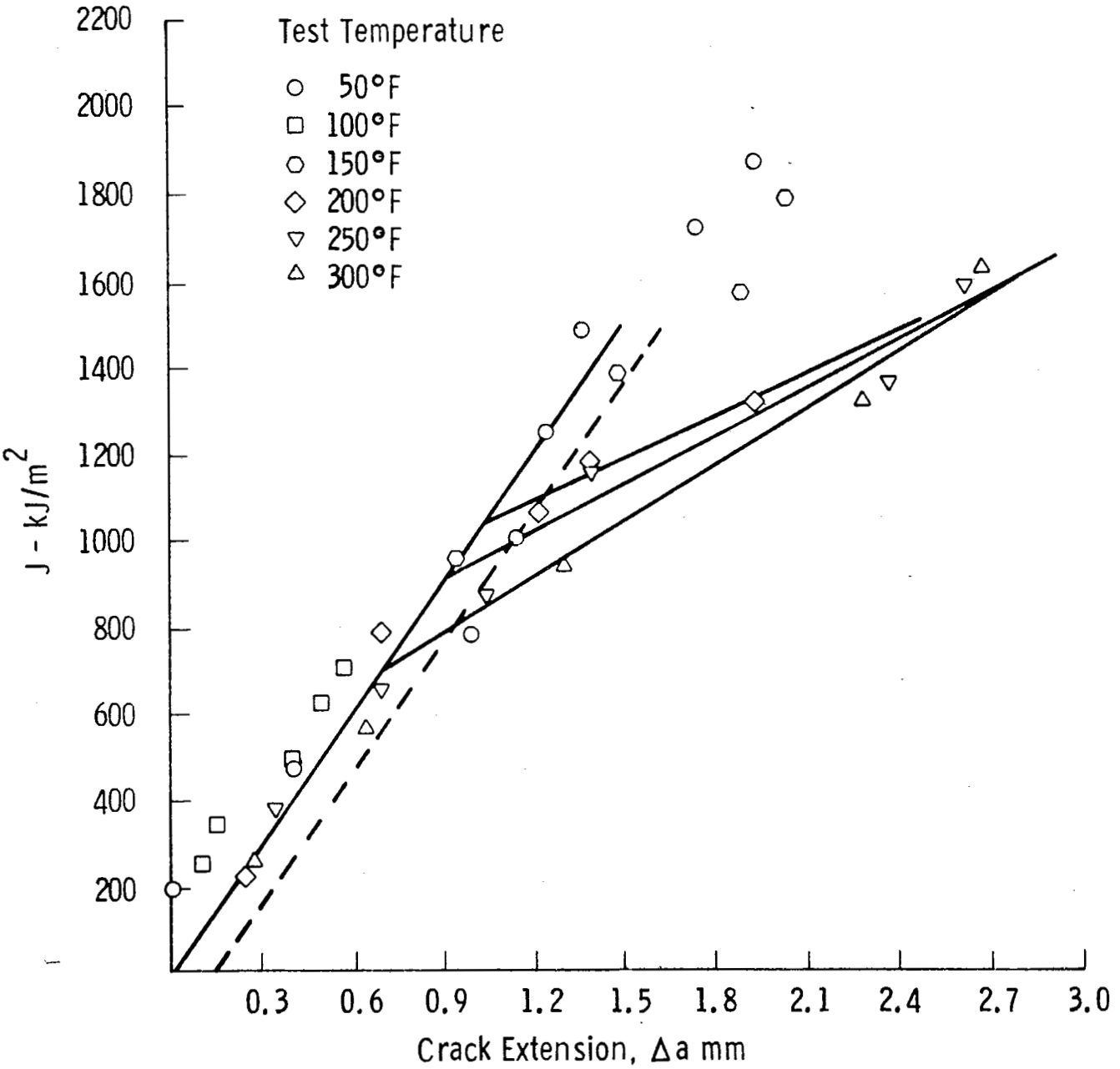

Fig. 57 J versus "a" for the unembrittled specimens of sample no. 75.

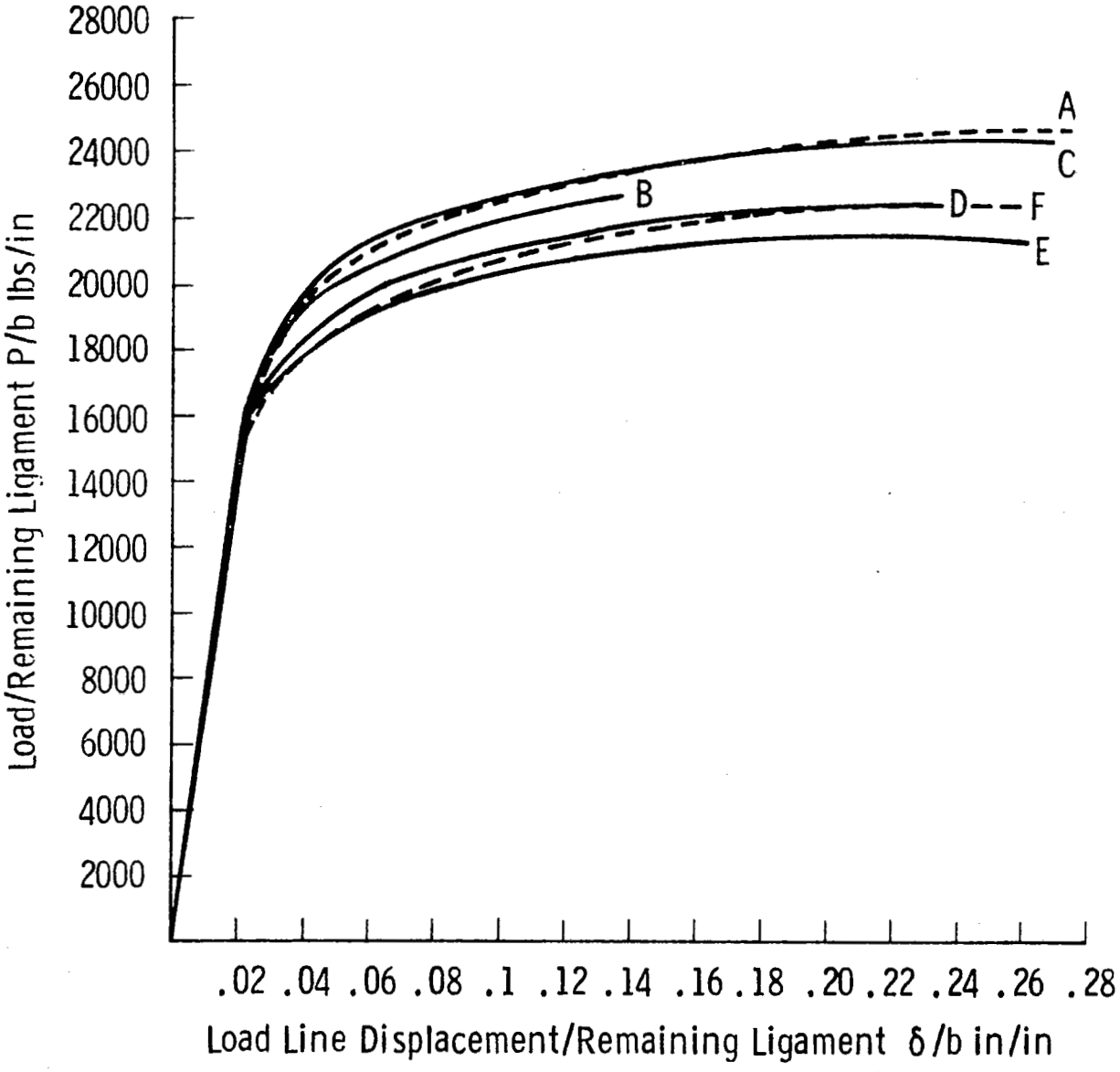

Fig. 58 Normalized load versus displacement curves for specimens of sample no. 75 tested at various temperatures.

Specimen	Test Temp. (°F)
A	50
B	100
C	150
D	200
E	250
F	300

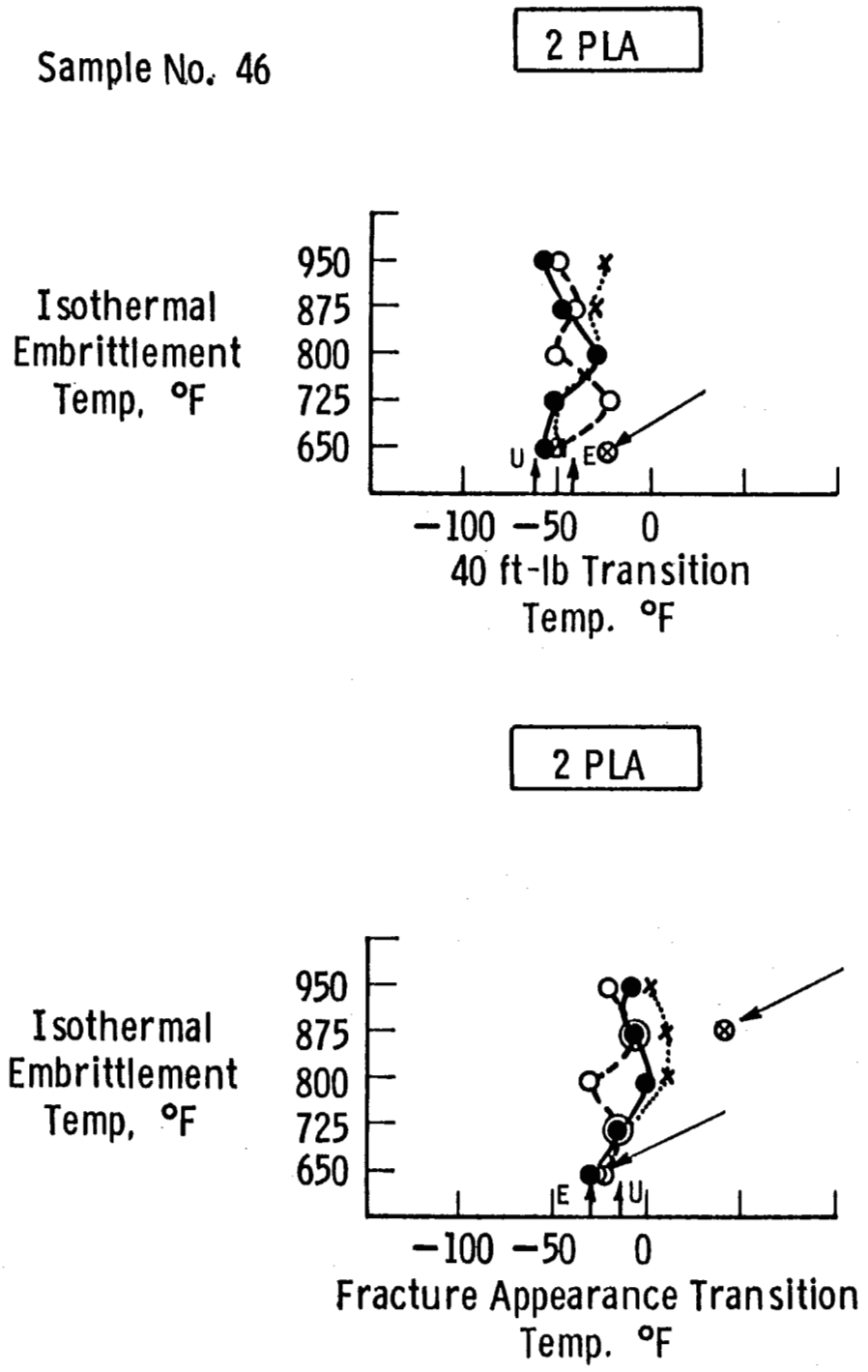

Fig. 59 The 40 ft-lb transition temperature and fracture appearance transition temperature plotted as a function of the isothermal annealing temperature after 1,000 hr ●, 10,000 hr ○ and 20,000 hr X . The bench mark ↑U represents the starting condition and ↑E the step-cooled embrittled condition. For comparison the data from a 3,500 psig H_2 environment after 1,500 hr at 650 and 875°F are represented by ⊗.

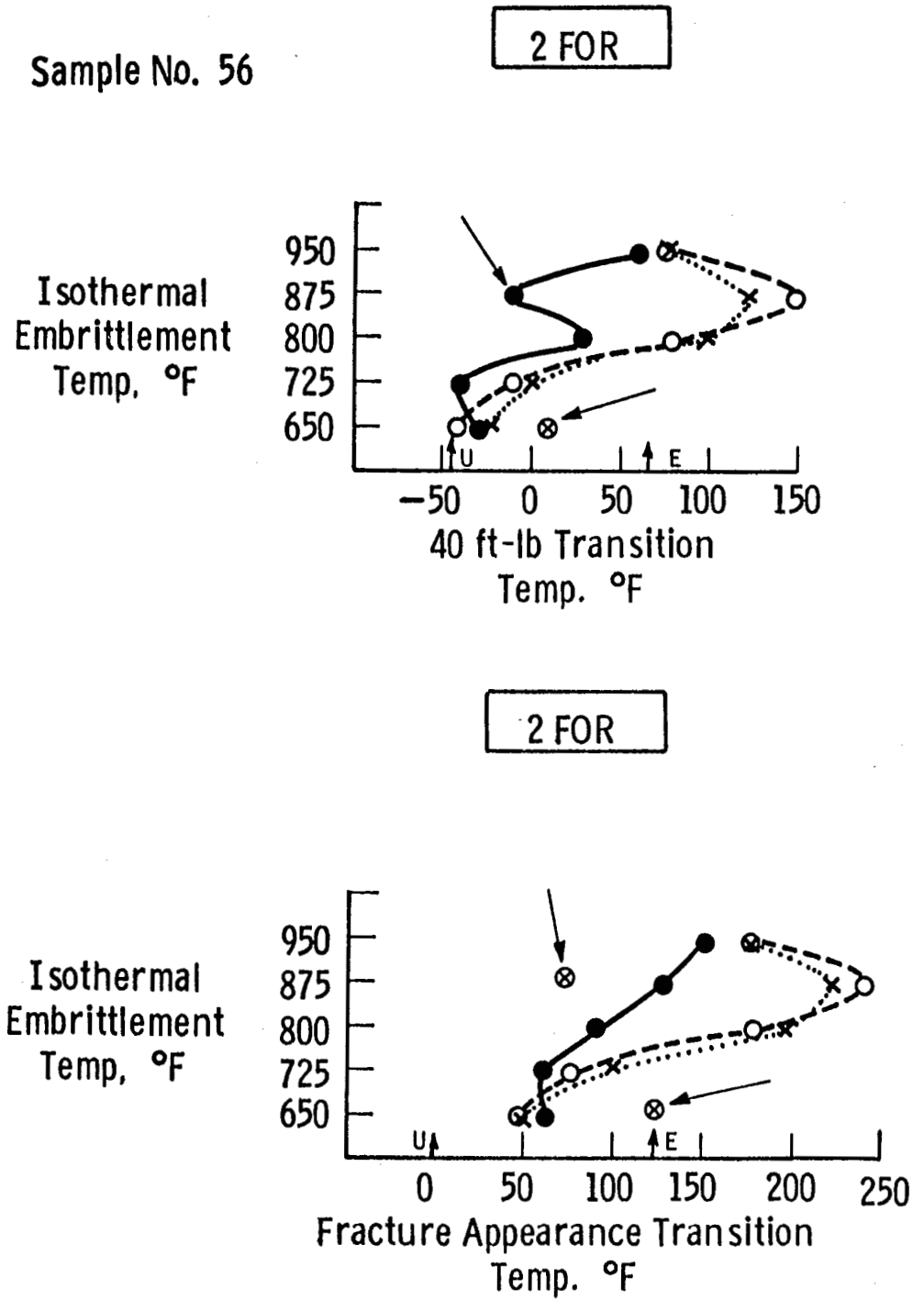

Fig. 60 The 40 ft-lb transition temperature and fracture appearance transition temperature plotted as a function of the isothermal annealing temperature after 1,000 hr●, 10,000 hr ○ and 20,000 hr X . The bench mark ↑U represents the starting condition and ↑E the step-cooled embrittled condition. For comparison the data from a 3,500 psig H_2 environment after 1,500 hr at 650 and 875°F are represented by ⊗.

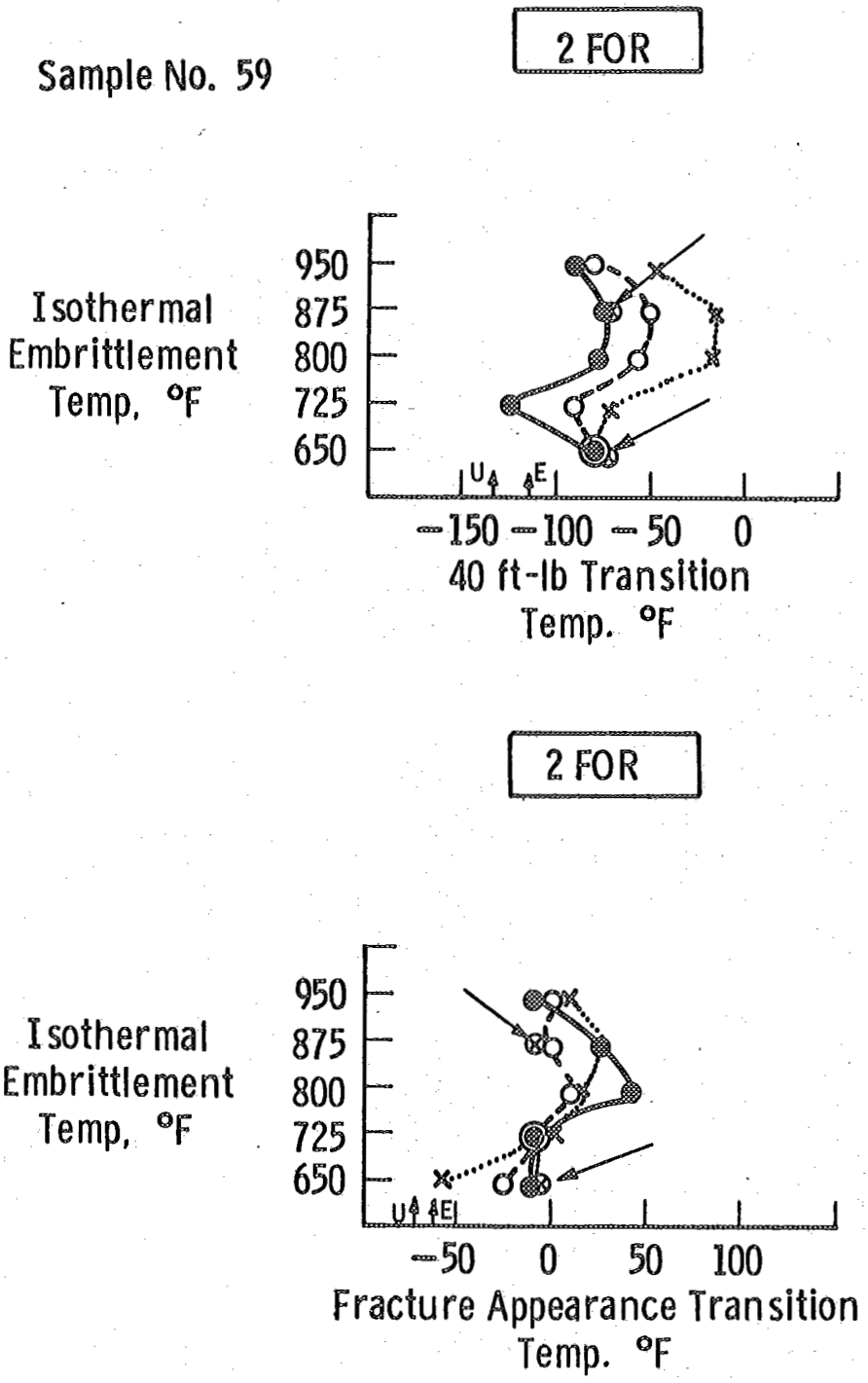

Fig. 61 The 40 ft-lb transition temperature and fracture appearance transition temperature plotted as a function of the isothermal annealing temperature after 1,000 hr ●, 10,000 hr ○ and 20,000 hr X . The bench mark ↑U represents the starting condition and ↑E the step-cooled embrittled condition. For comparison the data from a 3,500 psig H_2 environment after 1,500 hr at 650 and 875°F are represented by ⊗.

A

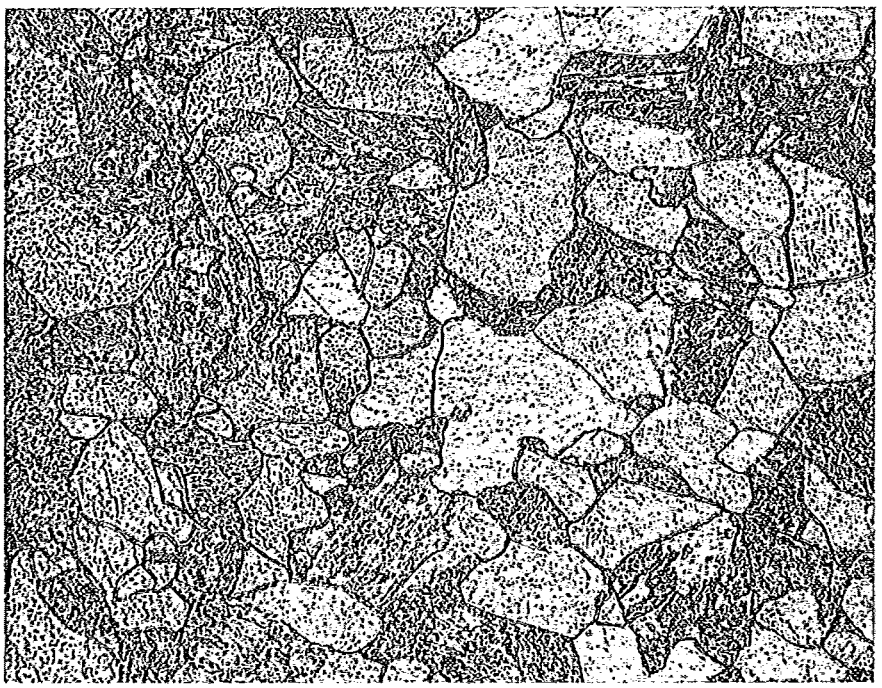

X500

B

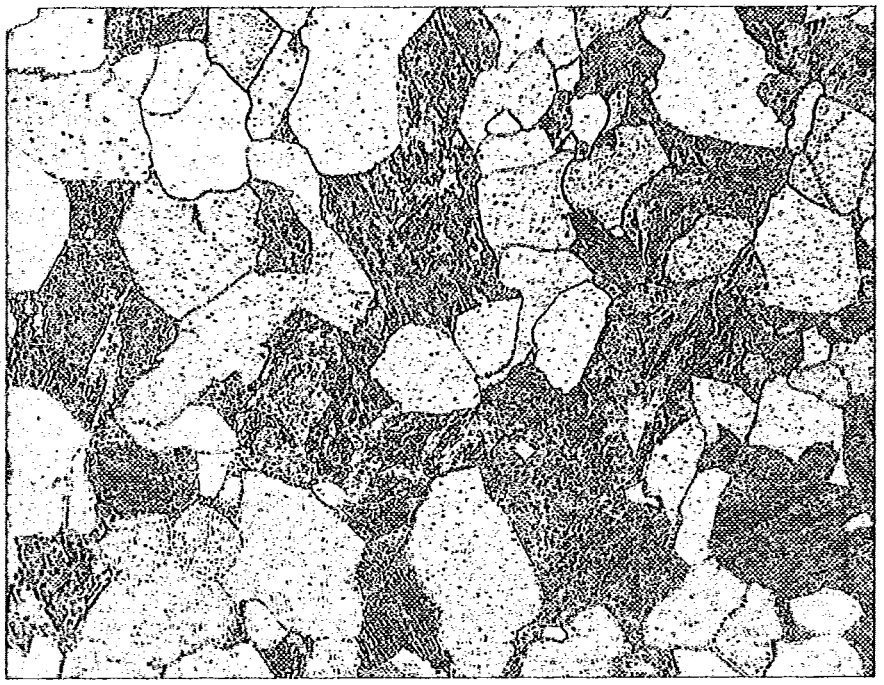

X500

Fig. 62 Metallographic sections of sample no. 46 (A) in the "as-received" condition and (B) after 1,000 hr at 875°F in air. Etch 2% Nital.

A

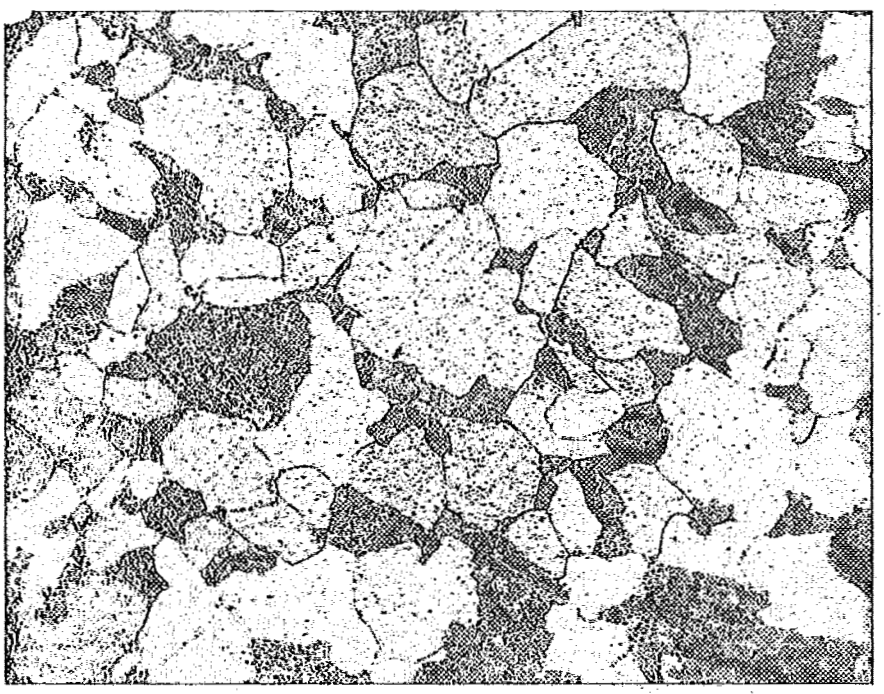

X500

B

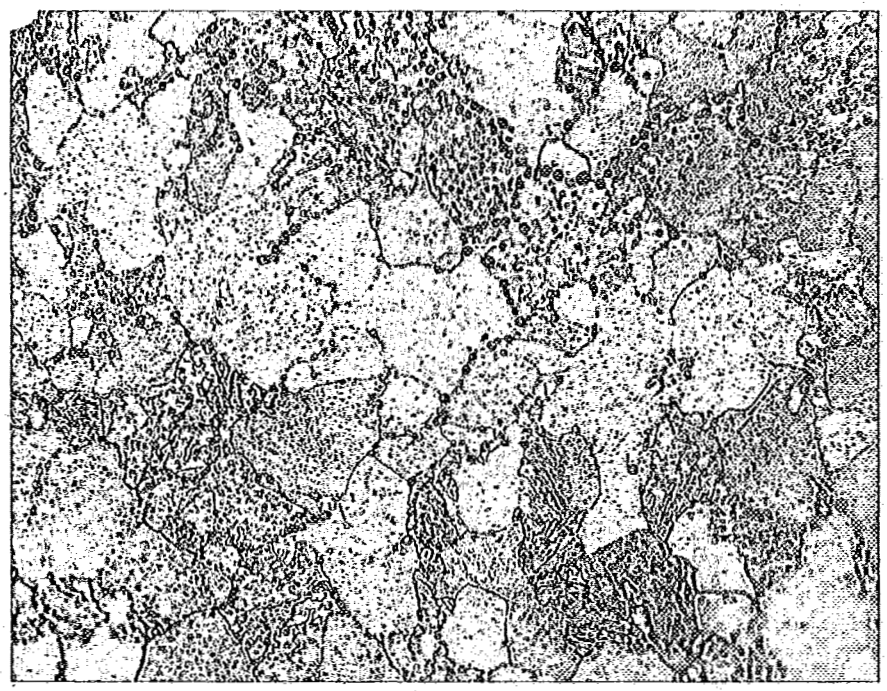

X500

Fig. 63 Metallographic sections of sample no. 46 (A) after 1,000 hr at 650°F in 3,500 psig H_2 and (B) after 1,000 hr at 875°F in 3,500 psig H_2. Etch 2% Nital.

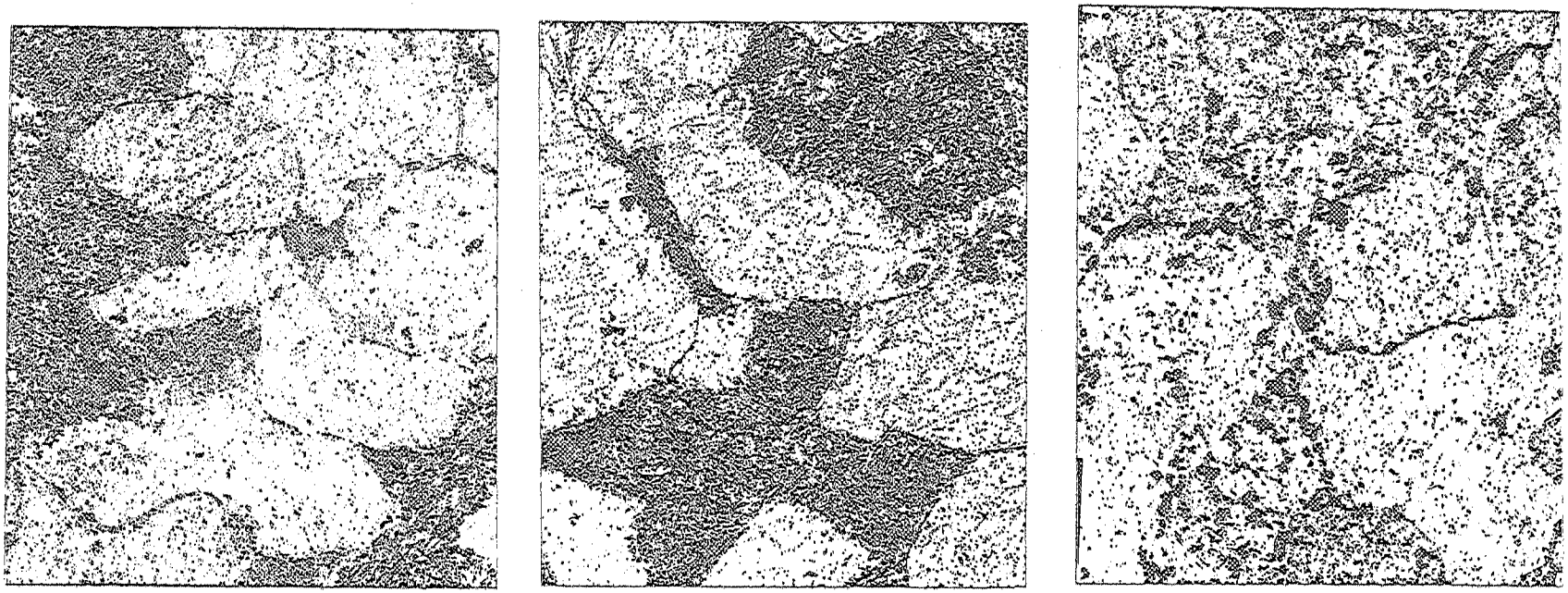

A B C

X1250

Fig. 64 Transmission electron micrographs of carbide extraction replicas from sample no. 46. Exposures (A) air at 875°F for 1,000 hr; (B) hydrogen at 3,500 psig and 650°F for 1,000 hr; and (C) hydrogen at 3,500 psig and 875°F for 1,000 hr.

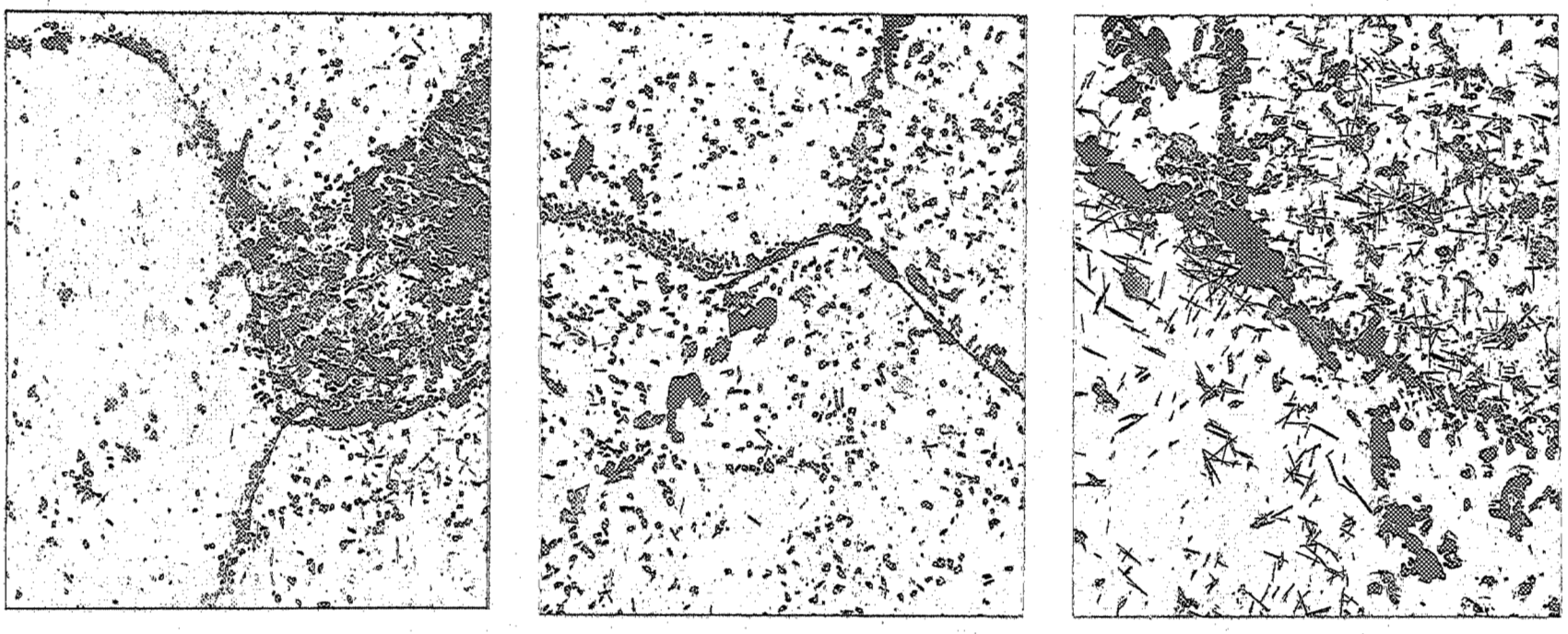

A B C

X5800

Fig. 65 Transmission electron micrographs of carbide extraction replicas from sample no. 46 showing details of the grain boundaries. Exposures (A) air at 875°F for 1,000 hr; (B) hydrogen at 3,500 psig and 650°F for 1,000 hr; and (C) hydrogen at 3,500 psig and 875°F for 1,000 hr.

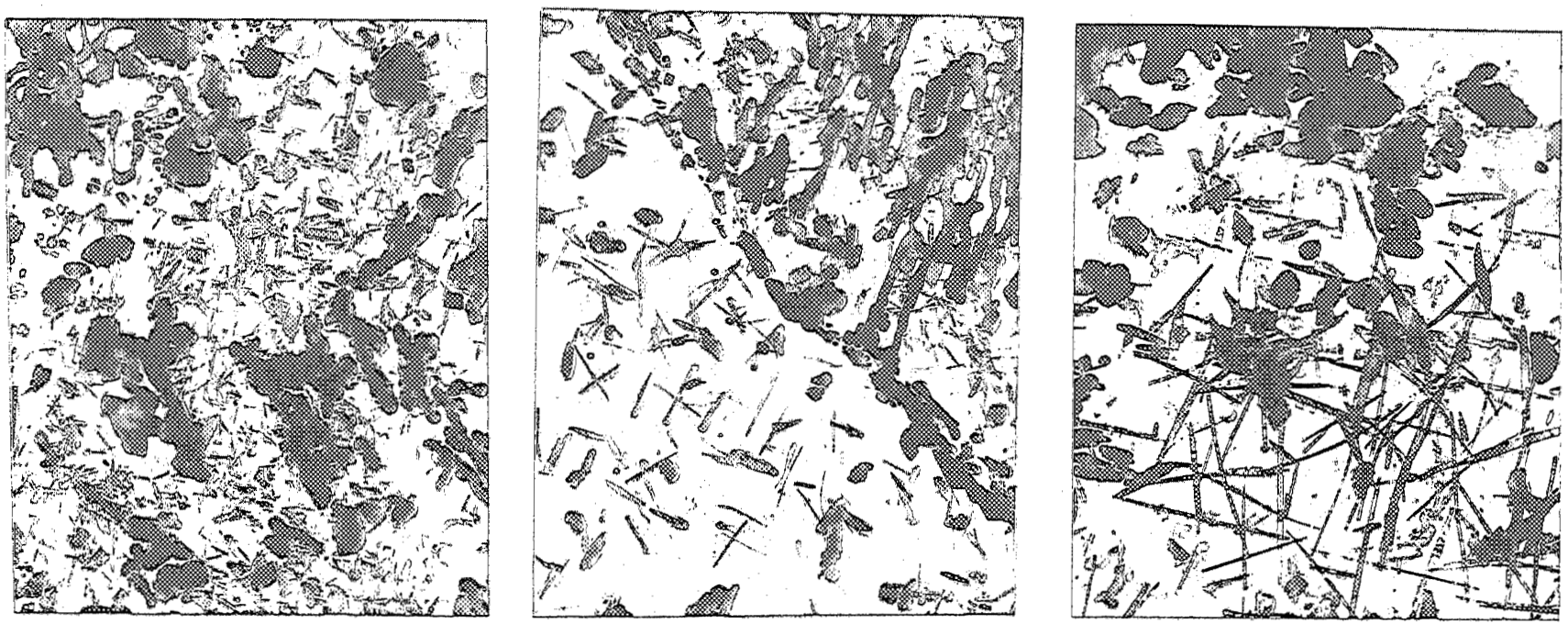

A B C

x 21000

Sample No. 46

Fig. 66 Comparison of acicular carbides from carbide extraction replicas viewed in a transmission electron microscope. Specimen exposures (A) air at 875°F for 1,000 hr; (B) hydrogen at 3,500 psig pressure at 650°F for 1,000 hr; and (C) hydrogen at 3,500 psig pressure at 875°F for 1,000 hr.

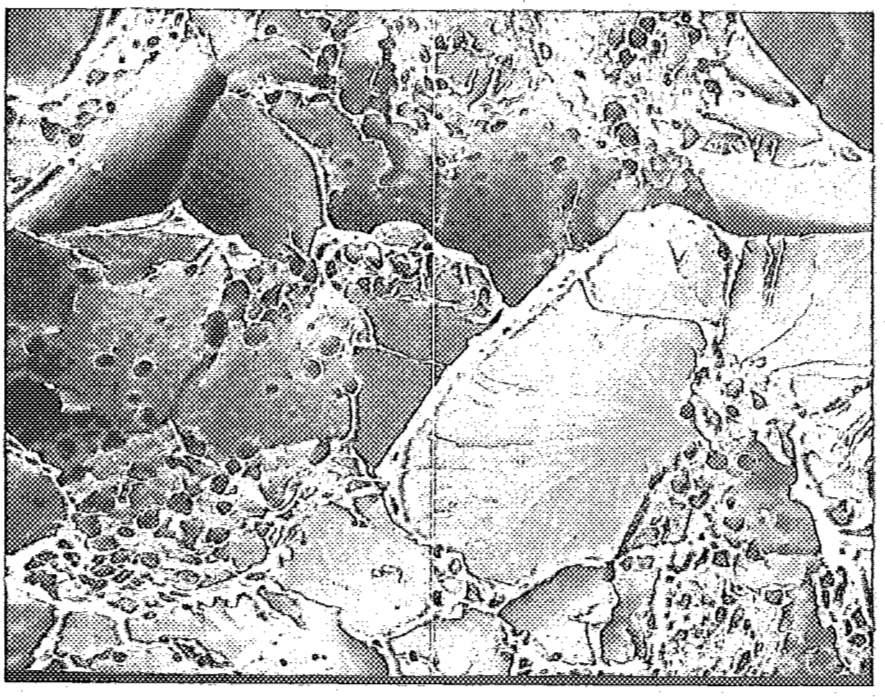

x1500

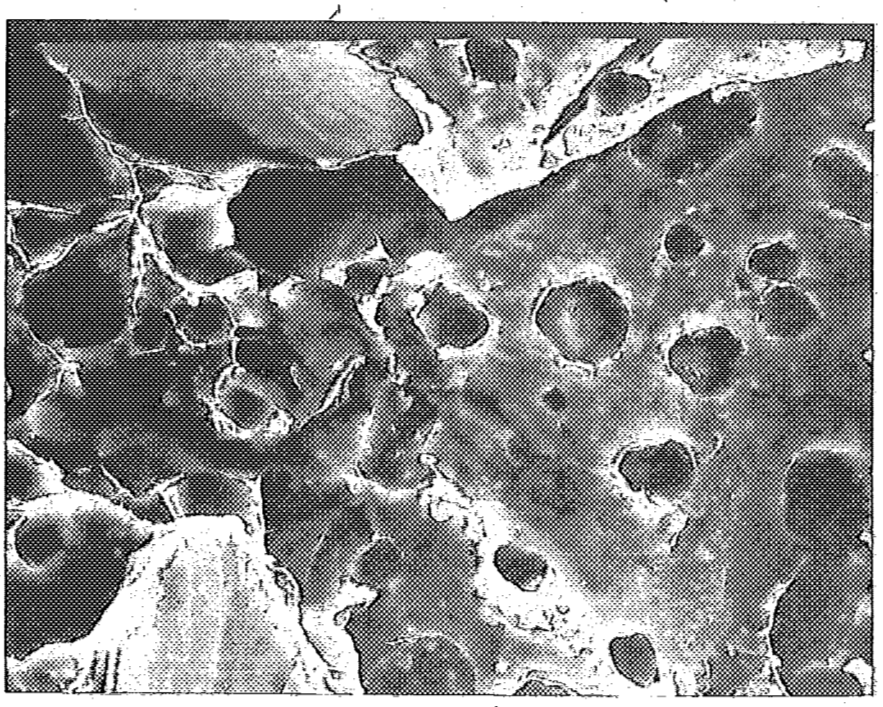

x5000

Fig. 67 Fracture surface of sample no. 46 after 1,000 hr at 875°F in 3500 psig of H_2. The x1500 fractograph shows a combination of cleavage and voids on intergranular facets. The x5000 fractograph shows detail of voids formed.

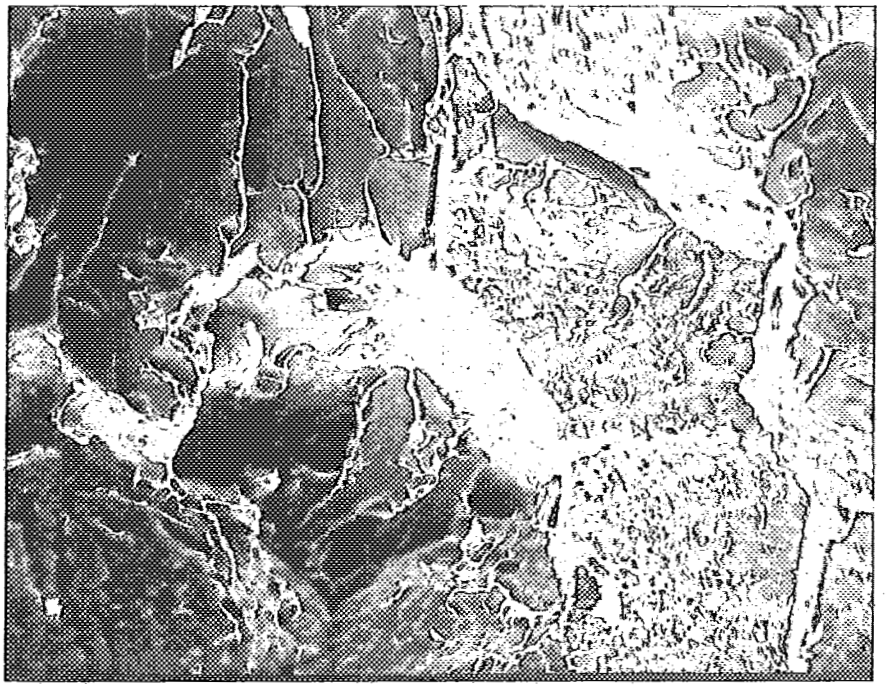

x1500

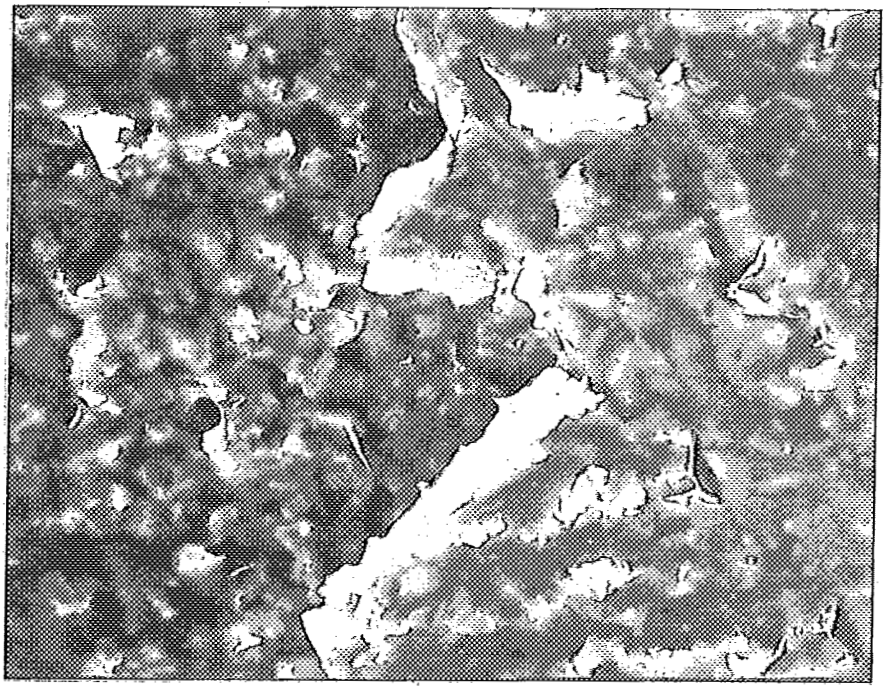

x5000

Fig. 68 Fracture surface of sample no. 56 after 1,000 hr at 875°F in 3500 psig H_2. The x1500 fractograph shows intergranular fracture and cleavage. The higher magnification shows a detail of the intergranular surface.

APPENDIX-DISCUSSION OF THE CHARPY TEST

(a) Sources of Error in Charpy Impact Test Data

The overall interpretation of the data depends to a large extent upon the significance of the numbers derived from the Charpy test. Throughout the program the Charpy testing procedure used at WRDC has been exactly that specified in the ASTM A370 ¶19 and E23 ¶6,8. Additionally the Charpy impact testing machine was periodically calibrated by using Charpy standards supplied by Watertown Arsenal. The tests were performed throughout by the same "operator" and the fracture appearances were "read" by the same operator and checked by two independent fracture surface readers.

Four major areas which might account for inconsistencies in the Charpy impact curve data are listed below.

- Material
  - Is the ingot correctly identified?
  - Is the rolling direction correctly marked?
  - Is the material chemically uniform?
  - Have additional heat treatments been introduced between comparative tests?
- Charpy Sample
  - Is the Charpy bar correctly orientated?
  - Is the notch in the Charpy bar correctly orientated?
  - Is the notch machining consistent from laboratory to laboratory?
- Testing
  - Is there an "operator" variable in testing?
    - time from bath to time of impact
    - temperature of bath
    - positioning of specimen
  - Has the Impact Testing Machine been maintained and calibrated?
- Data
  - Is the fracture appearance reading consistent from laboratory to laboratory?
  - Are sufficient tests run to reasonably assess Charpy impact curves?
  - Is there an inconsistency in defining the best Charpy curve to the data?

Taking all of these possibilities into account and bearing in mind the large number of samples provided for the program from diverse source, it would almost be remarkable if no inconsistencies occurred. Two of these considerations are discussed in the following sections.

(b) The Charpy Specimen Fracture Appearance

In 1976, Chicago Bridge and Iron (CB&I) and WRDC compared all aspects of the machining, machining tolerances, testing and "eye-ball" reading of percentage brittle fracture of the Charpy test. It was concluded that in every respect the procedures were identical except for minor differences in the machining. Even so the specimen tolerances were the same. J.E. Bonta of CB&I therefore supplied some SAW samples which had been tested for an independent evaluation of percentage brittle fracture at WRDC. The samples were given to the normal operators to read without any access to the data generated CB&I. The readings are tabulated below (% ductile).

	Westinghouse		
Sample	Operator A	Operator B	CB&I Reading
1C	10	5	10
1E	15	5	35
1F	30	35	75
2E	10	10	15
2F	15	10	30
2G	20	20	55
2H	5	5	15

It is immediately obvious that there is a significant difference between the readings. CB&I supplied the entire fracture appearance temperature data, which compared with the few samples evaluated at WRDC, showed about 100°F difference in FATT.

The reason for the differences was established after inspecting sample 1F, which represented extremes in the readings, in the SEM. Figure A1 shows schematically the appearance of the fracture surface. Zone A, adjacent to the notch, was found to be 100% dimpled rupture. The "shear lips," Zones C were mixed 50% cleavage and dimples rupture, Zone B in the center of the specimen 35% dimpled rupture mixed with cleavage, and Zone D at the back face of the sample 100% ductile. By conventional eye-ball reading, the apparent percentage of ductile fracture is either A + 2C + D, assuming that C is a ductile shear lip or A + D, assuming C is brittle. The former gives 70% ductile corresponding to the CB&I reading, whereas the latter gives 23% ductile corresponding to the WRDC reading. The correct percentage of ductile fracture derived from the table below is approximately 57%.

Area	% of Total Area	% Ductile in Each Area	% Ductile in Total Area
A	20	100	10.0
B	30	35	10.5
2C	47	50	23.5
D	13	100	13.0
			57.0% Ductile

A similar series of fractographic evaluations was carried out on 25 specimens which had been isothermally embrittled for 20,000 hr, mostly at 875°F. None of these specimens exhibited brittle modes of fractures in Zones, A, C and D (Fig. A1), but up to 25% dimpled rupture was found in the nominally brittle Zone B. An example is shown in Fig. A2. The areas of these zones were carefully measured on a binocular optical microscope and each zone of every specimen was inspected in the SEM to establish the mode of fracture. A simple calculation based upon the percentage of dimpled rupture in the area of Zone B yielded a corrected estimate of the amount of brittle fracture in each specimen. A comparison of the two measurements of fracture appearance is shown in Fig. A3 from which it can be concluded that there is a systematic error in the conventional visual readings. If this is the situation, one can only use the impact energy or the lateral expansion curve as a criterion for the ductile-to-brittle transition temperature. The 40 ft-lb temperature is an arbitrary criterion and is subject to error only if the upper or lower shelf energy is close to 40 ft-lb. However, if the impact energy curve is reasonably representation of the fibrosity curve, it would be more rational to use the impact energy corresponding to the average of the upper and lower shelf energies as a measure of the ductile-brittle transition temperature.

In the light of the fractographic study it is not too surprising to find that the shifts in the transition temperatures due to temper embrittlement, ΔFATT and ΔT(40), were not always equivalent. Since the 40 ft-lb TT is the least subjective of the measurements, it has been used as the primary measure to quantify temper embrittlement in this paper.

(c) Experimental Scatter in the 40 ft-lb Transition Temperature

Because of differences in the 40 ft-lb TT measured on steel samples at JSW and WRDC, it was thought that there might be some systematic testing difference between the two laboratories. Sample No. 61 (3Cr - 1Mo forging) had sufficient material for four sets of Charpy specimens to be taken out adjacent to one another. Thus variations in material characteristics were eliminated as far as possible. The machining and testing matrix was as follows:

Piece	Machined	Tested
61A	JSW	JSW
61B	WRDC	WRDC
61C	WRDC	JSW
61D	JSQ	WRDC

In this study, all possible variables except (1) machining and (2) testing apparatus were removed. The combined results are shown in Fig. A4. Here it can be seen that the effect of the notch machining may not be an important factor. Taking the data as a complete set, it can be represented by a broad band as shown in Fig. A4a. However, separating the WRDC and JSW test data reveals two overlapping bands without regard to origin, Fig. A4b. On this basis it would appear that there is a systematic difference between the JSW and WRDC Charpy impact test method. In discussion of this factor the only difference discovered was the recorded test temperature. JSW uses the temperature at time to impact where WRDC uses (the conventional) temperature of the bath. If any significant difference resulted from the two methods, the WRDC impact curve should lie above that of JSW. In fact, as can be seen in Fig. A4b, the reverse situation is found.

Irrespective of the slight inconsistencies in the data, an estimate of the experimental scatter for this class of steel (3CR - 1Mo) can be made. Using the curve in Fig. A4a, the maximum scatter (for the 30 tests) at the 40 ft-lb TT is approximately +25°F. Using the two curves in Fig. A4b, the scatter is ±15 to ±20°F. The scatter found in over 200 Charpy impact curves varied considerably. Typically the plate and forged steels exhibited a scatter of ±15°F, whereas in certain weld steels the 40 ft-lb TT could only be estimated to within ±35°F. This is a reflection of the relative homogeneity of plate and weld steel.

In order to obtain a better estimate of the transition temperature of steels with a large experimental scatter, it would be necessary to increase the number of test specimens to form the Charpy impact curve (i.e. effectively reducing the standard deviation but not the scatter).

Unfortunately in this study, the experimental scatter or the approximate standard deviation associated with estimates of the transition temperatures is comparable with the shift in transition temperature due to temper embrittlement in many of the steels assessed. This should be born in mind in the interpretation of the data.

At low temperatures the JSW data gives higher impact energy results than WRDC. However, taking the data as a whole, there are 30 points uniformly distributed in a broad band. Given that both laboratories use the same impact testing standard, and that both are competent in their testing techniques, the data shown in Fig. A4 can most reasonably be interpreted to mean that there is variability in the material.

In other words, a commercially-produced steel has enough variability in it (i.e. both composition and structure) that large scatter in the data is expected.

Dwg. 7731A36

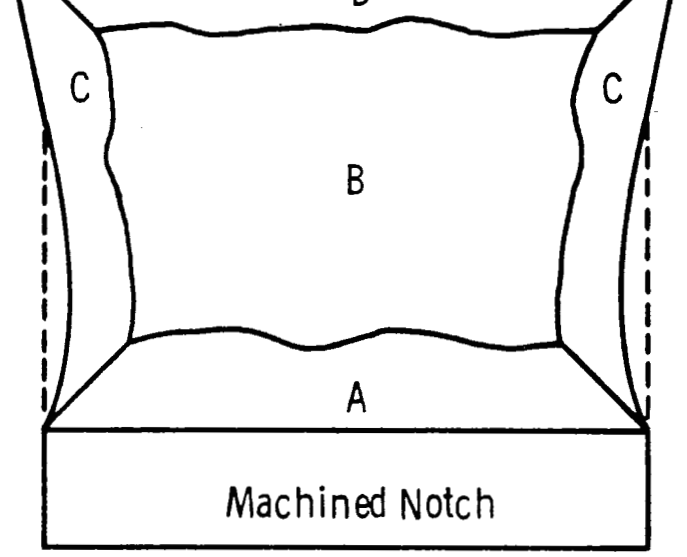

Fig. A1 Schematic diagram of the fracture surface of a standard Charpy specimen with approximately 50% "brittle" Area B.

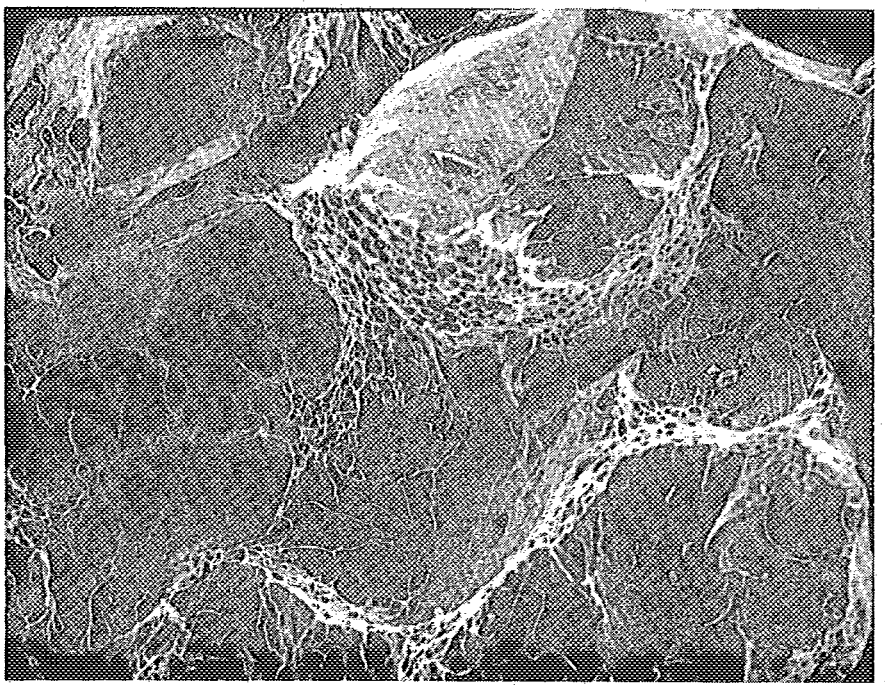

X500

Sample No. 4: 1 Cr-½ Mo Submerged Arc Weld (1 SAW)

Fig. A2 The fracture surface shows very clear cleavage along with islands of dimpled rupture which appear to be primarily on the grain boundaries.

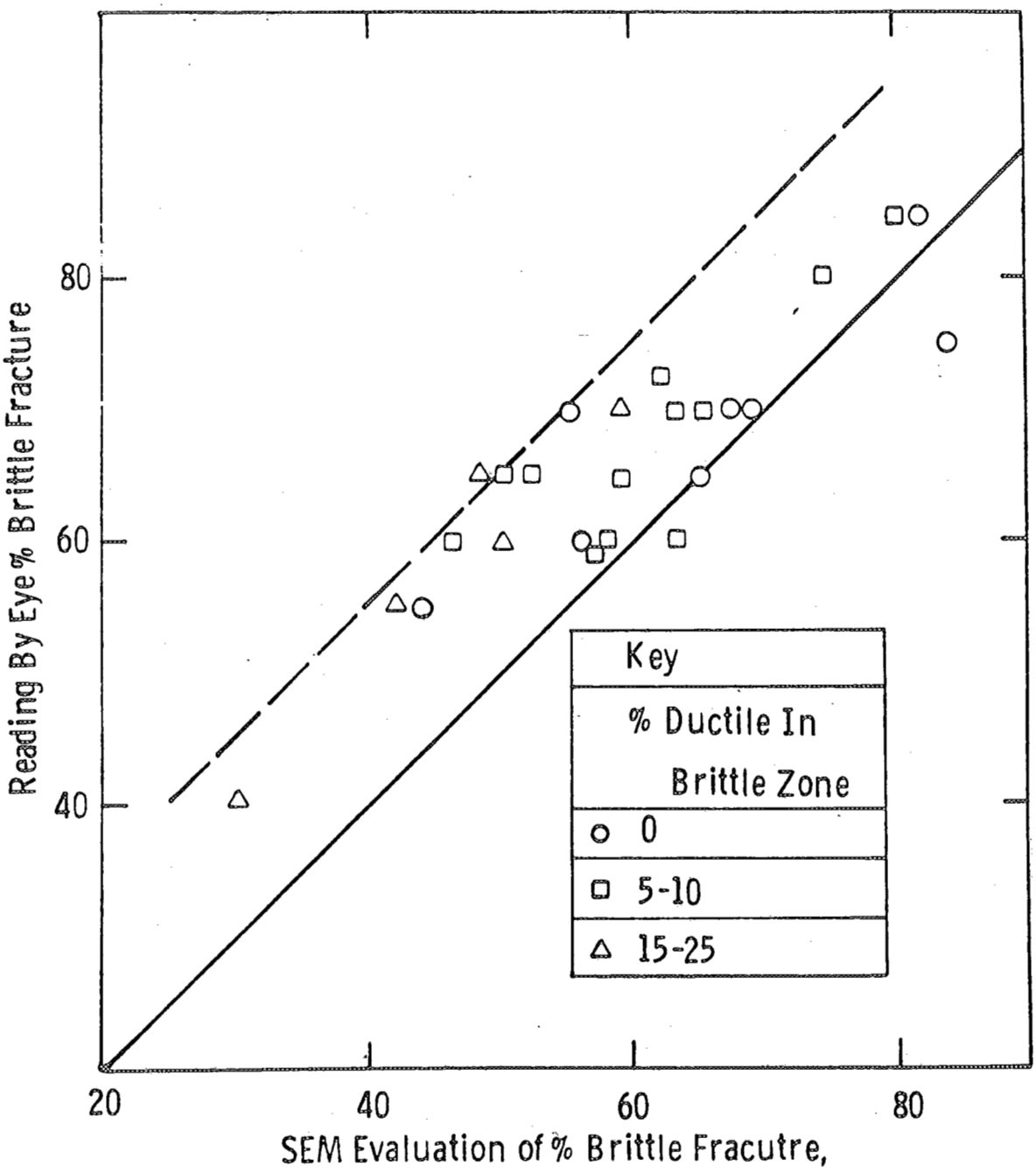

Fig. A3 Comparison of "eye-ball" readings of fracture surfaces with careful scanning electron microscope and optical evaluations. The main source of error stems from ductile regions in the nominally brittle zones.

(a)

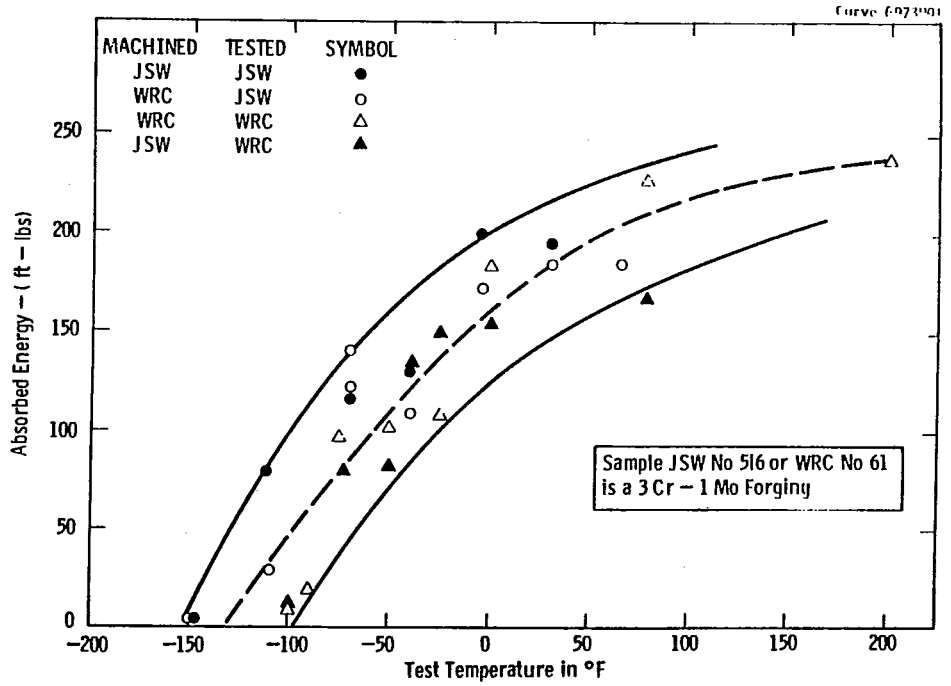

(b)

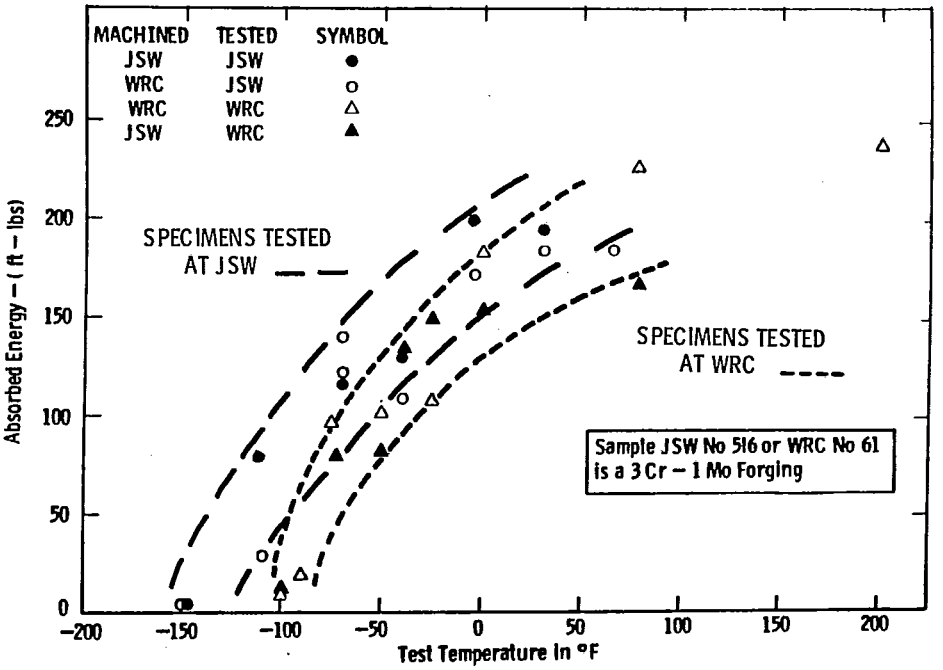

Fig. A4 Comparison of impact data from Charpies machined and tested at Westinghouse Research Center and Japan Steel Works.
(a) Scatter band for all data gathered
(b) Scatter bands for JSW and WRC tested specimens